The Thesis Committee for Yu-Chuen Chang
Certifies that this is the approved version of the following thesis:

Design of Desktop-scale Metal Wire-feed Prototyping Machine

APPROVED BY

SUPERVISING COMMITTEE:

Richard Crawford, Supervisor

Carolyn C. Seepersad

Design of Desktop-scale Metal Wire-feed Prototyping Machine

by

Yu-Chuen Chang, B.S.M.E

THESIS

Presented to the Faculty of the Graduate School of

The University of Texas at Austin

in Partial Fulfillment

of the Requirements

for the Degree of

MASTER OF SCIENCE IN ENGINEERING

THE UNIVERSITY OF TEXAS AT AUSTIN

December 2016

Acknowledgments

It is a pretty exciting and challenge experience for me to attend graduate school at UT Austin. I am not only learning how to do research but also exploring the culture of the United States. I would like to express my deepest appreciation to people who support me while I pursued my master degree.

I sincerely thank my supervisor, Dr. Crawford for encouraging and giving me full freedom to explore the fantastic field of design and manufacturing. His passion in design field motivates me to bring up assumption boldly while verifying it conscientiously and carefully. Also, I greatly appreciate his financial support of the work. I sincerely thank for Dr. SeepersadâĂŹs critical feedback for my research either. Her great advice helps me consider comprehensively and advance my research.

Besides, I am greatly appreciating the support for M.E. technical staff assistants. Mark Phillip always provides the great aid for the electrical problem, such as the current and voltage measurement experimental setup. Butch Cunningham shares his knowledge in the welding fields. Jamie Svrcek gives me much help on the brazing test setup. Daniel Smith gave me great suggestions on machining. Steve Ferraro provided the help when I was building the support for the welding torch. Danny Jares and Ricardo Palacios borrows me acetone and measuring tools.

Additionally, I sincerely appreciate the encouragement and support from

my parents and younger sister. They are people who share my joy and sorrow. Without their support, it would be difficult to complete my work.

Design of Desktop-scale Metal Wire-feed Prototyping Machine

Yu-Chuen Chang, M.S.E.
The University of Texas at Austin, 2016

Supervisor: Richard Crawford

The appearance of desktop 3D printers has inspired a trend toward increased personal fabrication. However, there are few desktop systems that can process metal for prototyping. This thesis reports on the design of a desktop scale prototyping machine that uses metal wire as a precursor material. The machine is intended for use by makers to produce wire-form prototypes, such as wire sculptures.

The design of the system assumes a layer-based fabrication approach. As such, the joining capability of the machine is the most important subsystem. During the research, various conceptual configurations were developed and investigated to determine their thermal bonding efficiency using a metallurgical welding simulation model. The selected bonding method is TIG welding. Two experiments were conducted to test the bonding speed and strength of the bonding spot to validate the feasibility of the concept. A wire bending subsystem was also developed. The selected wire bender is oriented vertically and uses a servo motor and solenoid to perform wire bending and cutting.

Table of Contents

List of Tables

List of Figures

Chapter 1

Introduction

Additive manufacturing (AM) or 3D Printing is a developing collection of disruptive fabrication technologies. In contrast to conventional subtractive manufacturing, namely cutting-based processes, AM builds up three-dimensional objects layer-by-layer. This layer-based approach can produce customized components economically in limited production runs and can be applied to both industrial production and personal fabrication [1].

The recent emergence of desktop or personal 3D printers suggests a trend towards a personal manufacturing revolution. By analogy with the development of the computer industry, AM shows promising potential to spur a manufacturing revolution: from industry to personal workshops [1–3]. One development that might stimulate this revolution is the availability of lost-cost AM processes that fabricate metallic parts. This is the focus of the research reported here.

1.1 Significance of the Problem

Although desktop AM machines offer benefits for the promotion of personal fabrication, these desktop machines still have inherent energy and material limitations which have hampered their application for creating metallic parts.

1.1.1 Material Limitations

Limited material selection is one of the primary challenges of desktop AM machines. Most desktop AM machines can only process polymers, not metals [3, 4]. This limitation comes from the lack of a softening point and high melting point (typically higher than $600\,^{\circ}\mathrm{C}$) of metals. The softening point is the temperature at which an amorphous or semicrystalline material exhibits viscous flow without causing significant dimensional deformation. Typical viscosity in this range is approximately $4 \times 10^{7}\,\mathrm{P}$ [5]. Fused Deposition Modeling (FDM), the most common process for desktop 3D printers [6], is the typical example to demonstrate the material property issues. FDM mainly uses materials which melt around $200\,^{\circ}\mathrm{C}$, such as polylactic acid (PLA) [7] and acrylonitrile butadiene styrene (ABS) [8]. Additionally, FDM utilizes the glass transition property of polymers to deposit semi-molten material. Unfortunately, most metals do not experience the softening stage [9] and move from solid to liquid state immediately at their melting points. This property demonstrates that a metal droplet does not have an appropriate viscosity to keep its shape.

Besides limitations in properties of materials, it is also important to consider cost and accessibility of precursor materials for desktop AM machines. The material for these machines should be easy to obtain and the price should be affordable for the general public.

1.1.2 Energy Limitations

Energy limitations result from the heating ability of desktop AM machines. Most AM processes include a heating stage to soften, sinter or melt the precursor material. In order to handle metals with melting points up to $600\,^{\circ}\mathrm{C}$, higher thermal energy is required. However, the ability of desktop machines to provide heat is limited by the domestic energy supply. A typical power receptacle in a residence in the United States can supply about $1800\,\mathrm{W}$ (The household voltage is $120\,\mathrm{V}$ and the common current breaker is rated at $15\,\mathrm{A}$ to $20\,\mathrm{A}$ in the United States [10]). This requirement makes it difficult to heat a metal to its melting temperature by traditional heating methods. Additionally, high thermal energy may result in cost, security, and even environmental issues [11].

1.2 Research Objective

To address the aforementioned material and energy limitations, this research aims to explore the feasibility of a new approach for desktop metal-based prototyping (RP) using readily available precursor materials [12].

The research is structured as a product design process and is illustrated in Figure 1.1. Metal wire is selected as the material resource because of its accessibility and affordability to the public, which is shown in Table 1.1. The deliverables of the research include:

1. **Clarify design constraints and requirements**

   It is necessary to clarify requirements and constraints to effectively develop

Metal Type	Shape of Wire	Price per foot	Source
Aluminum	Round	$0.07	Hobby Lobby
Copper	Round	$0.07	Home Depot
Copper	Half Round	$0.08	Wire-Sculpture.com
Brass	Round	$0.09	Home Depot
Stainless Steel	Round	$0.12	Wire-Sculpture.com
Sterling Silver	Half Round/Round	$0.51-0.99	Wire-Sculpture.com
Gold Filled	Half Round/Round/Square	$0.97-2.13	Wire-Sculpture.com

Notes. 22 gauge $\approx$ 0.64 mm.

Table 1.1: Price of 22 gauge metal wire

conceptual designs. The research presents a study of AM processes and applications to determine performance metrics. Additionally, general functional models are developed to provide design criteria for morphological analysis [12].

2. **Develop conceptual design**

   Evaluation of conceptual designs avoids the tedious and expensive trial and error process. Five concept variants are developed by morphological analysis and evaluated based on their estimated power consumption, processing time, and financial feasibility. A Pugh Chart [12] is used to compare these concept variants and select the preferred one.

3. **Concept-proof experiment**

   Concept-proof experiments are built to test its ability to create two-dimensional metal structures. The configuration of the desktop RP machine, such as the layout of its degrees of freedom, is developed in this stage. The result of the examination provides insights for further refinement of the design. How-

ever, parametric and detailed design steps are beyond the scope of the research.

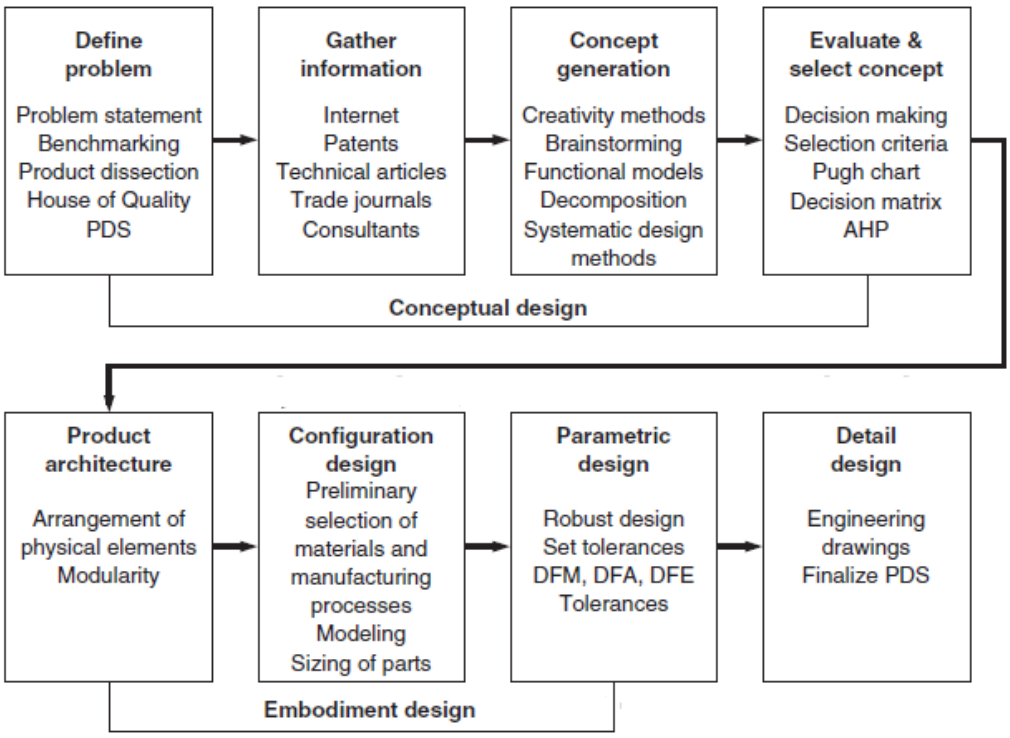

Figure 1.1: Roadmap of the product design process [13]

1.3 Thesis Organization

Chapter 1 highlights obstacles to the development of metal-based AM or RP machines for personal use. The chapter also discusses research objectives and organization of the thesis.

Chapter 2 provides a study of AM technology. The study includes three sections. The first section discusses general AM methods, including their material

limitations. The following section focuses on metal-based AM. Finally, the third section shows the existing solutions for desktop metal-based AM. This study of the state-of-the-art in metal-based AM technology informs the concept generation stage of the design process.

In Chapter 3, requirements and constraints of desktop metal-based RP machines are enumerated and required functions are identified for concept generation.

Chapter 4 shows five concept variants generated by morphological analysis. A theoretical model is built to demonstrate energy and financial feasibility. Finally, the concept variants are compared using a Pugh Chart to choose the preferred solution.

Chapter 5 focuses on the experimental design to validate its ability to create two-dimensional structures with metal wires. Chapter 6 illustrates the design of the wire bender system and develops the CAD Model and BOM.

Chapter 7 provides conclusions and recommendations for future work.

Chapter 2

Literature Review

This chapter 2 presents the problem context for the design of a desktop-scale metal wire-feed prototyping machine. The chapter first categorizes industrial additive manufacturing (AM) processes and then focuses on existing desktop-scale metal AM machines to identify common characteristics and limitations of AM processes.

2.1 Overview of Additive Manufacturing

AM is a computer-automated manufacturing process which can fabricate three-dimensional components by depositing material layer by layer. Figure 2.1 illustrates of the general process of AM. In Figure 2.1, users first build a virtual model by computer-aided design (CAD) software, such as SolidWorks (Concord, MA), AutoCAD (San Rafael, CA), and Pro-E (Needham, MA). Later, the CAD file is sliced by computer-aided manufacturing (CAM) software. A physical three-dimensional component is built based on the sliced CAD model by the selected AM process. The physical component is built up layer by layer until the final component is completely built.

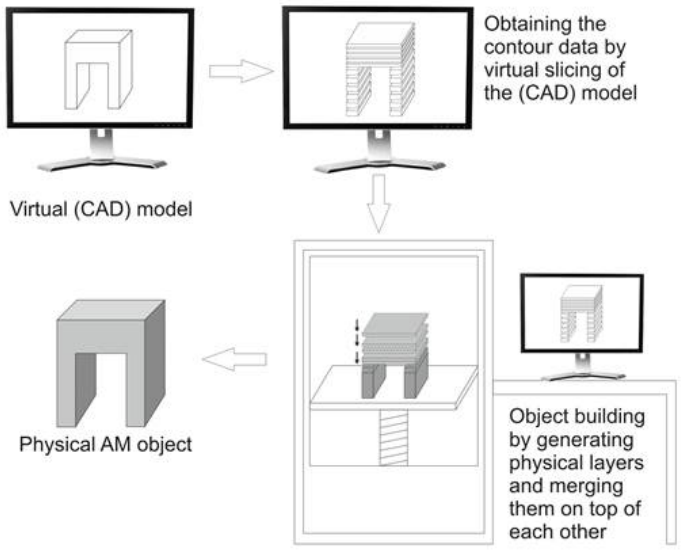

Figure 2.1: General AM process [14]

2.1.1 Characteristic of Additive Manufacturing

Most AM processes have three common characteristics even though these processes are based on significantly different physics.

- *Digital Fabrication:* One of the important characteristics is that all AM processes are controlled by computers. Digital fabrication tools produce objects from CAD models, typically STL files, for AM processes. This user-friendly feature allows users to create more complicated structures.

- *Part Flexibility:* In theory, AM can produce any design from an STL file. Thus, it is possible to create multi-functional structures on a single workpiece. Moreover, AM technology may have the ability to fabricate compo-

nents with gradient materials. It provides freedom to create a design with elaborate features, such as cellular structures.

- *Production Flexibility:* AM has a high degree of production freedom. Users can easily modify the design of a product by changing the STL file instead of the production set-up. Overall, AM can fabricate customized products economically compared to conventional manufacturing processes for mass production.

Part and production flexibility provides unique advantages for AM processes over conventional subtractive manufacturing, namely cutting-based processes. As a result, many manufacturers and research institutions are interested in AM (See Figure 2.2), such as Boeing [15] and NASA [16].

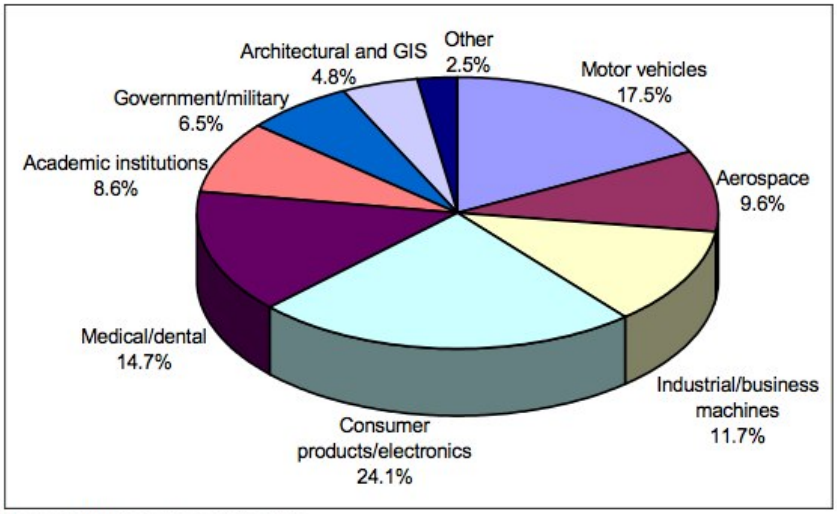

Figure 2.2: Industrial application of additive manufacturing[17]

2.1.2 Additive Manufacturing Process

There are many commercialized AM processes widely applied in manufacturing industries. Table 2.1 shows the most successful processes, including Stereolithography (SLA or SL), Fused Deposition Modeling (FDM), Ink Jet Printing (IJP), Laminated Object Manufacturing (LOM), Selective Laser Sintering/Melting (SLS/SLM), Three Dimensional Printing (3DP) and Laser Metal Deposition (LMD).

- **Sterelithography**

  Seterelithography (SLS) , developed by 3D systems (Rock Hill, SC, USA) in 1987, was the first commercial AM process. SLA has an elevator platform and ultraviolet (UV) laser light source. It utilizes the ultraviolet laser to cure or solidify a photosensitive polymer to create a resin layer. Next, the elevator platform descends, and the original layer is flooded with liquid photosensitive polymer. The new liquid resin is exposed to the ultraviolet laser and the process is repeated until the three-dimensional component is completely formed [18–20].

- **Fused Deposition Modeling**

  Fused Deposition Modeling (FDM), developed by S. Scott Crump and later commercialized by Stratasys (Eden Prairie, MN, USA), is widely applied to both industrial machines and desktop 3D printers. A thermoplastic filament is heated close to its melting temperature in a heating chamber. Then, a printing nozzle utilizes the softening process of the filament and extrudes

Process	Vendors
SLA/SL	3D Systems (USA)
	Aaroflex (USA)
	CMET (Japan)
	EnvisionTEC (USA)
	EOS (Germany)
	Formlabs (USA)
	Shaanxi Hengtong Intelligent Machine Co. Ltd (China)
	Shanghai Union Technology (China)
FDM	Beijing Yinhua Laser Rapid Prototype (China)
	MakerBot Idustries (USA)
	Stratasys (USA)
IJP	MicroFab Technologies (USA)
	Stratasys (USA)
LOM	3D Systems (USA)
	Cubic Technologies (USA)
SLS/SLM	3D Systems (USA)
	Blueprinter (Denmark)
	Concept Laser (Germany)
	EOS (Germany)
	Farsoon Hi-Tech Company (China)
	Realizer (Germany)
	Renishaw (England)
	SLM Solutions GmbH (Germany)
3DP	Voxeljet (Germany)
LMD	Optomec (USA)
	InssTek Inc. (South Korea)

Table 2.1: Commercialized additive manufacturing processes

the softened filament to defined locations in order to create target structures [18, 20, 21].

- **Ink-jet Printing**

  Ink-jet Printing (IJP) is analogous to a conventional inkjet printer. The main difference is that IJP deposits low viscous polymers, such as molten wax or thermoplastic material, instead of ink [18, 22]. This method is especially popular in electronic and medical industries [23, 24]. Many studies have proved the feasibility of printing scaffolds, organs, and biomaterials by IJP [24].

- **Laminated Object Manufacturing**

  Laminated Object Manfuacturing (LOM), developed by Helisys Inc. (Rochester, MI, USA), is a combination of additive and subtractive manufacturing. In the process of LOM, foil materials are glued or welded together layer by layer; then, material sheets are cut by laser or cutter to remove unwanted areas [18, 25]. This RP technique is applicable to paper, plastic or even metal processing [20, 26, 27].

- **Selective Laser Sintering/Melting**

  Selective Laser Sintering/Melting (SLS/SLM), developed by UT Austin in mid-1980s, is still the primary metal-based AM process. The system has a CO_2 or Nd:YAG laser and a powder bed. SLS/SLM uses the laser to fuse material powders to build up three-dimensional components.

  The concepts of SLS and SLM are slightly different. In SLM, the powder

fully melts. However, the SLS process experiences debinding, sintering, and infiltration stages [28,29]. Therefore, SLS typically requires the participation of a binder for metal parts.

There are two unique advantages of SLS/SLM. The first advantage is that SLS/SLM does not require support structures because unsintered powder in the powder bed keeps the processing component in place. Therefore, Selective Laser Sintering can be used to create more complicated geometry [18, 20, 30]. Additionally, unlike other AM processes that have limitations on heating capability, SLS/SLM can process a wide range of material, such as metal and ceramic, because of the high heating capability of the laser source and the use of low temperature binders.

- **Three Dimensional Printing**

  Three Dimensional Printing (3DP) was developed by MIT. 3DP has a roller to spread powder over a build platform. A printhead which is similar to the one for Ink-jet Printing extrudes binder. Subsequently, the binder selectively joints particles together [18,31]. This process is flexible enough to prototype sophisticated parts with various materials, such as ceramics [20,32,33], metals [34], polymers, and composites.

- **Laser Metal Deposition**

  Laser Metal Deposition (LMD) is relatively new compared to the other aforementioned AM processes. By means of laser cladding technology, powder is delivered by a nozzle and melted/sintered by a laser source [35]. LMD poten-

tially shows the ability to deposit material and repair an existing structure. A similar process includes electron-beam-induced deposition for microfabrication [36].

There are still many AM processes in development, such as Multi-Jet Modeling (MJM) [20], Rapid Freeze Prototyping (RFP) [20, 37], Freeze-form Extrusion Fabrication (FEF) [20, 38], and Robocasting [39]. However, these representative AM processes provide valuable insights for design requirement clarification and concept generation for this research.

2.2 Additive Manufacturing with Metals

Although AM technologies have part and production flexibility over traditional manufacturing processes, they can still only process limited materials. In fact, most AM processes can deal only with polymers, not metals. Differences in mechanical properties of polymers and metals make filament-based AM processes difficult for creating metallic objects. Filament-based AM processes, like FDM, utilize the softening point of an amorphous or semicrystalline material to extrude the semi-softened filament without deforming its shape. Thus, a filament extrusion system is useful to deal with thermoplastics, such as ABS, PLA, and Nylon. However, most metals do not experience the softening process. In other words, metals do not have high enough viscosity (typically over 4×10^7 P [5]) to maintain the shape of a droplet after depositing. As a result, not all AM processes are suitable for producing metallic components.

A high power heating source, such as a laser or electron beam, is commonly used for metal-based AM process. In order to fully melt or sinter metal powder, the heat source should have the capability to heat the metal powder close to or higher than its melting temperature. Therefore, melting/sintering capability is an important parameter for metal-based AM.

On the other hand, the use of metal powder is mainly enabled by the efficiency of laser power intensity absorption of metals for laser-based AM processes, such as SLS/SLM. Different material geometries, such as sheet and powder, have different reflectivities [40, 41], which is illustrated in Table 2.2.

Material	**Powder**	**Sheet**
Copper (rough)	$74\,\%$	$78.45\,\%$
Titanium	$41\,\%$	$91.87\,\%$

Table 2.2: Reflectivity ($\%$) of metal powder under CO_2 laser ($10.6\,\mu\mathrm{m}$)

The high reflectivity of metals causes significant power intensity reflectivity, shown in Equation 2.1, where I_t is the power intensity that the material absorbs, I_o is the original power intensity from the laser, and R represents the reflectivity of the metal. According to Equation 2.1, the loss of laser power intensity is directly proportional to the reflectivity of metal. For example, the reflectivity for copper powder is $74\,\%$, thus the loss of power is $74\,\%$. In other words, the laser power absorption efficiency of copper powder is $26\,\%$. Therefore, the geometry of the metal influences laser-based AM processes, which makes powder materials more preferable.

$$I_t = I_o(1 - R) \tag{2.1}$$

2.2.1 Thermal Aspects

Most metal-based AM processes need a high power energy supply, so thermal aspects of metal-based processes play a significant role. There are three types of thermal energy delivery methods for common commercialized metal-based AM processes: laser scanning processes, electron-beam scanning processes, and welding-based processes.

- **Laser scanning**

  Laser scanning processes, such as SLS/SLM, LMD, Laser Engineered Net Shaping Techniques (LENS) [42], and Three-Dimension Laser Cladding, are widely used in industry. CO_2 and Nd:YAG pulsed lasers [29] are common laser sources. A fraction of laser irradiation in laser scanning processes is absorbed by the metal powder, and the heat from the laser is conducted into the interior of powder and melts the powder particle. Besides the aforementioned influence coming from the geometry and the melting temperature of metal, the parameters shown in Table 2.3 influence laser-based processes.

- **Electron-beam scanning**

  Electron-beam scanning processes are also common metal-based AM approaches, especially in academic research. The collision of free electrons in a vacuum chamber can be converted into heat or kinematic energy to melt

Parameters	Material properties
Controlled	Viscosity
Laser scanners	Surface tension
Laser power	Particle size distribution
Mechanical layering of powder	Particle shape
Atmospheric control	Absorptivity/reflectivity
Air flow	Thermal conductivity
Heaters (bed temperature)	Specific heat
Machine-specific	Emissivity
Laser type	Melting temperature
Scan radius	
Geometry-specific	
Scan vector length	

Table 2.3: Process variables of SLS/SLM [9]

the target material. The power for Electron Beam Melting (EBM) can be higher than $4\,\mathrm{kW}$ [43]. This technique can melt the material independent of its surface conditions, such as reflectivity. Thus, the energy absorption and penetration is significantly improved in EBM processes. Furthermore, since EBM is applied under a vacuum, it can avoid gas contamination, which is one of the main issues for metal-based AM [16]. However, the capital cost and training cost of EBM techniques are significantly higher than laser-based processes, which make them less attractive for commercialization.

- **Welding**

  Welding technology is also an effective thermal approach for metal-based AM. The concept of Ultrasonic Object Consolidation (UC or UOC) is similar to LOM. UC/UOC utilizes ultrasonic welding and milling procedures to bond metal sheets together to create metal parts. Parameters of UC include

amplitude, welding speed, normal force, and substrate temperature [44]. On the other hand, welding metal sheets causes shear stress, which potentially results in plastic deformation and oxide layers (See Figure 2.3).

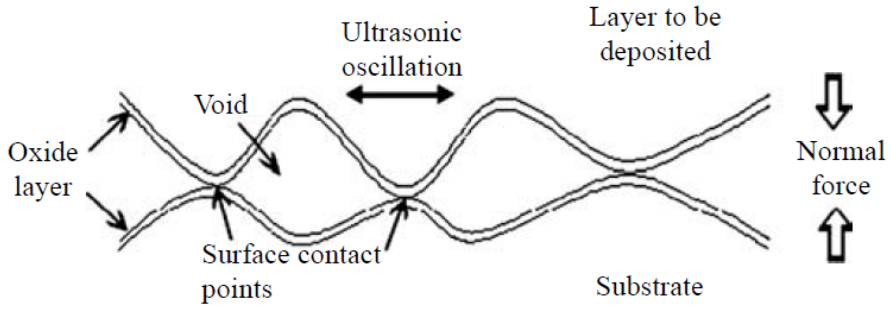

Figure 2.3: Oxide layers are generated during ultrasonic welding procedure[27]

These three thermal approaches in metal-based AM processes each require a high energy supply, as shown in Table 2.4. A high energy supply generally comes with a high cost, which makes the price of metal-based AM machines higher. The average price of the SLS process can be more than $\$350\,\mathrm{K}$ [45].

A low melting-temperature binder is often used in metal-based AM processes to make the bonding process more power efficient. A binder can be a pre-alloyed powder or a two-phase powder. Since the melting point of the binder is lower than the metal powder, it will melt first. Once the binder melts, the capillary force of the liquefying binder will cause the metal powder particles to attach together [9]. Therefore, an AM process with a binder requires a smaller energy supply to complete the melting/sintering process.

AM Process	Deposition Mode	Power Consumption	Citation
SLM	Laser melting	3.68 kW-6.4 kW	[46, 47]
SLS	Laser sintering	3.2 kW-10 kW	[48–50]
LDM	Laser cladding	10 kW	[51]
EBM	Electron beam melting	7 kW-60 kW	[52, 53]
UOC	Ultrasonic welding	4.5 kW-9 kW	[54]

Table 2.4: Total power consumption of commercialized metal-based AM

2.2.2 Other Metal-Based Additive Manufacturing

Some researchers intend to improve bonding in metal-based AM processes. This section details two methods: use of a chemical precursor and change of the nano-structure of the material.

- **The Use of Chemical Precursor**

  The participation of a chemical precursor can create a chemical reaction during the process and generate metal particles. This method has been used to form electrodes. The metal precursor is printed by an ink jet printer and then converted to metal. For example, copper hexanoate is extruded through the nozzle. Next, a metal-organic copper precursor is heated to 200 °C and decomposes to copper and copper oxide. Finally, the matrix totally converts to copper by forming gas annealing at 200 °C [23].

- **Change of Nano-structure of Material**

  Changing the nanostructure of a material is another potential solution, although this approach has not been commercialized yet. Once the shape or size of a nanoparticle changes, optical, thermal, and electrochemical properties of the material also improve. For example, the melting temperature

of a gold cluster ($130\,^{\circ}\mathrm{C}$) is much lower than the melting temperature of bulk gold ($1063\,^{\circ}\mathrm{C}$) [55]. Additionally, nanotechnology has been shown to improve the properties of a binder. Bai, J. G. et al. have demonstrated that a silver suspension binder can decrease the sintering temperature as low as $300\,^{\circ}\mathrm{C}$. Furthermore, the final product has less distortion and shrinkage [41].

2.3 Desktop-Scale Additive Manufacturing with Metal

The development of a desktop-scale metal-based AM machine has more constraints compared to industrial ones, particularly with respect to the energy supply, cost, and material choice. The energy supply limitation is very significant for desktop metal-based AM machines due to the limitation of domestic electric energy supply. The standard household voltage is $120\,\mathrm{V}$ in the United States and the common household circuit breaker is $15\,\mathrm{A}$ or $20\,\mathrm{A}$ [5]. Therefore, this suggests that the power for desktop metal-based AM machine should be less than $1800\,\mathrm{W}$. Cost is another significant consideration for the design of a desktop-scale machine. The price for commercialized desktop 3D printers ranges from $\$300\,\mathrm{to}\,\$6000\,\mathrm{in}$ [56]. Therefore, the price of desktop metal-based AM machine should be within the $\$6000\,\mathrm{price}$ range. The material for desktop metal-based AM machine should be generally accessible and affordable to the public. In addition, since a desktop machine is normally used in a studio or household, the material should be nontoxic during processing.

This section presents a study of four existing desktop metal-based AM ma-

chines: Mini Metal Maker, Open Source 3D Printer with gas-metal arc welding (GMAW), Selective Inhibition Sintering (SIS), and Liquid Metal Jetting (LMJ). Descriptions for these machines are based on limited available material. Only Mini Metal Maker is commercialized, asking funding by campaigns in Indiegogo and Kickstarter.

2.3.1 Mini Metal Maker: 3D Printer with Metal Clay

The Mini Metal Maker was developed by David Hartkop in 2013. The machine is similar to an FDM system. However, instead of extruding a semi-soften thermoplastic filament, the Mini Metal Maker extrudes metal clay, which consists of metal particles and a water-soluble organic binder, to create a green component. Later, this green component is heated in a furnace (typically $600\,^{\circ}\mathrm{C}$ to $900\,^{\circ}\mathrm{C}$ [57]) to remove the binder and fuse the metal particles together. Figure 2.4 shows metal parts built by Mini Metal Maker.

The unique concept of Mini Metal Maker is that the process separates the heating and forming process, much like the traditional wax-casting process. Specifically, there is no heat participation during printing. Additionally, metal clay serves as a mix of material and binder, which not only benefits the forming process but also effectively decreases the temperature in the kiln.

Figure 2.4: Stanford bunny test object built by Mini Metal Maker[57]

2.3.2 3D Printer with Gas-Metal Arc Welding

An open source metal 3D Printer with gas-metal arc welding (GMAW) was developed at Michigan Technological University. The group combined a Millermatic 140 welder with a delta RepRap to build a low cost metal-based 3D printer (See Figure 2.5) [4]. Carbon steel wire, ER 70S-6, is used as a material source to decrease the generation of sparks.

Different from the previously mentioned industrial AM processes, this 3D printer uses GMAW to heat the material. The price of a GMAW is comparatively cheap ($\$836$ for Millermatic 140 [4]) compared to other welding methods. Additionally, the energy requirement of the GMAW is suitable for most studios. For example, the input voltage requirement for the Millermatic 140 is $115\,\mathrm{V}$, and the input current is $20\,\mathrm{A}$, $60\,\mathrm{Hz}$ single phase [58].

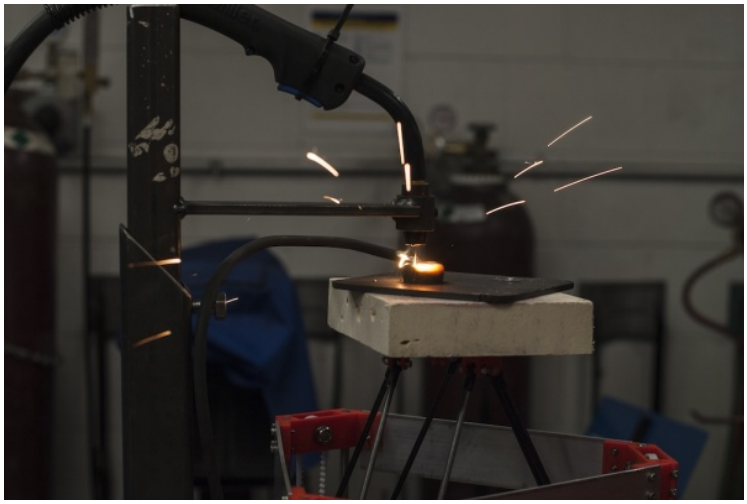

Figure 2.5: 3D Printer with Gas-Metal Arc Welding[59]

2.3.3 Selective Inhibition Sintering

Selective Inhibition Sintering (SIS) is an AM process similar to 3DP. The primary difference is that the print-head extrudes an inhibitor instead of the glue in SIS process. The print-head deposits the inhibitor along the contour of the geometry on the single powder layer. The piston platform moves down and the process is repeated layer by layer until completing building a powder block. Then, the powder block is moved into the furnace to start the sintering process. Most particles in the powder block will fuse except the part with the inhibitor. Later, the powder block cools down and is removed from the oven. The desired sintered geometry can be easily separated from the powder block (See Figure 2.6). Finally, the final sintered component is washed with water or an organic solution to remove the inhibitor.

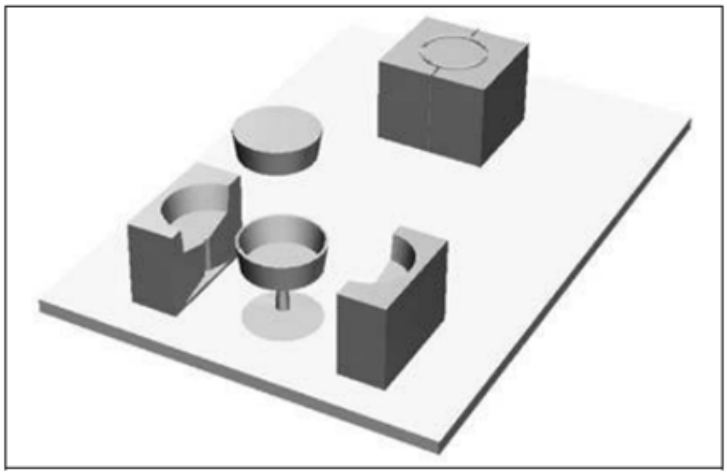

Figure 2.6: Separate sintering part based on inhibiter layer[60]

For the metal-based SIS process, microscopic mechanical inhibition is a common inhibition mechanism compared to macroscopic mechanical inhibition, chemical inhibition, and thermal inhibition [61]. Microscopic mechanical inhibition demonstrates that an inhibitor penetrates into the void between powder particles without changing the surface features of the powder particles. Microscopic mechanical inhibitors, such as salt water, silicone, and aluminum sulfate, prevent powder particles from joining together during the sintering process. Requirements of microscopic mechanical inhibitors in the SIS process include high solubility, low molecular mass, and low surface tension. Additionally, the melting temperature of the selected inhibitor should be higher than the metal powder. Based on selection criteria, the recommended inhibitor is aluminum sulfate for a bronze powder [60, 61].

2.3.4 Liquid Metal Jetting

Liquid Metal Jetting (LMJ) is another possible option for desktop metal AM technology. LMJ was developed at the University of Texas Arlington [62], and has a nozzle to deposit bulk metallic glass (BGM) or so-called liquid metal onto three-dimensional objects. The liquid metal is a metallic glassy alloy which fails to crystallize during solidification at low cooling rates. The liquid metal has better strength and elasticity compared to traditional solid metal, such as titanium alloys and steels. Therefore, a liquid metal 3D printer has potential to create metallic components with liquid metal at room temperature.

2.3.5 Comparison of Metal-Based Desktop Machines

Table 2.5 summarizes and compares these four desktop machines. All of these machines have their own disadvantages. For example, the primary disadvantage of the Mini Metal Maker is the price of the metal clay. Metal clay is available and easy to obtain via the Internet. However, the available metal clays are limited to gold, silver, copper, and bronze. Furthermore, the price of metal clay is comparatively expensive; for example, the price of $50\,\mathrm{g}$ of PMC 3 can be higher than $\$90$ [63]. This drawback makes the Mini Metal Maker unsuitable for common prototyping needs. For 3D Printer with GMAW, safety issues are significant. Appropriate fire protection is required in order to protect the user from the splatter generated from the welding process. For SIS and LMJ, the primary problem is the material (inhibitor and material powder for SIS and BGM for LMJ) is not easy to obtain for the general public. Furthermore, the efficiency of the sintering process

of SIS still depends on the melting point of the metal powder; in other words, the sintering process mainly depends on the heating capability of the furnace.

Machine	Material	Layer Creation Technique	Challenge
Mini Metal Maker	Metal clay	Continuous extrusion	High price of metal clay
3D Printer with GMAW	Consumable electrode	Welding	Safety issue
SIS	Metal powder	Inhibitor extrusion	Inaccessibility of inhibitor and metal powder for the public; safety issue
LMJ	Liquid metal	Continuous extrusion	Inaccessibility of liquid metal for the public

Table 2.5: Summary of four desktop AM machines

However, these four studies still provide two important insights. First, the separation of printing and the heating process might be a possible solution for desktop AM process. The Mini Metal Maker and SIS both separate printing and heating processes. The Mini Metal Maker uses a metal clay, comprising metal particles and a binder, to help metal particles adjoin together when the printed component is in the oven. On the other hand, SIS uses an inhibitor to prevent material powder particles from fusing together in the oven.

Second, a low cost welding method may be another possible solution for the development of desktop metal-based AM machine. The cost of a 3D printer with GMAW is less than $2000. Additionally, many welding machines are suitable for the studio; in other words, it fits the energy supply requirement for the design

of desktop machines.

These two insights are valuable for the development of conceptual design in the following chapter.

2.4 Chapter Summary

Chapter 2 summarizes the related literature about additive manufacturing. Here are the primary contributions of this chapter:

- Identify common characteristic of additive manufacturing
- Review commercialized metal-based additive manufacturing
- Compare four existing desktop-sized metal-based additive manufacturing machines

Insights gained from these four desktop machines are used to develop conceptual designs in Chapter 4.

Chapter 3

Define Problem

Chapter 3 focuses on defining the objective and identifying requirements and constraints for the design of a desktop metal wire-feed prototyping machine. Section 3.1 demonstrates the challenge for creating wire art sculpture and specifies the problem context. Section 3.2 describes the problem statement. In Section 3.3, functional models for SLS, FDM and LOM are identified to generate the functional requirements of desktop AM machines. Finally, performance metrics for the device are developed in Section 3.4.

3.1 Problem Context

The design of the desktop-scale metal wire-feed prototyping machine is inspired by metal-wire handcrafts. Metal-wire has a long history as an art medium. The early record of metal-wire handcrafts can be traced to ancient Egypt. Gold or silver strips are woven and used to decorate sarcophaguses [64]. At the time, metal wire or metal strip was used for decoration purposes. By 1823, metal wire became a common art medium because of the inspiration from Henry Stammler, who earned recognition for his exceptional metal-wire artworks at the Exposition of French Industrial Products [65]. Later, metal-wire was even used to create sculptures, as

shown in Figure 3.1.

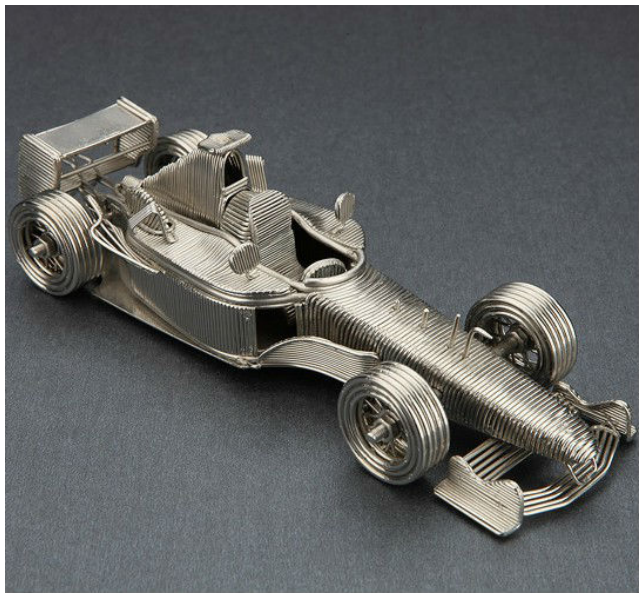

Figure 3.1: Car Wire Sculpture[66]

There are different diameters of metal wire that serve different purposes (See Table 3.1). The recommended diameter and hardness of the wire depends on the applications. Typically, 22 guage, approximately 0.64 mm, is the most common diameter of metal wire for wire sculpture design.

Diameter (guage)	**Application**
30-28	Fine jewelry (weaving)
26	Wrapped wire
24	Easy to kink
22	Common
20-18	For chains
16-14	Heavy jewelry

Table 3.1: Different diameters of metal wire and its handcraft application (ref. [65])

Making metal-wire artwork is a labor-intensive and time-consuming process. Furthermore, there is a steep learning curve to create complicated structure, especially wire art sculpture. For example, a wire artist needs to have skill in brazing and soldering. Additionally, the artist must have several tools, such as various pliers, cutters, hammers, and so on. Therefore, the difficulties of creating wire art sculptures inspires the question: is it possible for artists to create wire sculptures with automatic machines?

The machine is expected to create both two-dimensional and three-dimensional structures with metal wire, such as spiral structures and wire sculptures, with an additive manufacturing approach.

3.2 Problem Statement

The challenge for the design of a desktop metal wire-feed prototyping machine mainly comes from the limitation of domestic energy supply. Traditional industrial methods, such as SLS/SLM, UOC, and EBM, are not suitable for the design due to large energy supply requirement for material-bonding processes, which also results in the high cost of those metal-based AM processes. Therefore, new design approaches are required in order to design a desktop-scale metal wire-feed prototyping machine.

Additionally, the desktop-scale metal prototyping machine is expected to not only work in studios but also in households. Therefore, the precursor material for the machine should be affordable and easy to obtain by the general public. Metal wire is chosen as the material resource for the desktop-scale metal proto-

typing machine since it is easy to obtain by the general public compared to metal powder and metal sheet. Users can buy metal wire even in craft stores. Prices and vendors for common metal wire are listed in Appendix **??**.

As the result, the problem statement of the research is:
Design a low-cost desktop-scale metal wire-feed prototyping machine which can create metallic components with domestic power in an appropriate time period.

3.3 Functional Requirements of the Design

Three common characteristics (digital fabrication, part flexibility, and production flexibility) of AM processes imply that there are common functional requirements for AM processes. In order to identify these functional requirements, Selective Laser Sintering (SLS), Laminated Object Manufacturing (LOM), and Fused Deposition Modeling (FDM) are analyzed by using function structures. The reason why these AM processes are selected is because they use very different material forms; specifically, powder for SLS, sheet for LOM, and filament for FDM.

A function structure is a flow chart that identifies the internal functions of a product or system. Specifically, a function structure illustrates the relations between component and transfer flow (in this case, energy, material, and signal flow). By developing function structures for SLS, LOM, and FDM, basic functional requirements of the metal wire-feed prototyping machine can be identified. The function structures only develop a single-layer building process instead of a complete process. Because AM is a layer-approach process, a single-layer building process represents the main functional requirements of a complete AM process.

3.3.1 Function Structure of Selective Laser Sintering

While there are differences among SLS systems, most of them have a powder delivery system, build chamber, laser, and computer control system. The precursor material for the SLS process is powder. An example of the common interior of a SLS machine is shown in Figure 3.2. For the powder delivery system, the powder is first stored in a feed chamber. The powder feed piston moves upward to deliver the powder, and the roller moves and spreads the powder on the surface of the build chamber. For the laser delivery process, the computer controls the power input and scanning speed of the laser. An X-Y scanning mirror controls the direction of the laser, and the lens increases the laser power intensity by decreasing the radius of the laser spot. The laser spot heats in the selected path and sinters powder particles. Once a single layer is created, the build piston moves downward, and the roller spreads new powder on the surface of the build chamber. The process is repeated until the final component is created.

Based on the SLS system in 3.2, the function structure is constructed (See Figure 3.3). The process can be separated into three modules: controller, energy supply system, and material delivery system. While Figure 3.2 depicts the interior structure of a SLS machine, the diagram lacks information on the preheating system of a SLS machine. Likewise, the function structure in Figure 3.3 ignores details for the preheating system.

The first module in the function structure is the controller. The controller regulates set-up parameters, such as laser power, laser scanning speed, and part-bed temperature. Additionally, the laser path is processed by the controller based

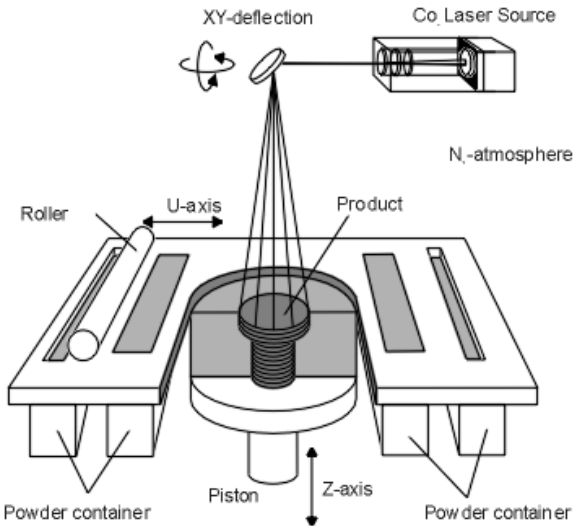

Figure 3.2: Process of Selective Laser Sintering [67]

on the input STL file. Then, the controller actuates and controls the energy supply system (in this case, the laser system) and material delivery system.

The second module is the energy supply system, which is the laser system for the SLS process. The laser system contributes to the sintering process to combine metal powder particles. After actuation and receiving process parameters from the controller, the laser beam passes through lenses. The lenses decrease the radius of laser spot to increase the laser power intensity. The laser is guided by the XY mirror to a specific location of the powder bed. The optical energy from the laser is converted to thermal energy conducted into the interior of the powder particles to start the sintering process. There is also a loss of laser power intensity due to the reflectivity of the powder.

The precursor material of the SLS process is powder. The third module, the

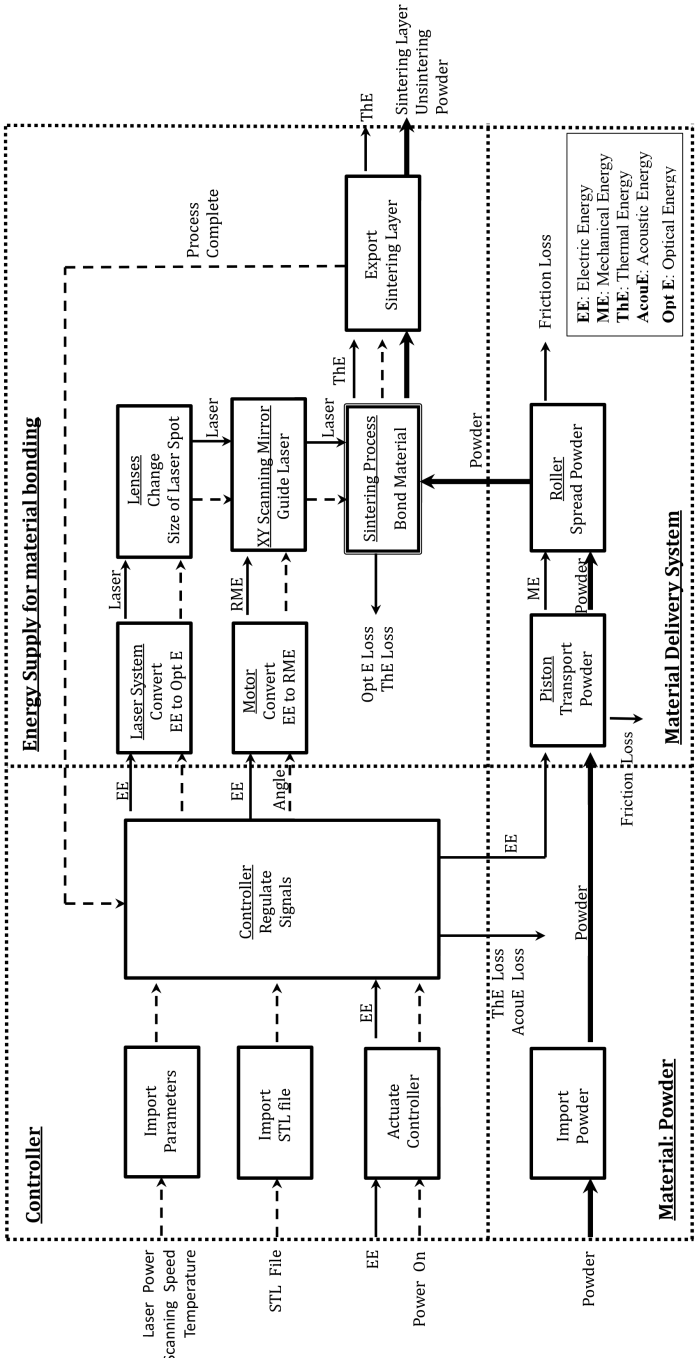

Figure 3.3: Function Structure of Selective Laser Sintering

material delivery system, stores and transports material to the build chamber. In the SLS process, the material delivery system includes a piston and a heated roller. Once a single layer of the sintering process completes, the unsintered powder stays in the building chamber until the end of the complete SLS build.

3.3.2 Function Structure of Laminated Object Manufacturing

The basic components in Laminated Object Manufacturing include a controller, cutting system (a laser or cutter), supply roller, heated roller, and a moving platform. The precursor material for the LOM process is in sheet form. A schematic of the process is illustrated in Figure 3.4. When the controller imports the basic set-up information, the material supply roller starts to deliver the material sheet. The heated roller provides pressure and heat to bond the material sheet with the previous sheet layer. Then the laser cuts the contour of the geometry. After the laser cutting process, the build platform moves downward, and a new layer of material sheet is delivered and covers the previous layer. The process is repeated until the part is complete.

The function structure of the LOM process is shown in Figure 3.5. There are four primary modules in the LOM machine: controller, energy supply system for both bonding and cutting processes, and material delivery system.

The controller actuates and controls the material delivery system, the welding (bonding) system, and the laser cutting system. The controller system reads the bonding parameters (for example, input voltage and welding speed for ultrasonic consolidation) and laser cutting parameters (laser power and laser cutting

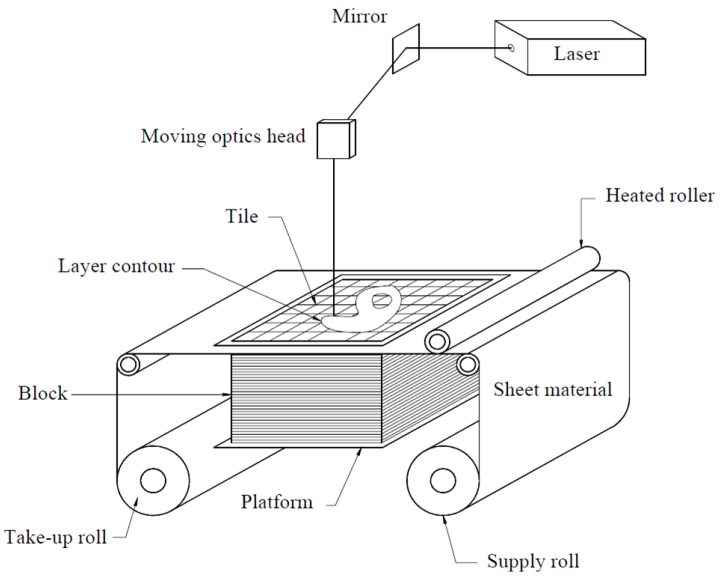

Figure 3.4: Process of Laminated Object Manufacturing[68]

speed). The controller also reads the STL file that is converted to the laser cutting path. The bonding speed signal is transferred to the supply roller to start the delivery and bonding process.

The welding (bonding) system uses pressure and high temperature to bond the material sheet which is delivered by the supply roller. The bonded block is then cut by the laser. The mechanism of the laser system is similar to the SLS laser system. The laser passes through the lenses and is reflected by the XY scanning mirror to cut the bonding block.

The precursor material pattern of LOM is in sheet form. The material supply roller delivers the material sheet to a platform. The material sheet is bonded or welded by a heated roller and then cut by a laser. The waste take up roll recycles

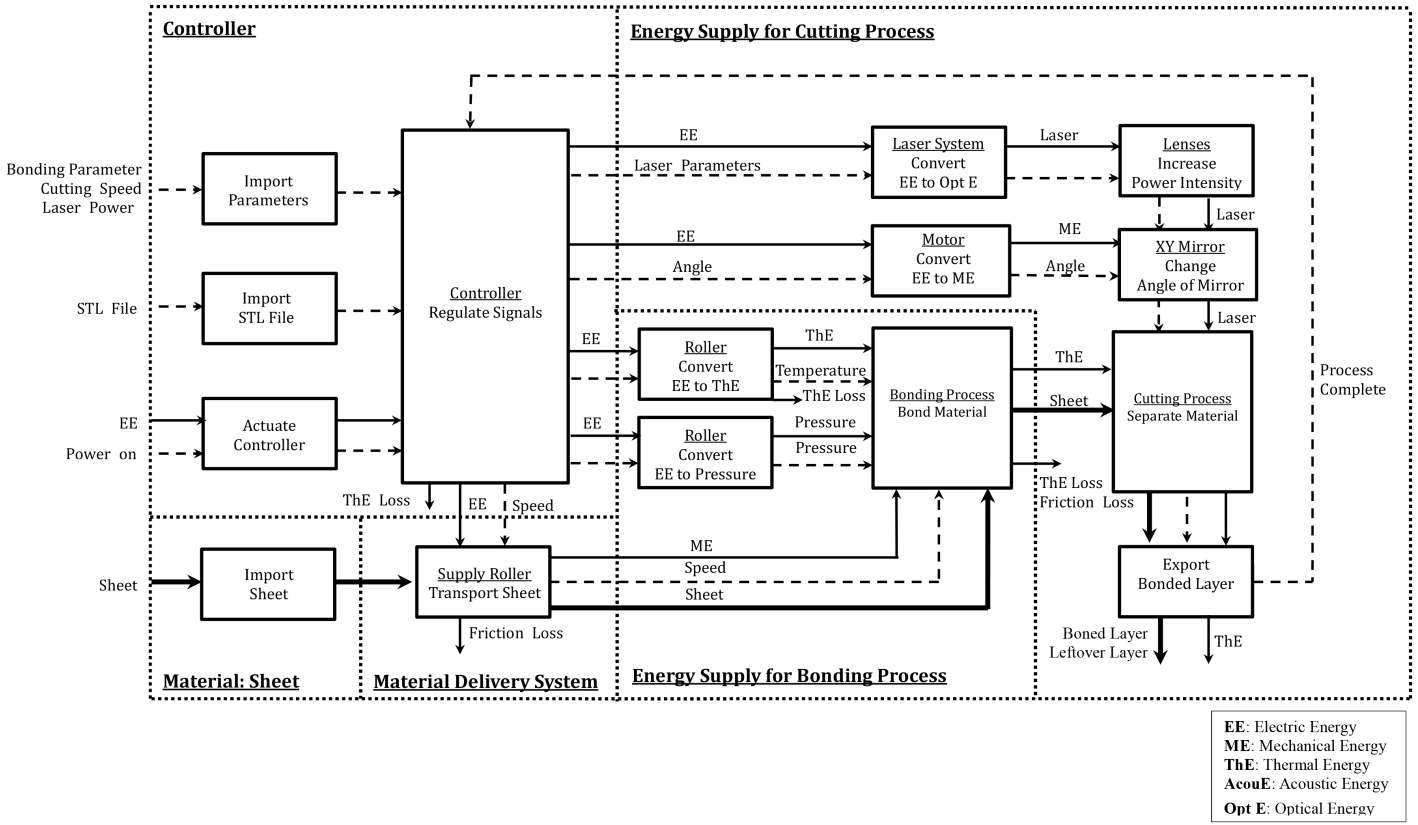

Figure 3.5: Function Structure of Laminated Object Manufacturing

the leftover material. The process continues until the part is complete.

3.3.3 Function Structure of Fused Deposition Modeling

Fused Deposition Modeling (FDM) is a representative process that uses a filament as the precursor material. Figure 3.6 shows the process of FDM. The FDM system contains a roller, electric-resistance heater, extrusion nozzle, and a build platform. In Figure 3.6, the roller delivers the material filament to an electric-resistance heater. The material filament is heated by the electric-resistance heater close to its melting temperature. The softened filament is then extruded through a nozzle to a platform to create the three dimensional component.

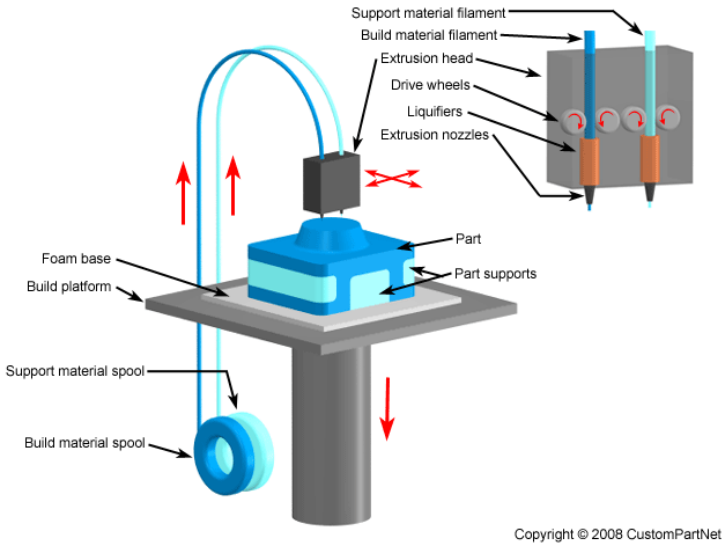

Figure 3.6: Process of Fused Deposition Modeling[69]

The function structure for the FDM process is illustrated in Figure 3.7. The modules for the process include the controller, the energy supply for the bonding

process, and the material delivery system.

The controller reads user set-up parameters, such as temperature of the heater and extrusion speed. These parameters are delivered to an energy supply system and material delivery system.

The energy supply system of FDM is an electric resistance heater. The temperature of the heater is determined by user input. The temperature is close to the softening point of the material filament. After the heating process, the softened filament is extruded through a nozzle to a specific position on the platform.

The precursor material for the FDM process is in filament form. The material delivery system is a wire feed system. The controller drives motors connected to rollers. The friction between the rollers and the material filament moves the filament translationally. Furthermore, the rollers also help to straighten the material filament in the process.

3.3.4 Identify Functional Requirements

In the previous sections, function structures for Selective Laser Sintering, Laminated Object Manufacturing, and Fused Deposition Modeling were presented. Table 3.2 compares these three processes.

Considering the function structures of SLS, LOM, and FDM, they share three common modules: controller, energy supply system for bonding process, and material delivery system.

- *Controller:* The controller receives the process parameters for the energy

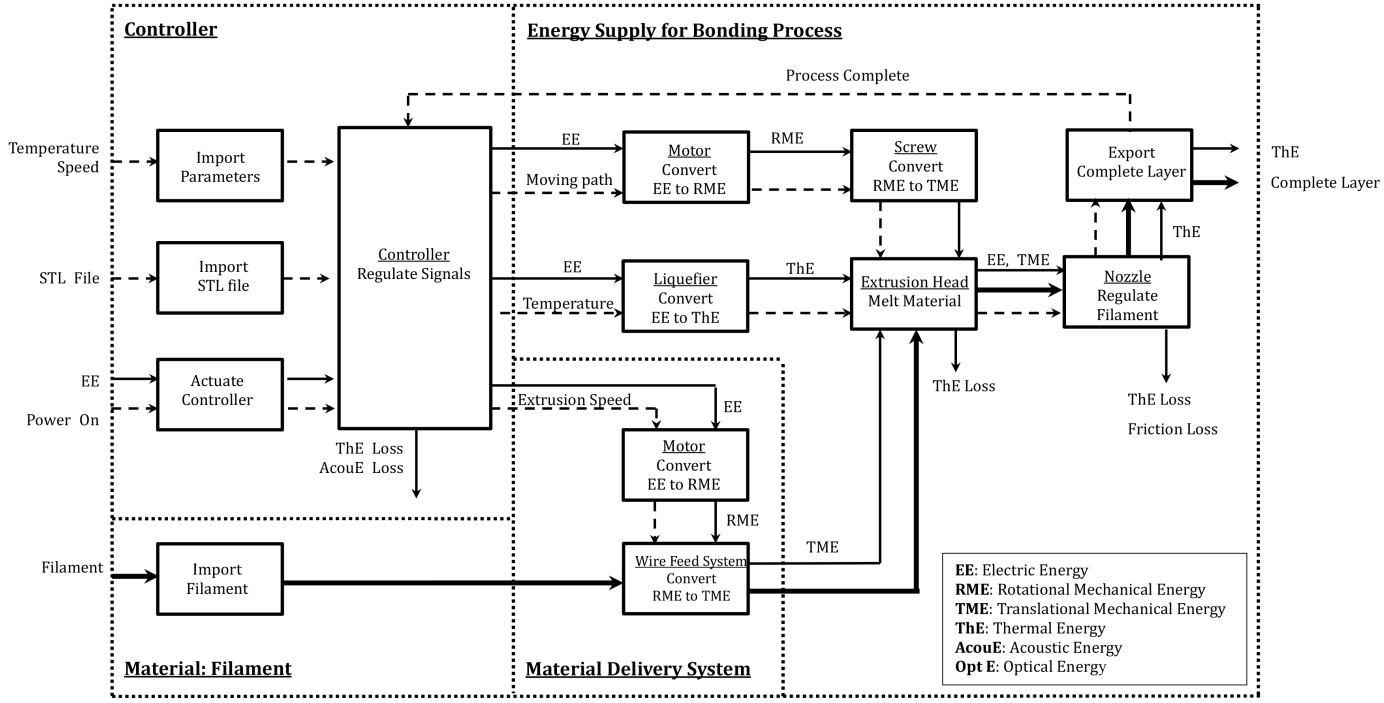

Figure 3.7: Function Structure of Fused Deposition Modeling

supply system, delivery speed for the material delivery system, and uses a STL file to determine the movement of the machine.

- *Energy Supply System for material bonding and geometry creation:* These three processes each have an energy supply to stack material and create the geometry of printed parts. The comparison of these processes also interprets that thermal energy system is the most common energy supply system for AM.

- *Material Delivery System:* The design of the material delivery system is mainly determined by the format of the material of the AM process. The roller set is a common design for the material delivery system. The use of the roller provides a way to effectively convert rotational motion from motors to translational motion in order to move the material.

	SLS	**LOM**	**FDM**
Material	Powder	Sheet	Filament
Have controller?	Yes	Yew	Yes
Energy supply	Laser scanning	Welding	Electric heating
Material delivery	Piston and roller	Roller	Wire feed roller
Cutting process	-	Laser cutting	-
Supports	Unsintered powder	leftover sheet	Extrusion supports

Table 3.2: Function modules comparison for SLS, LOM, and FDM

Besides these three modules, there is one important characteristic that cannot be identified from these three function structures because only single-layer building processes are depicted. However, if there is more than one layer, *support*

is required to stabilize printed components, especially overhangs. For example, FDM deposits extra material as supports to stabilize the printed parts while unused material supports the printed structures for SLS and LOM.

The four primary modules (controller, energy supply system, material delivery system, and supports) represent different functions. The controller is mainly responsible for *signal regulation*. The energy supply system provides energy to *melt* and *bond* precursor material. The material delivery system *transports* precursor material. Support *stabilizes* the printed part.

However, functions "melt material" may contain more than one sub-function. For example, the melting processes in both FDM and SLS not only bond material but also change the shape of precursor material. Additionally, softened filament can be separated easily by moving the extrusion head. It is necessary to identify the exact meaning for "melting material". Original complicated function structures are simplified and depicted below. Only the energy supply system, the material delivery system, and the build platform are considered in these simplified function structures.

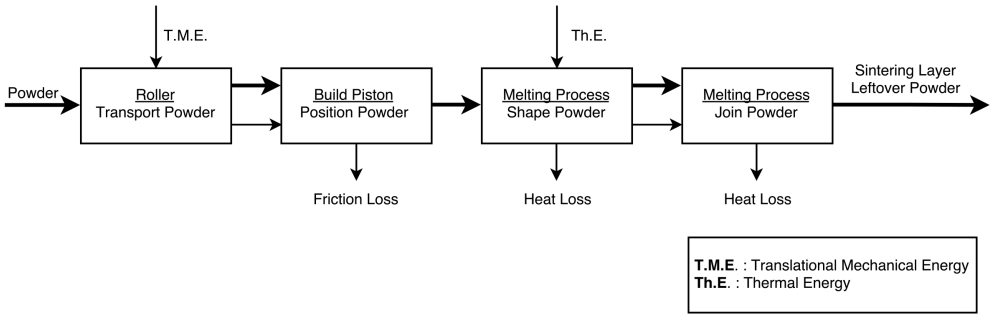

Figure 3.8: Simplified function structure of selective laser sintering

Figure 3.8 illustrates a simplified function structure of the SLS process. The detailed concepts of the build piston and melting process is considered. The build piston locates the printed component to an accurate Z position. In the melting process, thermal energy is conducted to powder particles and joins them. Additionally, the melting process also determines the shape of the final printing components. Therefore, it is reasonable to take “shape material” into consideration.

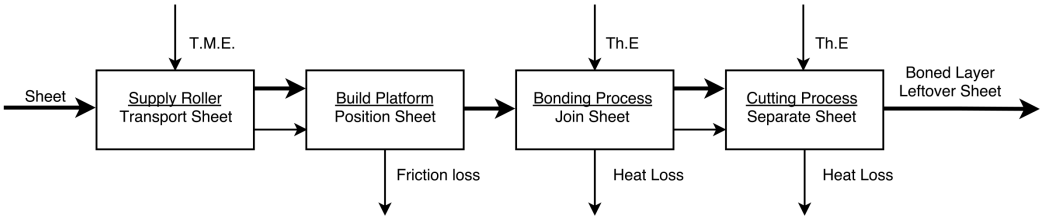

Figure 3.9: Simplified function structure of laminated object manufacturing

The simplified function structure of the LOM process is depicted in Figure 3.9. The supply roller transports material to the build platform. The energy supply system, such as welding system, provides thermal energy to bond sheets. The laser is applied to separate material to create the desired contour.

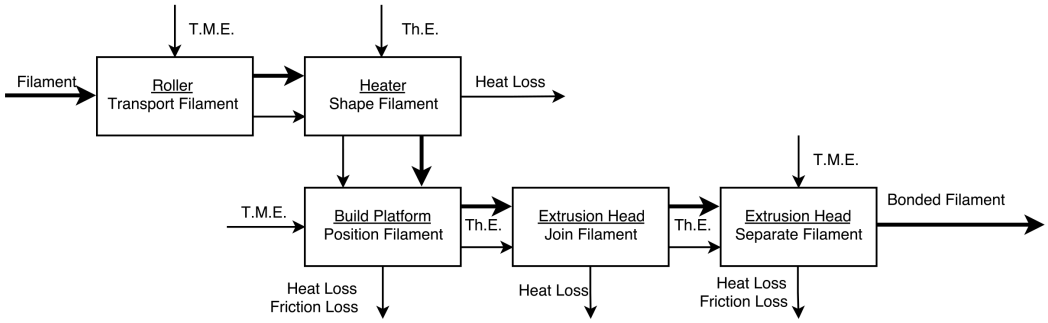

Figure 3.10: Simplified function structure of fused deposition modeling

The similar idea is applied to the FDM system. The simplified function structure of FDM is shown in Figure 3.10. The filament is transported to the extrusion head by rollers. The melting process softens the filament and determines the geometry of the final printing part by controlling the movement of the extrusion head. The softened filament is extruded through the nozzle to the platform and bonded with previous layers. Finally, when the single layer is complete, the extrusion head can move up and separate the filament.

Overall, the function, melting filament/wire, actually includes three subfunctions: *shape material*, *join material*, and *separate filament*. Additionally, the movement of the extrusion head and the build platform determines the position of material. These functions are included in the morphological matrix.

3.3.5 Summary of Functional Requirements

The SLS, LOM, and FDM processes utilize different precursor material: powder for SLS, sheet for LOM, and filament for FDM. Although details of the

additive manufacturing processes are different, they have common functional requirements:

1. The AM process should be automatic. In other words, the AM system should have a controller.
2. The AM process should include an energy supply system for the bonding process.
3. The AM process should include a material delivery system to deliver and store material. The design of the material delivery system is based on material form (powder, wire, or sheet).
4. Support helps to stabilize materials.
5. The movement of platform locates material.

Besides these common characteristics, the filament-based system needs to include two additional functions, *shape material* and *separate material*. Therefore, six functional requirements (transport material, position material, shape material, couple material, stabilize material, and separate material) are proposed to develop the morphological matrix for the conceptual design. The controller is not concluded because it is not different between different AM processes.

3.4 Further Constraints and Requirements

Besides the functional requirements for the AM processes, there are additional constraints and requirements for the design of the desktop-scale metal

wire-feed prototyping machine. This section enumerates the details of related performance metrics, which are summarized in Table 3.3.

Performance Metrics for Desktop Rapid Prototyping Machine			
D/W	**Metric**	**Value**	**Units**
Geometry			
W	Width of the Machine	50-80	cm
W	Length of the Machine	80-120	cm
D	Diameter of Material Wire	0.64	mm
W	Weight of the Machine	≤ 13	kg
Material			
D	Material	Copper or Bronze	-
Operation			
D	Energy Supply	≤1800	W
D	Processing Speed for Wire Extrusion	≥30	mm/s
Cost			
D	Cost	≤6000	US Dollars
Production			
W	Accuracy of the Machine	≤11	μm
W	Feature Size	~0.64mm	mm

Table 3.3: Performance Metrics for Desktop Rapid Prototyping Machine

- **Energy Supply**

  The energy supply is the primary limitation for developing a desktop machine. The limitation comes from the domestic household power supply. The typical household voltage in the United State is 120 V, and the common

circuit breaker is $15\,\mathrm{A}$ or $20\,\mathrm{A}$. Therefore the suggested energy requirement should be less than $1800\,\mathrm{W}$.

- **Cost**

  The desktop machine should be affordable for the public. Therefore, the price range for commercially available desktop 3D printers was benchmarked. The price range for desktop 3D printer is from $\$300$ to $\$6000$ US [56]. Therefore, the suggested cost for the desktop-scale metal wire-feed prototyping machine should be within this price range.

- **Material**

  Although the final design goal is not limited to copper or bronze, copper and bronze are selected due to their low cost and availability. The average prices and retailers for 22 guage copper and bronze wire are listed in Appendix **??**.

- **Diameter of Metal Wire**

  There are six diameter ranges for metal wire in handcraft industries, as shown in Table 3.1. 22 guage, approximately 0.64 mm, is selected because this diameter is the most common one used for handcrafts.

- **Weight**

  One of the characteristics of the desktop machine is portability. According to [70], the maximum weight that can be manual lifted causing back-pain is approximately $13\,\mathrm{kg}$, which is shown as Figure 3.11. Therefore, it is appropriate to assume that the weight of the desktop prototyping machine should be within $13\,\mathrm{kg}$.

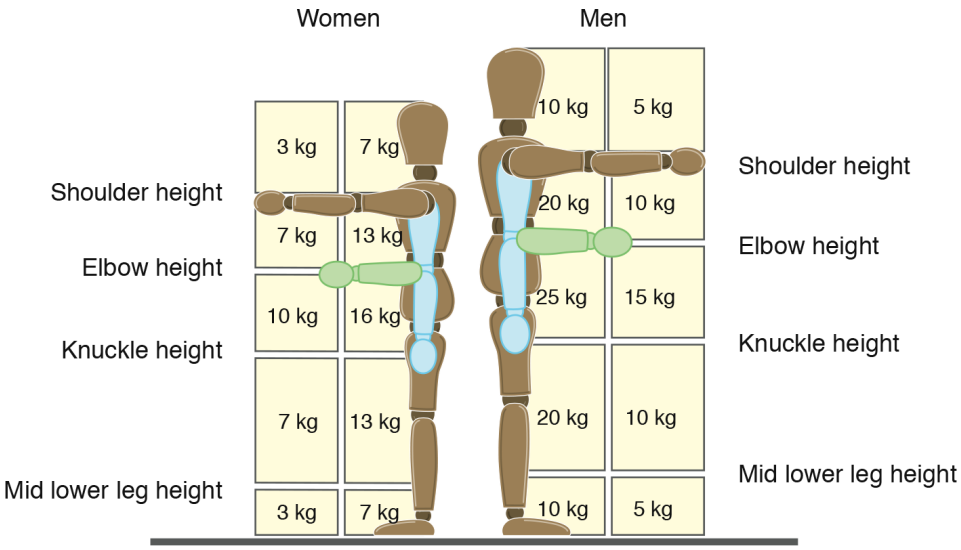

Figure 3.11: Manual lifting for different gender and position[70]

- **Feature size**

  The diameter of the metal wire limits the resolution of a single layer. Therefore, the expected feature size should be as close to $0.64\,\mathrm{mm}$ as possible.

- **Precision of the Machine**

  The machine movement accuracy is much more precise compared to feature size. Considering the precision of the MakerBot is $11\,\mu\mathrm{m}$ for XY position and $2.5\,\mu\mathrm{m}$ for Z position [71], the machine precision of the desktop machine is approximately $11\,\mu\mathrm{m}$.

- **Dimensions of the Machine**

  One of the design goals of the machine is that it is available for household or office usage. Therefore, the size limitations of the machine should be suitable for standard sizes of desks or tables. The typical width of a desk is

approximately $20\,\text{in}$-$30\,\text{in}$, and the typical length of desk is approximately $30\,\text{in}$-$60\,\text{in}$ [72]. In other words, the width of the machine is expected to be within $50\,\text{cm}$-$80\,\text{cm}$, and the length of the machine is expected to be within $80\,\text{cm}$-$120\,\text{cm}$.

- **Build Time and Speed**

  The build time of AM processes is affected by many variables, such as resolution, geometry, and mechanical properties [73]. It is difficult to establish the absolute target speed. However, the relative speed range can be obtained by comparing the building time based on different building methods. In order to have a more specific speed range, geometry and material properties are taken into consideration.

  1. **Geometry**

     The build times for a six layer spiral structure (wire diameter is $0.64\,\text{mm}$ without any gap) by using a wire spiral making tool (see Figure 3.12) and MakerBot Replicator are shown in Table 3.4. This table illustrates that using a specific device to create specific geometry (such as spiral) can result in a larger build speed. However, if much larger and complicated components are built, the spiral making tool becomes very limited and time-consuming. For general geometry, the default print speed for the MakerBot Replicator is $80\,\text{mm/s}$ [71], which is much faster than the hand-making speed.

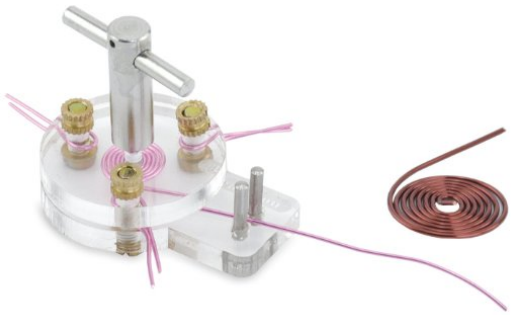

Figure 3.12: Wire spiral making tool[74]

Method	**Build Time**	**Build Speed**
Wire spiral making tool	$26\,\mathrm{s}$	$2.78\,\mathrm{mm/s}$
MakerBot Replicator	$60\,\mathrm{s}$	$1.206\,\mathrm{mm/s}$

Table 3.4: Build time comparison with different methods

2. **Material Properties**

   Material properties are also important consideration. Although MakerBot Replicator can have a print speed as high as $80\,\mathrm{mm/s}$, the machine can only deal with thermoplastic materials, which typically have a printing temperature around $200\,^{\circ}\mathrm{C}$. If an AM machine deals with metal wire, additional time is required due to the high melting temperature of metal. Therefore, the actual printing speed with metal wire is much slower than $80\,\mathrm{mm/s}$. $30\,\mathrm{mm/s}$ is proposed as the minimum build speed to have extra heating time.

Besides these performance metrics, there are four requirements which are difficult to quantify. These four requirements are as follows:

- The machine can create complex geometry.
- The material should be available to the general public.
- The machine does not require a special operating environment.
- The manufacturing process should avoid potential safety issues, such as the generation of toxic gases.

3.5 Chapter Summary

This chapter defines the problem and identifies constraints and requirements for the desktop metal wire-feed prototyping machine. The specification sheet (Table 3.3) provides important design constraints and performance metrics, especially energy supply, cost and processing speed.

Christopher Williams et al. [75] decompose the sub-functions of additive manufacturing into six modules, which are *store material*, *pattern material*, *pattern energy*, *create primitive*, *provide new material*, and *support previously material*. Table 3.5 shows the comparison of sub-functions of additive manufacturing between [75] and this work.

From [75]	**This Work**
Store Material	Transport Material
Pattern Material	Position Material
Pattern Energy	Shape Material
Create Primitive	Couple Material
Provide New Material	Separate Material
Support Previously Deposited Material	Stabilize Material

Table 3.5: Comparison of sub-functions of additive manufacturing

In this work, three function structures of common AM processes, Selective Laser Sintering, Laminated Object Manufacturing, and Fused Deposition Modeling, are created to clarify functional requirements for the design. There are four common modules in general AM processes: controller, energy supply for bonding material, material delivery system, and support based on function structures. Six functional requirements (*transport material*,*position material*, *shape material*, *couple material*, *stabilize material*, and *separate material*) from these four modules are used to develop conceptual designs in the next chapter.

Chapter 4

Conceptual Design

Conceptual design is an important phase of the design process. In this design step, several concept variants are generated by brainstorming methods and evaluated for feasibility. Then, feasible concepts are compared with each other based on specific criteria to select the final concept for prototyping.

Chapter 4 presents concept generation for the desktop-scale metal wire-feed prototyping machine. Section 4.1 describes concept variants generated by morphological analysis. Section 4.2 focuses on exploring the feasibility of each concept variant and selecting the final concept for embodiment design.

4.1 Concept Variants Development

A morphological matrix is a concept generation method which systematically explores possible solutions based on functional requirements. In Chapter 3, four common elements in the AM system have been identified, which are the controller, the material delivery system, the energy supply system, and supports. These modules are converted into functional requirements in order to set up the morphological matrix besides the controller, which mainly processes the signals.

- *Material Delivery System:* A material delivery system transports material from the material store to the build platform. Therefore, two functions, "Transport Material" and "Position Material", are included in this system.

- *Energy Supply System:* The energy supply system includes geometry creation and material additive. When the material is transported to the build platform by the material delivery system, there is a geometry creation method to determine the geometry of material. Therefore, the function, "Shape Material", is primarily completed by the geometry creation method. A material additive method provides energy (in most cases, thermal energy) to join material layers together. Therefore, the function of material additive method is "Couple Material".

- *Supports:* Supports are used to stabilize the material during the build process. Therefore, the support can be viewed as "Stabilize Material".

Additionally, considering the filament-based AM processes, when the extrusion head stops extruding the filament, it "separates" the filament. Therefore, it is reasonable to include the "Separate Material" function in the morphological matrix.

Overall, *Transport Material*, *Position Material*, *Shape Material*, *Couple Material*, *Separate Material* and *Stabilize Material* are the functions used to develop the morphological matrix.

Table 4.1 presents the results of morphological analysis. Five concept variants are developed based on this morphological matrix. These five concepts in-

clude bending configuration, winding configuration, laser configuration, welding configuration, and brazing configuration.

Transport Material	Roller	Belt	Segment screw	Push mechanism			
Position Material	Manipulator	Extrusion nozzle	Moving platform	Fixture	Gravity	Magnetostatics	Electrostatics
Shape Material	Laser	Welding	Bending	Winding	Cutting	Chemical reaction	
Couple Material	Welding	Brazing	Soldering	Laser melting	Melting in the oven	Adhesive	Chemical reaction
Stabilize Material	No support	Removable support	Truss structure	Material itself	Fluid		
Separate Material	Cutting	Melting	Shearing	Blanking	Chemical milling		

Table 4.1: Morphological matrix for the design

4.1.1 Bending Configuration

The first concept variant is the bending configuration. Elements in the first configuration include a roller group, a wire bender, a solder gun, a cutter, and a moving platform. Metal wire is delivered by a group of rollers. Next, the wire bender bends the wire to the desired geometry. After that, the solder gun joins the wire together. If wire stops delivery, the cutter cuts the wire. The bending configuration is shown in Figure 4.1, and the morphological matrix for the bending configuration is illustrated in Table 4.2.

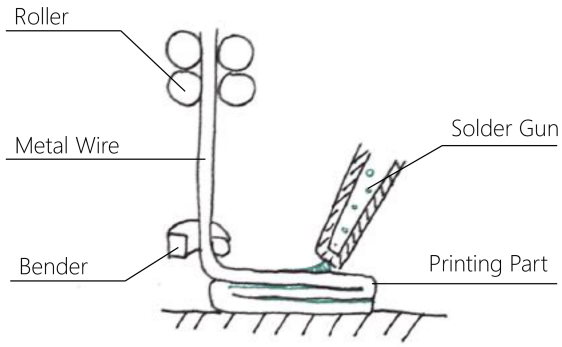

Figure 4.1: Schematic of the bending configuration

Transport Material	Roller	Belt	Segment screw	Push mechanism			
Position Material	Manipulator	Extrusion nozzle	Moving platform	Fixture	Gravity	Magnetostatics	Electrostatics
Shape Material	Laser	Welding	Bending	Winding	Cutting	Chemical reaction	
Couple Material	Welding	Brazing	Soldering	Laser melting	Melting in the oven	Adhesive	Chemical reaction
Stabilize Material	No support	Removable support	Truss structure	Material itself	Fluid		
Separate Material	Cutting	Melting	Shearing	Blanking	Chemical milling		

Table 4.2: Morphological matrix for the bending configuration

4.1.2 Winding Configuration

The winding configuration comes from the traditional winding process, which is shown in Figure 4.2. In the traditional winding process, the filament is wound by a rotating mandrel to create a composite part. Therefore, the winding configuration can be used to create axisymmetric components, such as vases.

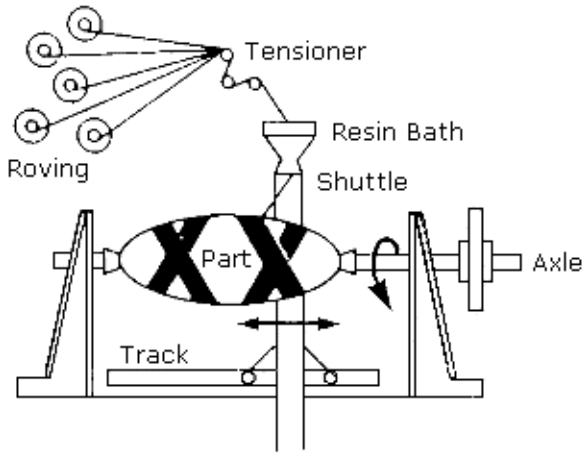

Figure 4.2: Traditional winding process [76]

Details of the winding configuration are illustrated in Figure 4.3. Metal filler wire is wound by the rotating mandrel to build the expected winding component. Later, the rotating mandrel is removed, and the winding part is heated in the kiln to melt the filler wire to strengthen the component. The morphological matrix of the winding configuration is illustrated in Table 4.3.

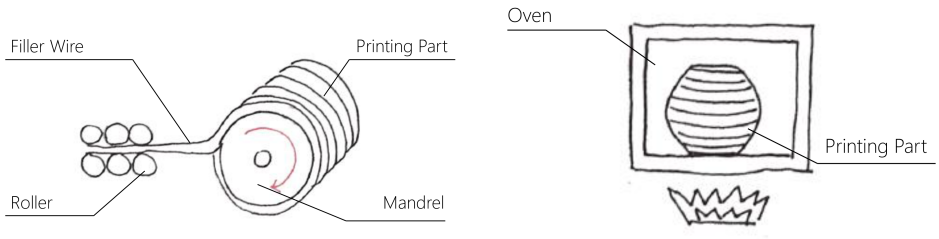

(a) Rotating mandrel winds filament to create a component

(b) Once the winding process completes, the part is heated in an oven

Figure 4.3: Schematic of the winding configuration

Transport Material	Roller	Belt	Segment screw	Push mechanism			
Position Material	Manipulator	Extrusion nozzle	Moving platform	Fixture	Gravity	Magnetostatics	Electrostatics
Shape Material	Laser	Welding	Bending	Winding	Cutting	Chemical reaction	
Couple Material	Welding	Brazing	Soldering	Laser melting	Melting in the oven	Adhesive	Chemical reaction
Stabilize Material	No support	Removable support	Truss structure	Material itself	Fluid		
Separate Material	Cutting	Melting	Shearing	Blanking	Chemical milling		

Table 4.3: Morphological matrix of the winding configuration

Similar to the idea Dave et al. [77] describe electron beam solid freeform fabrication with a rotating mandrel. The primary difference is that the research uses the electron beam to join layers together.

4.1.3 Laser Configuration

The laser configuration comes from electron beam freeform fabrication [78]. In the laser configuration, the electron beam is replaced by a diode or CO_2 laser to melt metal wire. A schematic of the laser configuration is illustrated in Figure 4.4. One of the primary issues for this concept variant is the needed power of the laser required to melt metal wire and the cost of the laser system. Therefore, the feasibility of using a low power laser in the system is explored in Section 4.2. The morphological matrix of the laser configuration is shown in Table 4.4.

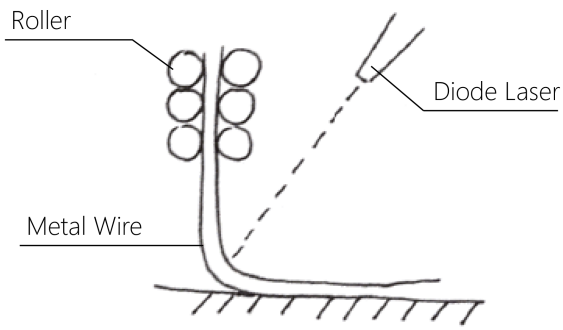

Figure 4.4: Schematic of the laser configuration

Transport Material	Roller	Belt	Segment screw	Push mechanism			
Position Material	Manipulator	Extrusion nozzle	Moving platform	Fixture	Gravity	Magnetostatics	Electrostatics
Shape Material	Laser	Welding	Bending	Winding	Cutting	Chemical reaction	
Couple Material	Welding	Brazing	Soldering	Laser melting	Melting in the oven	Adhesive	Chemical reaction
Stabilize Material	No support	Removable support	Truss structure	Material itself	Fluid		
Separate Material	Cutting	Melting	Shearing	Blanking	Chemical milling		

Table 4.4: Morphological matrix for the laser configuration

4.1.4 Welding Configuration

The welding concept variant includes two configurations: the spot welding configuration and the induction welding configuration. Other common welding methods can also be used to develop the welding concept variant, such as Gas

Metal Arc Welding (GMAW) and Tungsten Inert Gas (ITG Welding). Since these two welding approaches have been developed in the previous research [4,79], this research intends to explore other welding methods which may apply to AM processes.

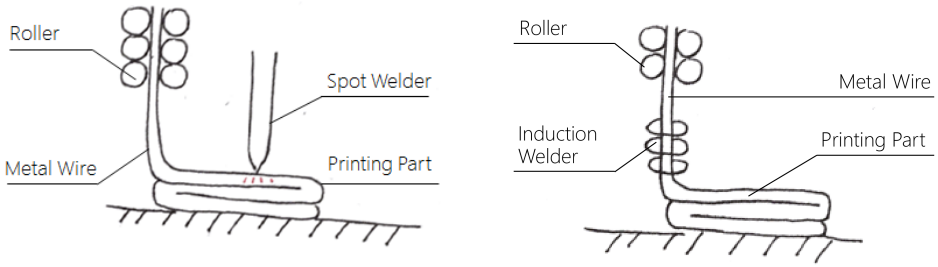

(a) Spot welding configuration (b) Induction welding configuration

Figure 4.5: Schematic of the welding configuration

Figure 4.5 shows the schematic of the spot welding configuration and the induction welding configuration. Spot welding uses electrodes to concentrate electric current into a single spot. The heat generated from the resistance melts the material at the spot and joins the material together. On the other hand, induction welding configuration utilizes electromagnetic induction to combine the material.

Details of the morphological matrix of these welding configurations are presented in Table 4.5.

Transport Material	Roller	Belt	Segment screw	Push mechanism			
Position Material	Manipulator	Extrusion nozzle	Moving platform	Fixture	Gravity	Magnetostatics	Electrostatics
Shape Material	Laser	Welding	Bending	Winding	Cutting	Chemical reaction	
Couple Material	Welding	Brazing	Soldering	Laser melting	Melting in the oven	Adhesive	Chemical reaction
Stabilize Material	No support	Removable support	Truss structure	Material itself	Fluid		
Separate Material	Cutting	Melting	Shearing	Blanking	Chemical milling		

Table 4.5: Morphological matrix for the welding configuration

4.1.5 Brazing Configuration

The brazing configuration is similar to [4]. Instead of using a welder to join material, a brazing gun or a torch is used in this concept variant. The schematic of the brazing configuration is shown in Figure 4.6. The precursor material is filler instead of pure metal wire. The filler filament is transported by rollers to the build platform and is melted by the brazing gun to create the geometry of the components. One of the primary issues in the process is maintaining the shape of metal filler droplet. Metal filler does not experience the glass transition process and converts to liquid directly once the temperature is higher than its melting temperature. Therefore, an additional cooling system is required to maintain the shape of metal filler droplets. The morphological matrix of the brazing configuration is illustrated in Table 4.6.

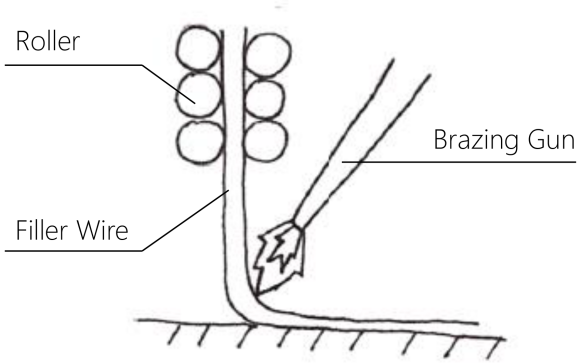

Figure 4.6: Schematic of the brazing configuration

Transport Material	Roller	Belt	Segment screw	Push mechanism			
Position Material	Manipulator	Extrusion nozzle	Moving platform	Fixture	Gravity	Magnetostatics	Electrostatics
Shape Material	Laser	Welding	Bending	Winding	Cutting	Chemical reaction	
Couple Material	Welding	Brazing	Soldering	Laser melting	Melting in the oven	Adhesive	Chemical reaction
Stabilize Material	No support	Removable support	Truss structure	Material itself	Fluid		
Separate Material	Cutting	Melting	Shearing	Blanking	Chemical milling		

Table 4.6: Morphological matrix for the brazing configuration

4.2 Concept Selection

Among these five concept variants, the most important functional requirement is whether the material can be completely joined with a reasonable power input. Laser, welding, and brazing configurations generate thermal energy to com-

bine material continuously, namely continuous joining processes. Therefore, the joining speed becomes a significant variable in these processes.

On the other hand, bending and winding configurations have two independent procedures to shape and join the material. These two processes do not create the geometry by heating methods, so the joining process can be discontinuous, namely discontinuous joining processes. Thus, the joining speed is not the primary consideration. Table 4.7 categorizes these five concept variants into continuous and discontinuous joining processes.

Continuous Joining	**Discontinuous Joining**
• Laser Configuration	• Bending Configuration
• Welding Configuration	• Winding Configuration
• Brazing Configuration	

Table 4.7: Category of concept variants

4.2.1 Continuous Joining Capability Investigation

The laser, welding, and brazing configurations melt the precursor material continuously, thus the joining speed is considered as the most important parameter for investigating feasibility. The joining speed should be higher than $30\,\mathrm{mm/s}$ as the discussion in Chapter 3.

In order to evaluate the relationship between joining capability, joining speed, and the input power for continuous joining concepts, a heat conduction model with a moving heat source is built. Equation 4.1 shows the heat conduction model with a moving heat source and assumes that the heat source is originally located at y=z=0 in the infinite medium. In Equation 4.1, T is transient temperature

(K), k is the conduction coefficient ($\mathrm{W\,m^{-1}\,K^{-1}}$), q is the rate of energy production by a specific heat source (W), υ is the constant velocity of heat source ($\mathrm{m\,s^{-1}}$), α is the diffusion coefficient ($\mathrm{m^2\,s^{-1}}$), and $\delta(x)$ is Dirac's delta function.

$$\bigtriangledown^2 T + \frac{1}{k} q\delta(x - \upsilon t)\delta(y - 0)\delta(z - 0) = \frac{1}{\alpha}\frac{\partial T}{\partial t} \tag{4.1}$$

Equation 4.1 is used as the governing equation to develop the model for the joining process. Considering that the model is under quasi-steady states conditions ($\frac{\partial T}{\partial x} = 0$) and $\varepsilon = x - \upsilon t$, Equation 4.1 can be written as

$$\frac{\partial^2 T}{\partial \varepsilon^2} + \frac{\partial^2 T}{\partial y^2} + \frac{\partial^2 T}{\partial z^2} + \frac{1}{k} q\delta(\varepsilon)\delta(y)\delta(z) = -\frac{\upsilon}{\alpha}\frac{\partial T}{\partial \varepsilon} \tag{4.2}$$

The purpose of this simulation is to investigate the heat conduction influence of the metal wire. Therefore, Equation 4.2 is simplified to an one-dimensional equation (Equation 4.3).

$$\frac{\partial^2 T}{\partial \varepsilon^2} + \frac{1}{k} q''\delta(\varepsilon) = -\frac{\upsilon}{\alpha}\frac{\partial T}{\partial \varepsilon} \tag{4.3}$$

For one-dimensional analysis, the heat source is assumed as a planar heat source and only moves in the x direction. Therefore, Equation 4.2 becomes

$$\theta' + \frac{\upsilon}{\alpha}\theta + \frac{1}{k} q''\delta(\varepsilon) = 0 \tag{4.4}$$

$$\theta(\varepsilon) = \frac{\partial T}{\partial \varepsilon} \tag{4.5}$$

If ε does not equal to zero, the solution of Equation 4.4 can be presented as

$$\theta = -\frac{q''}{k} e^{-\frac{\upsilon}{\alpha}\varepsilon} \tag{4.6}$$

Assuming that $\theta \rightarrow 0$ as $\varepsilon \rightarrow 0$, the solution for one-dimensional heat source is

$$T = \begin{cases} T_o + \frac{q''}{\upsilon \rho C_p} & , x < 0 \\ T_o + \frac{q''}{\upsilon \rho C_p} e^{-\frac{\upsilon}{\alpha}x} & , x > 0 \end{cases} \tag{4.7}$$

where T_o is the initial temperature of the medium.

However, Equation 4.7 only considers the influence of heat conduction. If convection is taken into consideration, the governing equation (Equation 4.4) becomes

$$\theta' + m\theta + \frac{1}{k} q'' \delta(x) = 0 \tag{4.8}$$

$$m = \frac{\upsilon}{\alpha} - \frac{hP}{Ak} \tag{4.9}$$

In Equation 4.9, P is the uniform lateral perimeter (m), h is the convective heat transfer coefficient ($\mathrm{W\,m^{-2}\,K^{-1}}$), and A is the uniform cross-sectional area of the medium.

Assume that $\frac{dT}{d\varepsilon} \rightarrow 0$ for $\varepsilon \rightarrow 0$, the solution for one-dimensional heat source is

$$T = T_o + \frac{q''}{k} e^{-mx}\,, x > 0 \tag{4.10}$$

It is necessary to compare the influence of convection in the heat transfer model with a moving heat source before developing the Excel program for laser and brazing process.

4.2.1.1 Convection Influence Evaluation

Aluminum is selected as the test material, and the thermal properties of aluminum are shown in Table 4.8. The reflectivity of aluminum is about 0.8 (See Table 4.9). It is assumed that the heat flux is provided by a $45\,\mathrm{W}$ laser heat source with $1\,\mathrm{mm}$ spot size. If the laser has a flat-top intensity, the laser intensity (q'') is approximately $11.46\,\mathrm{MW/m^2}$. The geometry of metal wire with a $0.64\,\mathrm{mm}$ diameter gives a perimeter (P) of $2.011\,\mathrm{mm}$ and area (A) as $0.322\,\mathrm{mm^2}$. The result is shown in Figure 4.7.

Material	k ($\frac{\mathrm{W}}{\mathrm{m\,K}}$)	C_p ($\frac{\mathrm{J}}{\mathrm{kg\,K}}$)	ρ($\frac{\mathrm{kg}}{\mathrm{m^3}}$)	α($\frac{\mathrm{m^2}}{\mathrm{s}}$)	T_m(K)
Aluminum	237	903	2702	97.1×10^{-6}	933
Copper	401	385	8933	117×10^{-6}	1358
Iron	80.2	447	7870	23.1×10^{-6}	1810

Table 4.8: Thermal properties of metals (Adapted from [80])

The heat transfer coefficient for free convection is typically around $5\,\mathrm{W/(m^2\,K)}$-$20\,\mathrm{W/(m^2\,K)}$ [80]. However, even h=$20\,\mathrm{W/(m^2\,K)}$, the difference between the two models (without convection and with convection model) is approximately $5.31\,\%$. Overall, it is reasonable to ignore the influence of heat convection in the following analysis.

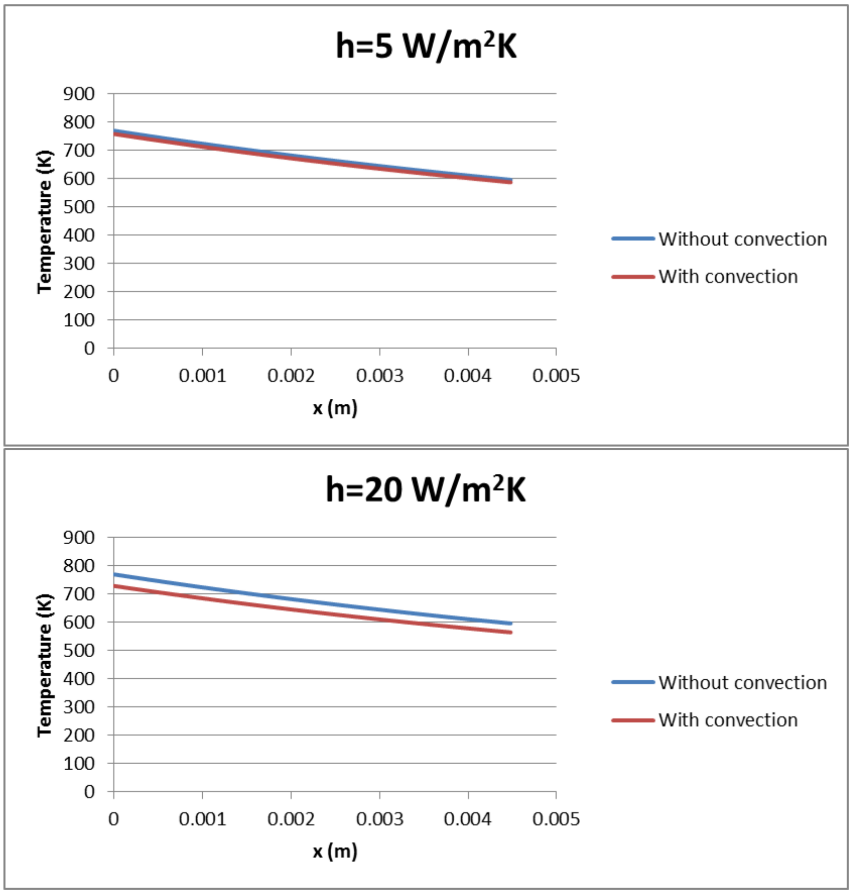

Figure 4.7: Conduction model and combination model with different heat transfer coefficients

4.2.1.2 Laser

The wavelength of the laser has a significant influence on the reflectivity of metal, which is shown in Table 4.9. The three laser ranges in Table 4.9 present three primary laser systems used by industry: $10.6\,\mu\mathrm{m}$ for a CO_2 laser, $1.06\,\mu\mathrm{m}$ for a Nd:YAG laser, and $300\,\mathrm{nm}$-$600\,\mathrm{nm}$ for a green laser. Reflectivity influences how much energy the material can absorb. For example, iron can absorb about $12\,\%$

of input laser energy under a CO_2 laser. When exposed to a Nd:YAG laser, iron can absorb $0.25\,\%$-$0.32\,\%$ of the energy. Based on Equation 2.1, high reflectivity metal (in other words, low absorptivity metal) reflects more input laser energy. Therefore, the actual laser energy that the metal receives is much less than the original input laser energy.

Material	300–600 nm	1.06 μm	10.6 μm
Aluminium, smooth		0.06–0.2	0.03–0.06
rough		0.2–0.4	0.1–0.4
Copper, polished	0.05	0.04	0.01–0.03
rough	0.05	0.1–0.3	0.05–0.10
oxidized	0.85	0.5	
Gold		0.02–0.04	0.01–0.02
Iron, polished	0.37–0.40	0.25–0.32	0.12
Molybdenum, polished	0.4–0.5	0.25–0.35	0.05–0.15
Nickel	0.5	0.15–0.35	0.05–0.15
Platinum		0.25–0.30	0.03–0.08
Silver		0.03	0.02–0.10
Tungsten	0.5	0.35	0.03–0.3
Carbon (graphite)	0.75	0.8–0.9	0.7–0.9
Alumina (Al_2O_3)		0.05–0.1	0.90–0.99
Magnesia (MgO)		0.2	0.93–0.98
Silica (SiO_2)	Transparent	Transparent	0.9
Zirconia (ZrO_2)		0.1–0.2	0.85–0.98
Silicon carbide (SiC)	0.8–0.9	0.85–0.95	0.8–0.9
Silicon nitride (Si_3N_4)	0.6–0.7	0.6–0.8	0.9

Table 4.9: Absorptivity of different materials under different laser wavelength [81]

Before creating the laser model, it is necessary to select the appropriate laser power based on cost constraints. Table 4.10 shows Full Spectrum H-series CO_2 laser cutters for wood and acrylic. The cost in Table 4.10 includes the basic cutter system without a water cooling system.

Full Spectrum H-series Laser			
Power	40 W	45 W	90 W
Focus lens	1.5	2.5	5.0
Beam diameter	5 mm		
Cost	$3499	$3749	$6249

Table 4.10: Specifications for Full Spectrum H-series laser [82]

Based on Table 4.10, the power of a desktop CO_2 laser system is assumed as $90\,\mathrm{W}$ with a $5\,\mathrm{mm}$ beam diameter.

Another variable to consider is the spot size of the laser. The focus lens provides a smaller spot size, which increases the laser power intensity. Therefore, the theoretical spot size can be calculated according to Equation 4.11 [83], where λ is the wavelength of the laser, f is the lens focal length, and r_o is the beam radius.

$$r_{\text{theoretical}} = \frac{f\lambda}{\pi r_o} \tag{4.11}$$

Based on Equation 4.11, the ideal spot size can be as small as $100\,\mu\mathrm{m}$ with a 1.5" focus lens. However, the spot size of a CO_2 laser actually is influenced by beam propagation factor, M^2, which is the ratio between ideal Gaussian beam and actual beam divergence. Therefore, Equation 4.11 becomes

$$r_{\text{actual}} = M^2 \frac{f\lambda}{\pi r_o} \tag{4.12}$$

In this study, M^2 is assumed as 2.2 [84]. Therefore, the spot size in the simulation is $220\,\mu\mathrm{m}$.

For the Nd:YAG laser, the laser parameters come from the iWeld Laser System (980/990 Series) [85]. The iWeld laser system is a desktop laser welder for

jewelry. The system utilizes a $35\,\mathrm{W}/60\,\mathrm{W}$ Nd:YAG laser to complete spot welding. The beam diameter of the iWeld laser system is $2\,\mathrm{mm}$.

For a wavelength around $300\,\mathrm{nm}$-$600\,\mathrm{nm}$, the green laser is selected as the representative. The typical wavelength of a green laser is approximately $523\,\mathrm{nm}$. However, a laser in this wavelength range typically has lower power. $10\,\mathrm{W}$ [86] is defined as the power of the green laser, and the spot size is around $1.5\,\mathrm{mm}$ [87].

The laser parameters in the heat transfer model are summarized in Table 4.11.

Laser Type	**Power(W)**	**Spot Size (mm)**
CO_2 Laser	90	0.22
Nd:YAG Laser	60	2
Green Laser	10	1.5

Table 4.11: Laser parameters in the heat transfer model

The selected material in the simulation is copper, which is one of the most common wire materials used in the benchmarks and artist application. Additionally, copper has high reflectivity and conductivity, which can indicate the limitations of the laser system. The thermal properties of copper are shown in Table 4.8. The ambient temperature is assumed as $300\,\mathrm{K}$.

The appropriate joining depth depends on the joint type. In order to create a strong joint, wire with a $0.64\,\mathrm{mm}$ diameter should be completely melted for the butt joint. For an overlap joint, the laser should have the capability to melt metal wire to a depth of $1.28\,\mathrm{mm}$. Figure 4.8 shows a butt joint and an overlap joint. Therefore, the appropriate joint depth should be between $0.64\,\mathrm{mm}$-$1.28\,\mathrm{mm}$.

(a) Butt joint (b) Overlap joint

Figure 4.8: Different joint types [88]

Figure 4.9 to Figure 4.12 show the relationship between temperature and depth from the laser source under the CO_2 laser, the Nd:YAG laser, and the green laser.

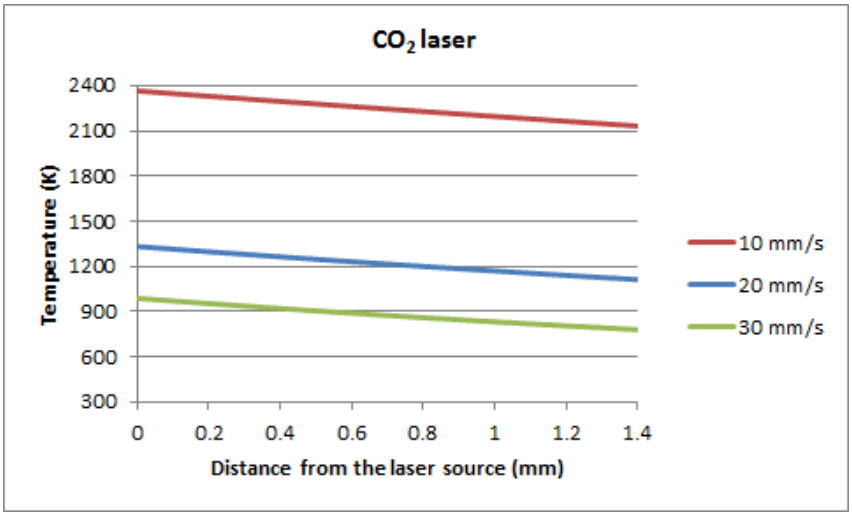

Figure 4.9: Copper under $90\,\mathrm{W}$ CO_2 laser with different laser scanning speed

Figure 4.9 shows the copper temperature change with different laser scanning speeds. This diagram ignores the influence of vaporization of copper. By using a $90\,\mathrm{W}$ CO_2 laser, it is possible to process copper wire within the scanning speed range of $10\,\mathrm{mm/s}$ to $20\,\mathrm{mm/s}$.

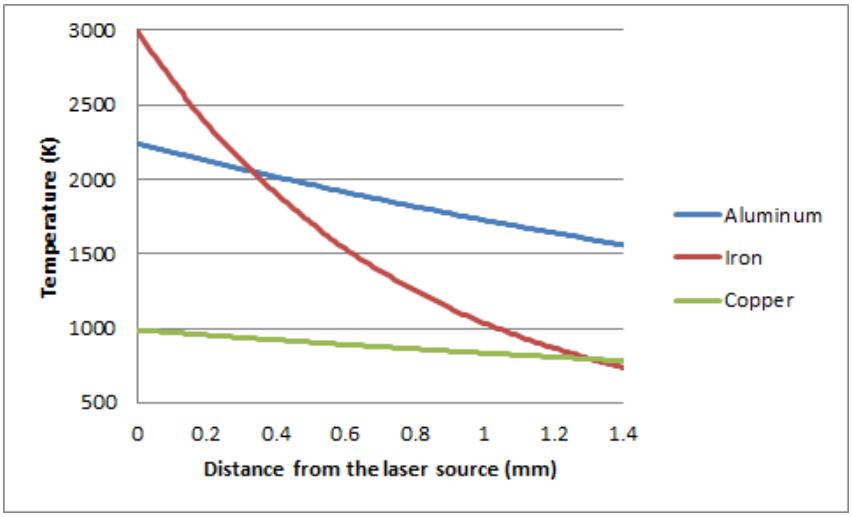

Figure 4.10: Aluminum, copper, and iron under $90\,\mathrm{W}$ CO_2 laser with $30\,\mathrm{mm/s}$

Figure 4.10 illustrates the temperature change aluminum, iron, and copper under $90\,\mathrm{W}$ CO_2 laser with $30\,\mathrm{mm/s}$. Both aluminum and iron are melted, and the figure illustrates the potential to process in higher scanning speed or lower laser power.

However, the cost of the desktop metal wire-feed prototyping machine should be less than $\$6000$. A $90\,\mathrm{W}$ laser system needs to have an additional cooling system, enclosure, and shield gas, which makes the cost of the system greater than $\$6000$. As a result, a CO_2 laser is infeasible in this case due to the cost constraint.

Figure 4.11 and Figure 4.12 show the relationship of temperature and depth under Nd:YAG and green laser when the laser scanning speed is $10\,\mathrm{mm/s}$. According to the results of these two models, a $60\,\mathrm{W}$ Nd:YAG laser with $2\,\mathrm{mm}$ spot size and a $10\,\mathrm{W}$ green laser with $1.5\,\mathrm{mm}$ spot size cannot process the selected metal

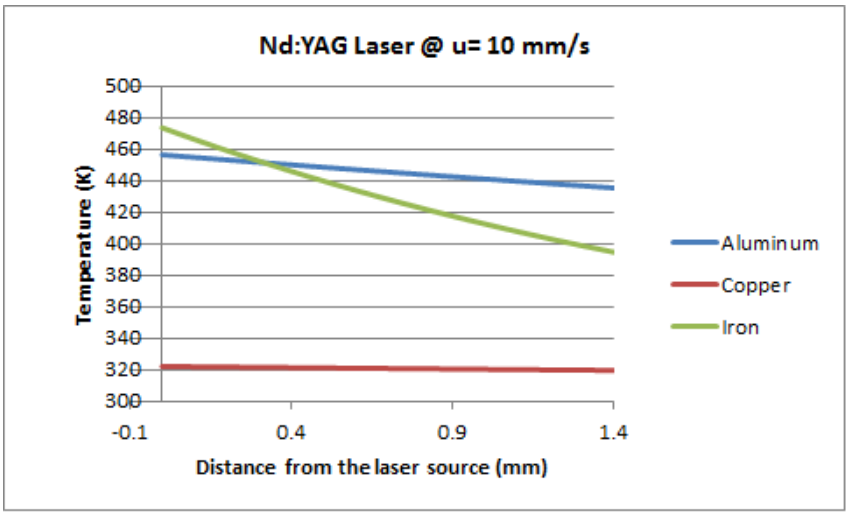

Figure 4.11: Aluminum, copper, and iron under 60 W Nd:YAG laser with 10 mm/s laser scanning speed

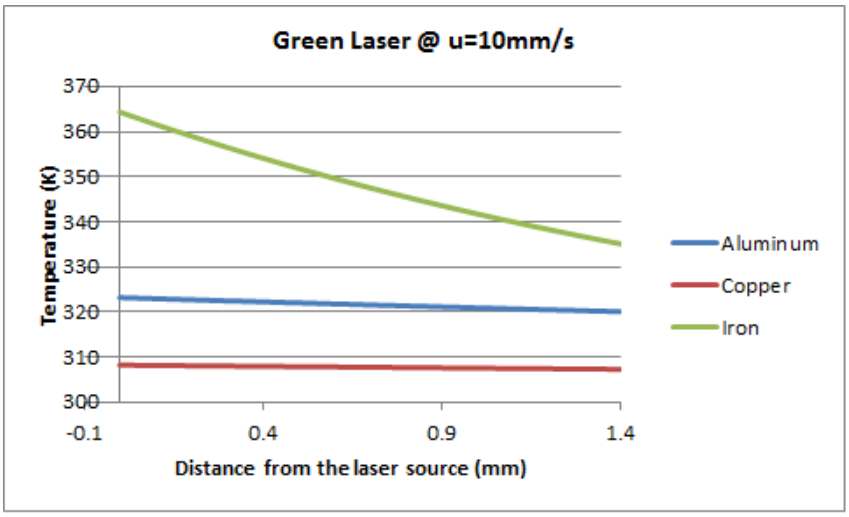

Figure 4.12: Aluminum, copper, and iron under 10 W green laser with 10 mm/s laser scanning speed

due to high reflectivity of material, even with the laser scanning speed as slow as 10 mm/s.

In summary, the continuous joining faster than $30\,\mathrm{mm/s}$ is infeasible for copper wire due to the high reflectivity and conductivity of copper wire. However, this analysis shows the potential to process aluminum and iron. The concept is eliminated mainly due to the cost constraint.

4.2.1.3 Laser with a Preheating System

Another possibility to increase the joining capacity of the laser system is to add a preheating system. The preheating system can heat metal to specific temperature to decrease the reflectivity of metal, which is shown in Figure 4.13.

However, oxidation of metal is a significant issue for preheating. Therefore, the preheating temperature should be lower than the temperature at which the metal experiences significant oxidation.

Copper is selected as the target material. Copper under different temperatures generates an oxidation layer with a different chemical composition (Figure 4.14). Significant oxidation occurs after region 4 in Figure 4.14. Therefore, the preheating temperature of copper is assumed blow $200\,^{\circ}\mathrm{C}$.

The thermal properties of copper are slightly changes when the temperature increases. Table 4.12 shows the thermal properties of copper under the room temperature and $400\,\mathrm{K}$. According to Figure 4.13, the reflectivity of copper decreases when the temperature increases.

Since the cost of a $90\,\mathrm{W}$ CO_2 laser exceeds the $\$6000$ constraint, the heat transfer model uses $60\,\mathrm{W}$ CO_2 laser with a $220\,\mu\mathrm{m}$ spot size.

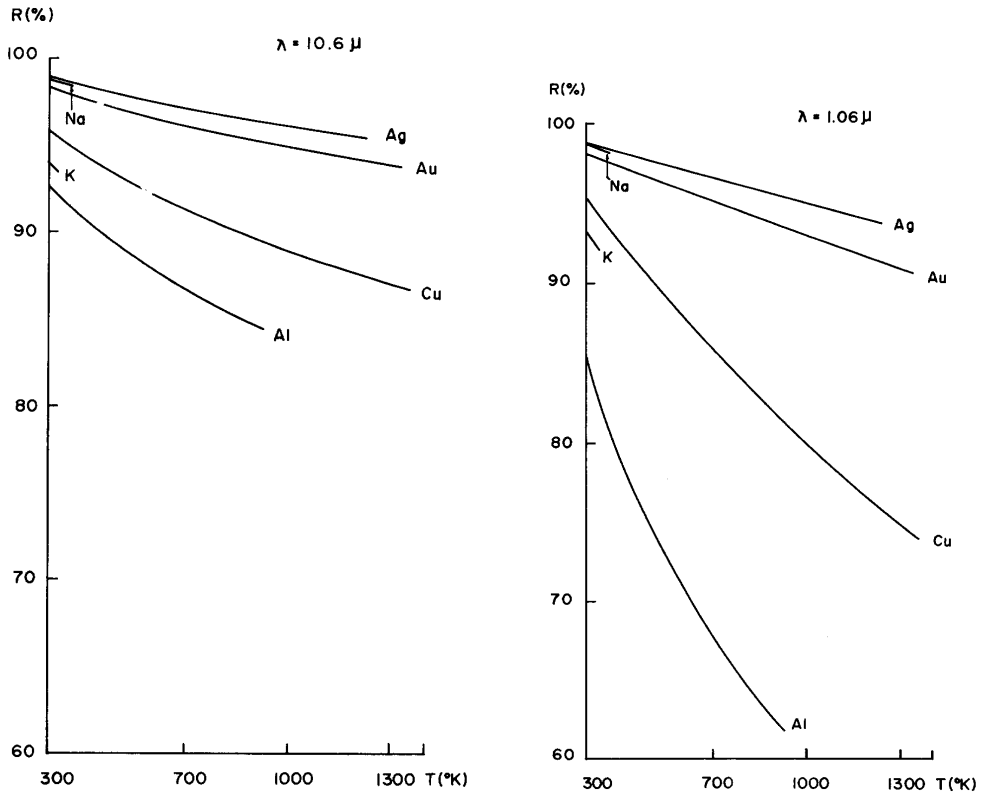

(a) CO_2 laser (b) Nd:YAG laser

Figure 4.13: Reflectivity of various metals changes due to temperature under CO_2 and Nd:YAG lasers [89]

Figure 4.15 and Figure 4.16 depict the $60\,\mathrm{W}$ CO_2 laser without and with a preheating system. The maximum scanning speed is $10\,\mathrm{mm/s}$-$30\,\mathrm{mm/s}$. Figure 4.15 presents the laser system without the preheating system, and Figure 4.16 shows the system with the preheating system. Comparing Figure 4.15 and Figure 4.16illustrates that the heating capability of a laser improves when there is an additional preheating system. However, the scanning speed still cannot be higher than $30\,\mathrm{mm/s}$. Therefore, direct melting with a laser on a desktop machine is infeasible

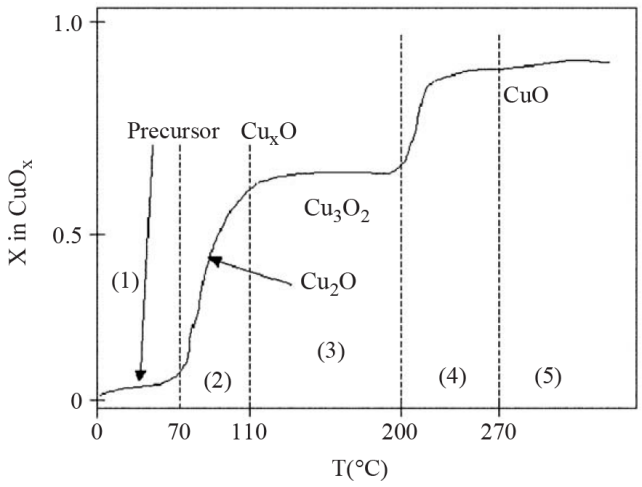

Figure 4.14: Copper oxidation formation under different temperature[90]

		Copper (Pure)	
Property	Unit	300 K	400 K
Heat Capacity	$\frac{J}{kg\,K}$	385	398.6
Thermal Conductivity	$\frac{W}{m\,K}$	401	393.7
Density	$\frac{kg}{m^3}$	8933	8933
Reflectivity	-	0.97	0.95

Table 4.12: Properties of copper under the room temperature and 400 K [80,89,91, 92]

even with a preheating system.

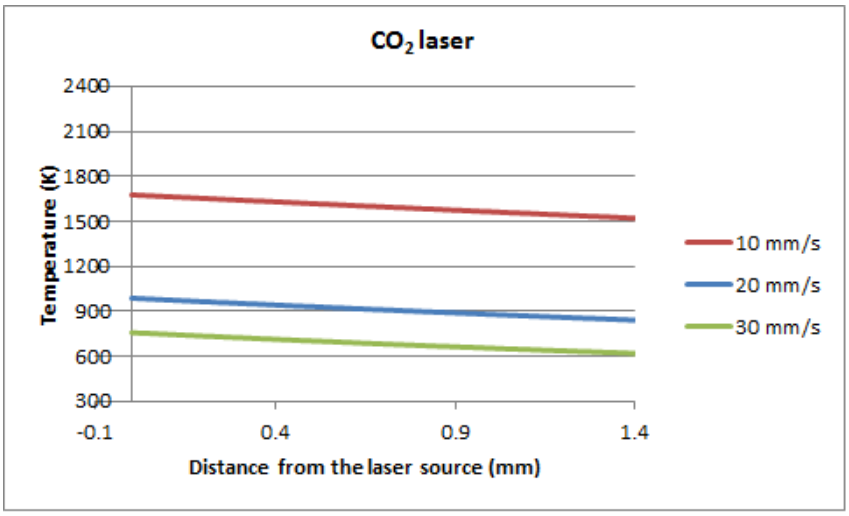

Figure 4.15: Copper temperature changes under 60 W CO_2 laser without preheating system

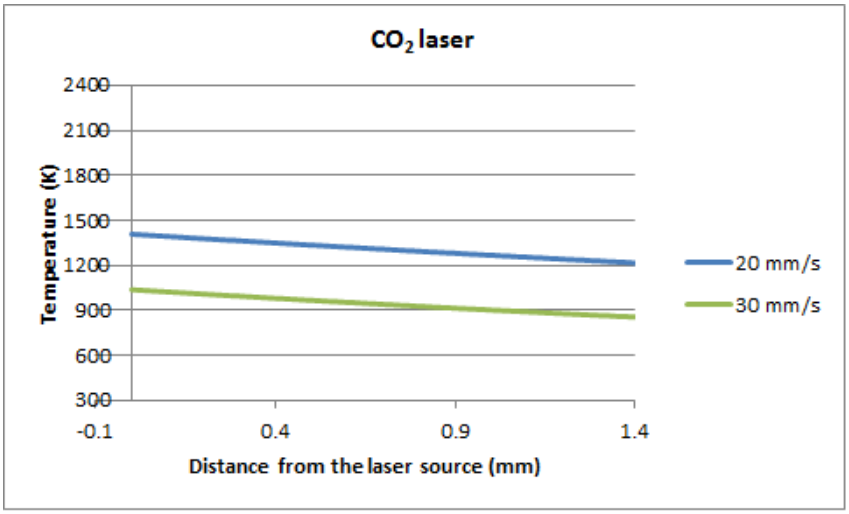

Figure 4.16: Copper temperature changes under 60 W CO_2 laser with preheating system

4.2.1.4 Brazing

Brazing processes include a filler metal and a base metal. Only filler metal melts in the brazing process. Therefore, the following section investigates whether filler metal can melt under scanning speed of $30\,\mathrm{mm/s}$.

Table 4.13 shows thermal properties of filler metals. These filler metals were selected because complete property data is available for the simulations.

Material	k ($\frac{\mathrm{W}}{\mathrm{m\,K}}$)	C_p ($\frac{\mathrm{J}}{\mathrm{kg\,K}}$)	ρ($\frac{\mathrm{kg}}{\mathrm{m^3}}$)	α($\frac{\mathrm{m^2}}{\mathrm{s}}$)	T_m(K)
Al-1Mn	140	900	2400	64.1×10^{-6}	922
Al-10Si	145	910	2408	66.17×10^{-6}	858
Cu-30Zn	110	380	8530	33.9×10^{-6}	1188

Table 4.13: Thermal property of filler metals [80, 93]

Common fuels for brazing include propane and oxy-acetylene. The heat fluxes generated from propane and oxy-acetylene are shown in Table 4.14. These values are utilized to construct the welding metallurgy model. Additionally, the model also includes MIG welding.

Torch type	Heat flux ($\mathrm{W/m^2}$)
Propane torch	10^5
Oxy-acetylene torch	10^6

Table 4.14: Heat flux for common brazing torch [94]

Figure 4.17 and Figure 4.18 show the heat transfer simulation results from the brazing process with a brazing speed at $10\,\mathrm{mm/s}$. The model shows that the filler metal does not melt completely even at this slow speed. The primary reason

is due to insufficient heat flux. Therefore, it is infeasible to perform continuous joining for the desktop metal prototyping machine.

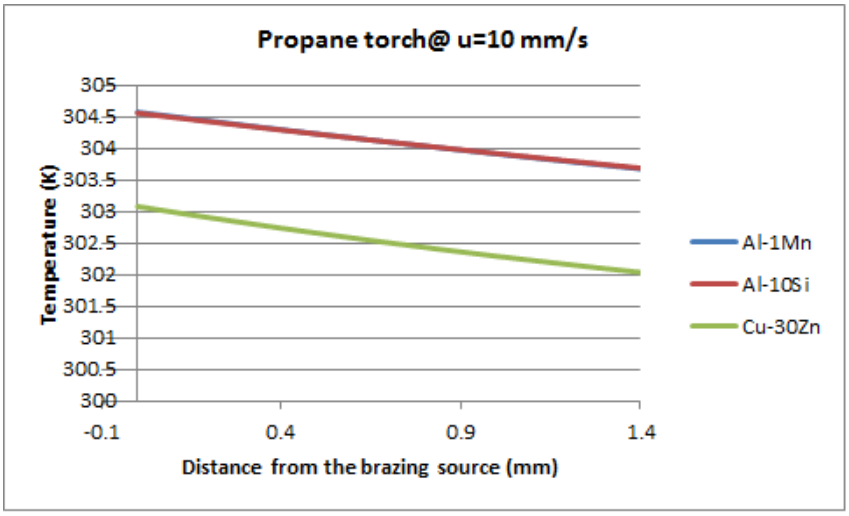

Figure 4.17: Welding metallurgy model with propane torch

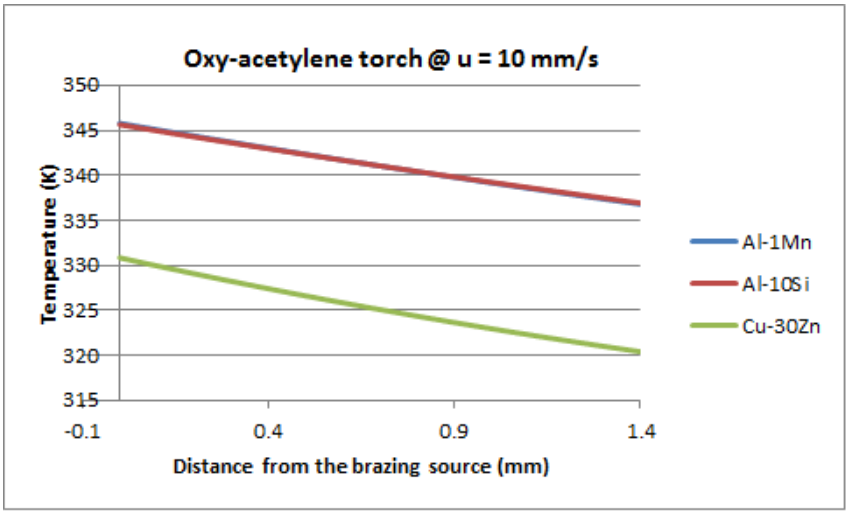

Figure 4.18: Welding metallurgy model with oxy-acetylene torch

4.2.1.5 Induction Welding and Spot Welding

Besides the aforementioned continuous joining processes, welding speed is also an issue for the induction welding and spot welding configurations.

For induction welding, the price of the induction equipment, UPT S-5 (See Table 4.19), is more than $\$9000$ according to the information provided by Ultra-Flex Power Technology with melting speed of $30\,\mathrm{mm/s}$. As a result, this concept variant is eliminated due to the cost consideration.

Power Supply Model

	UPT–S4	UPT–S5	UPT–S5-3
Output Power, kW	4.0	5.0	5.0
Frequency, kHz	50-250	50-250	50-250
AC Line, Volts (50/60Hz)	230 ±10%	230 ±10%	230 ±10%
Line Phases	1	1	3
Weight, Lb (kg)	43 (19.5)	43 (19.5)	43 (19.5)
Dimensions, Inch (cm) LxWxH	14.2 x 14.2 x 11.8 (36 x 36 x 30)	14.2 x 14.2 x 12.2 (36 x 36 x 31)	15.4 x 17.3 x 12.6 (39 x 44 x 32)
Compatible Heat Stations	HS-4, HS-8	HS-4, HS-8	HS-4, HS-8

Figure 4.19: Specification sheet for UPT-S5 [95]

For spot welding, the desktop spot welding machine can only complete 30 welds/min [96]. The spot welding configuration is not suitable for continuous joining. Therefore, the concept is temporarily eliminated. However, spot welding is possible to combine with a bending subsystem, which is discussed in detail in the next chapter.

Overall, continuous joining is infeasible for the desktop wire-feed metal prototyping machine due to the limitation of the heat flux and cost.

4.2.2 Pugh Chart

According to the discussion above, a Pugh Chart is used to compare the winding and bending subsystems without regard to the heating processes. The criteria for the Pugh chart include energy usage, build time, cost, and freedom to create geometry. The comparisons of power consumption and cost are based on the primary component in these two concept variants; specifically, a wire bender and a laser welder for the bending configuration. On the other hand, the winding configuration includes a stepper motor for the mandrel and an additional kiln to melt the wound part. The complete Pugh Chart is shown in Table 4.15.

Criteria	Bending	Winding
Power consumption	0	-1
Build time	0	0
Freedom to create geometry	0	-1
Cost	0	+1
Total	0	-1

Table 4.15: Pugh chart for the desktop metal wire-feed prototyping machine

- **Power consumption**

  The power consumption for a desktop CNC wire bender is approximately $216\,\mathrm{W}$ ($100\,\mathrm{V}$-$24\,\mathrm{V}$ and $1.8\,\mathrm{A}$ at $50\,\mathrm{Hz}$-$60\,\mathrm{Hz}$ [97]) and $400\,\mathrm{W}$ for a desktop pulse TIG welder [96]. Therefore, the energy consumption for the bending configuration is less than $1000\,\mathrm{W}$. On the other hand, for the winding configuration, since the wire component has light weight, a $100\,\mathrm{W}$ DC motor [98] is selected for the Pugh chart comparison. The kiln typically requires power higher than $1440\,\mathrm{W}$ ($120\,\mathrm{V}$ and $12\,\mathrm{A}$ [99]). Therefore, the winding

configuration requires much higher power compared to the bending configuration.

- **Build time**

  For the build time, if only the shaping process is considered, the winding process can have higher build speed. However, if the joining process is considered, there is no significant time difference. The reason is the heating process in a klin may take several hours. Therefore, it would be better to assume that they have similar speed ranges.

- **Geometry**

  One of the primary disadvantages of the winding configuration is that the geometry of the component is limited to symmetrical components. The bending configuration provides more freedom to create the geometry.

- **Cost**

  Considering the primary components in both machines, costs are listed in Table 4.16. The commercial desktop CNC bender costs $\$3750$ [100] (including program, cutter, and bender). The pulse TIG welder for jewelry is approximately $\$400$ [96]. Considering that there is extra cost for additional components, such as a platform, the estimated cost for the bending configuration is approximately $\$5000$. For the winding configuration, a $100\,\mathrm{W}$ DC motor is used for the mandrel, and the price of the DC motor is less than $\$100$ [101]. The cost of kiln should also be considered, which is typically less than $\$800$ [102]. The estimated cost for the winding configuration is

about $2000. As a result, the winding configuration has an advantage over the bending configuration based the cost.

Bending		Winding	
Bender	$3750	100 W DC motor	∼$100
Pulse TIG welder	$400	Kiln	≤$800
Estimated cost	≤$5000		≤$2000

Table 4.16: Cost estimation for concept variants

Based on Table 4.15, the bending configuration is better than the winding configuration. The next chapter focuses on the design of the discontinuous heating system. There are two possible options for the design: TIG pulse welding and brazing.

4.3 Chapter Summary

This chapter discusses five concept variants, which are the bending configuration, the winding configuration, the laser configuration, the welding configuration, and the brazing configuration. Bending and winding configurations separate the shaping process and the joining process. The other three configurations create the geometry by melting material directly.

After developing the welding metallurgy model, the direct methods suffer from the slow welding/brazing speed, which makes them infeasible for the desktop metal wire-feed prototyping machine. Therefore, the Pugh Chart only includes the winding configuration and the bending configuration. Since the bending configuration provides more freedom to create the geometry, the bending configuration

is selected to explore its feasibility in the next chapter.

Chapter 5

Design of Discontinuous Joining System

Chapter 5 focuses on the design validation for the spot welding subsystem. The bending sybsystem utilizes a bender to create the geometry of metal wire. To make a funtional part requires, it is possible to do discontinuous joints at the points that users want to connect. The possible discontinuous joining processes include pulse TIG welding and brazing. The discontinuous joining concepts do not include a laser system due to the cost issue, as discussed in Chapter 4.

5.1 Design Criteria for Discontinuous Joining System

The criteria for discontinuous joining processes are different than continuous processes. For discontinuous joining processes, joining speed is not the primary consideration. Therefore, it is necessary to redefine the design criteria for the discontinuous joining process.

Tensile strength, time for joining at a single point, control, cost, and area of oxidation are considered for these processes.

- **Tensile test**

  The first criterion is tensile strength of the joint. Tensile strength is selected because it determines whether final printed parts can be damaged easily.

- **Time for joining single point**

  If there are several points that need to be joined, the join speed difference is amplified. Thus, time for joining at a single point is one of the criteria for the discontinuous joining processes.

- **Control**

  An automatic system should adapt to variations in the environment and the wire. Therefore, the ideal discontinuous method should be easy to control.

- **Cost**

  Since the design also includes a bender system, it is necessary to ensure the design does not exceed the cost constraint.

- **Area of oxidation**

  One of the significant issues with thermal processing is oxidation. Post-processing is required to clean the area of oxidation. A smaller area of oxidation preferable. Therefore, the cleaning area is taken into consideration in the Pugh Chart.

5.2 Discontinuous Joining Concept Introduction

This section discusses the brazing and pulse TIG welding systems used for tensile testing and time for joining single point experiments.

5.2.1 Brazing

The brazing process is the common material joining process for makers and jewelry artists. They often use metal filler or silver solder paste to join copper. Since these people are target customers, the equipment in the experiment should approach how they braze copper.

In the experiment, a Worthington 310184 WT3401 propane torch is used to join annealed 22 AWG copper wire (ASTM B3 [103]). The WT3401 propane torch can generate a neutral flame of approximately 10 cm. The filler metal is SS-75 silver solder paste sold by EURO TOOL, Inc (a typical chemical composition for hard silver solder is $75\,\%$ Ag, $22\,\%$ Cu, and $3\,\%$ Zn [104]).Before brazing, the copper wire is cleaned with acetone. The brazing process is outlined in AWS C3.2M [105].

5.2.2 Pulse TIG Welding

The TIG pulse welder in the experiment is a DingXing DX-YQ0505. The welder is connected to a $120\,\mathrm{V}$ power supply. Figure 5.1 shows this TIG pulse welder. In the experiment, the original electrode is replaced with a $2\,\%$ lanthanated electrode (color code: blue). The diameter of the lanthanated electrode is $1/16$", and the tip angle is 38°. In the experiment, there is no shield gas or filler metal.

One of the primary issues for this welder is that it does not provide a range of output current and output voltage, which are critical parameters to control welding penetration depth. Therefore, voltage and current measurement experiments were conducted to collect these values.

Figure 5.1: DingXing DX-YQ0505 pulse TIG welder

5.2.2.1 Current Measurement

The experimental set-up for the current measurement is shown in Figure 5.2. The output current is connected to a $200\,\mathrm{A}$, $50\,\mathrm{mV}$ shunt and measured by an Agilent Technologies DSO1012A Oscilloscope.

Figure 5.3 shows the current wave form ($2\,\mathrm{V/div}$ and $1\,\mathrm{ms}$) when the current adjustment knob is set to 1.5, which is the setup that welds the 22 AWG annealed copper wire completely. One of the primary issues with the welder is that the peak current varies for a given adjusted value. Therefore, the current shown below is the average weighted current. The first peak is the inrush current, so the RMS current is from the second wave. The RMS current is about $2828\,\mathrm{A}$ over $5\,\mathrm{ms}$.

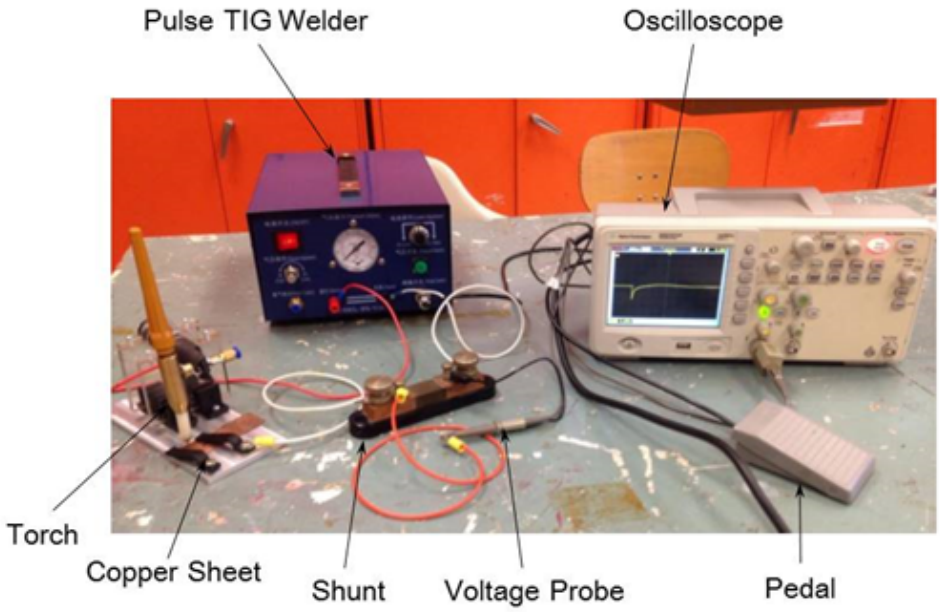

Figure 5.2: Experimental setup of current measurement

5.2.2.2 Voltage Measurement

Based on the current measurement result, a bridge rectifier is used to change the AC to DC and a filter capacitor to generate the impulse signal. Therefore, the output voltage of the welder can be obtained by measured the voltage difference of the bridge rectifier. The simplified electric circuit of the inside of the welder is shown in Figure 5.4. Figure 5.5 shows the inside of the welder, and Figure 5.6 shows the D6SB 60 L bridge rectifier.

Measured by Fluke 325 clamp meter, the voltage of the bridge rectifier D6SB is $161\ \mathrm{V}$. Therefore, the output voltage of the welder machine is $161\ \mathrm{V}$. The result is validated by measuring the voltage difference at the switch in the electric circuit

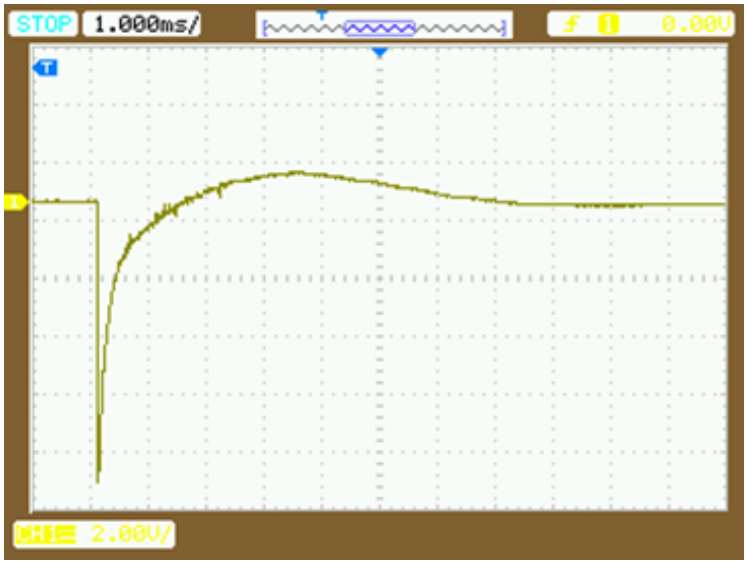

Figure 5.3: Current measurement of DingXing DX-YQ0505 TIG Pulse Welder

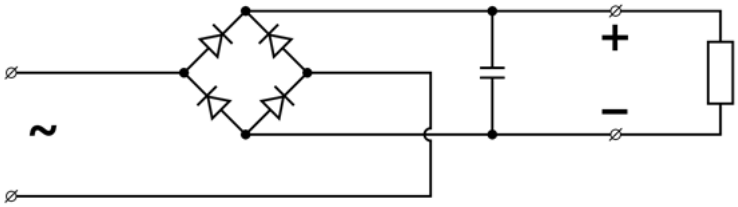

Figure 5.4: Simplified sketch of the circuit to generate impulse signal [106]

of the DingXing welder.

5.3 Tensile Test

Tensile testing is conducted to measure the joint strength for both the brazing and welding processes. The tensile test is performed with an Instron Model 2519-107. The material specimen is annealed copper (ASTM 3B, 22 AWG). The

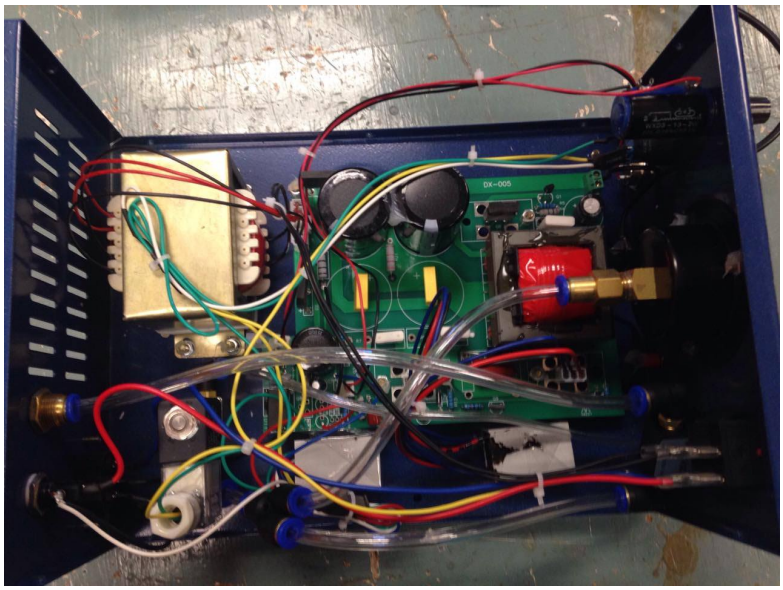

Figure 5.5: Inside of the pulse TIG welder

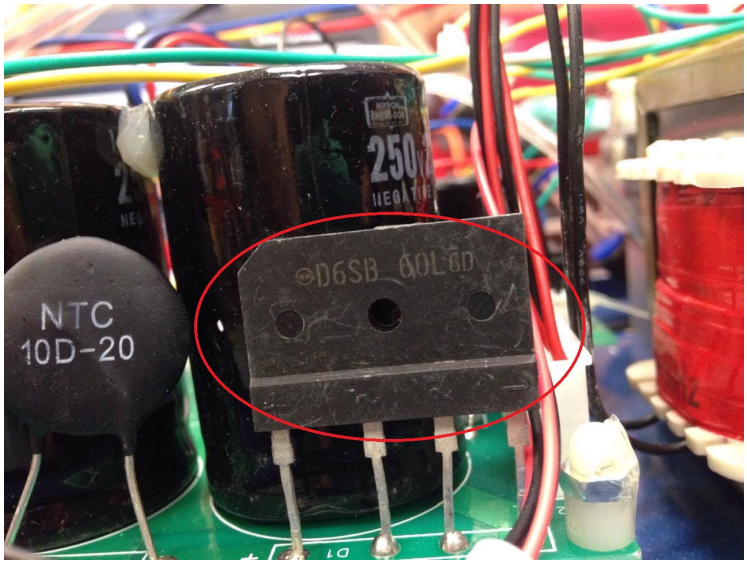

Figure 5.6: The bridge rectifier D6SB in the pulse TIG welder

gauge length of the specimen is $30\,\mathrm{mm}$. All the wire is straightened before brazing or welding. The specimen is created with a butt joint as shown in Figure 5.7. The speed of the tensile machine is $1\,\mathrm{mm\,min^{-1}}$ at room temperature. The tensile test is outlined in ASTM E8 [107].

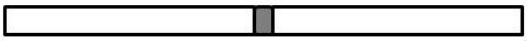

Figure 5.7: Schematic of butt joint

5.3.1 Copper Wire

Figure 5.8 shows the tensile test results of copper wire without brazing or welding. The results indicate that the maximum force that the copper wire can tolerate is about $56\,\mathrm{N}$. Additionally, Table 5.1 presents the maximum load for each specimen.

Trial	Maximum Load (N)
1	56.53654
2	56.01073
3	55.9769
4	56.06808

Table 5.1: Maximum Load of each copper wire specimen

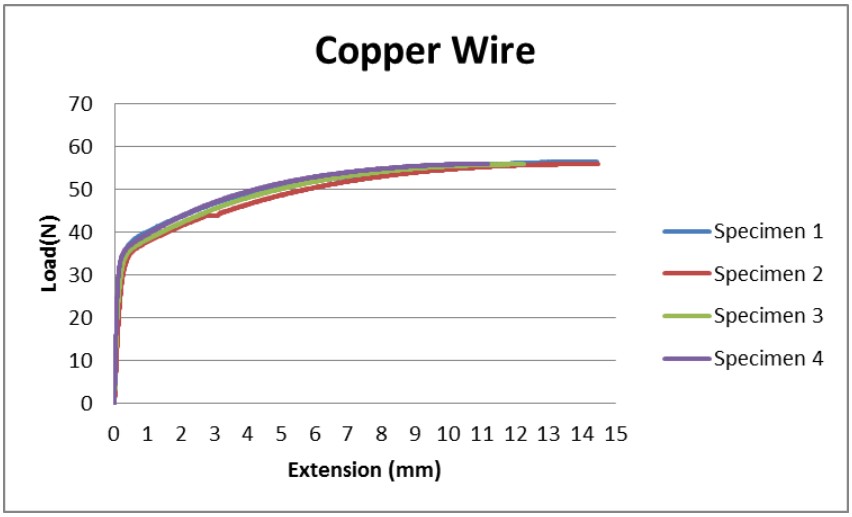

Figure 5.8: Tensile test result of ASTM B3, 22 AWG copper wire

5.3.2 Brazing Joint

Figure 5.9 shows the tensile test result for the brazed specimens. The experiment includes four trials. None of these four specimens broke at the joint. The average maximum breaking force is approximately $54\,\mathrm{N}$ (See Table 5.2), which is similar to the breaking force of copper wire.

Trial	Maximum Load (N)
5	54.86052
6	55.24443
7	54.32339
8	52.7428

Table 5.2: Maximum Load of brazing joints

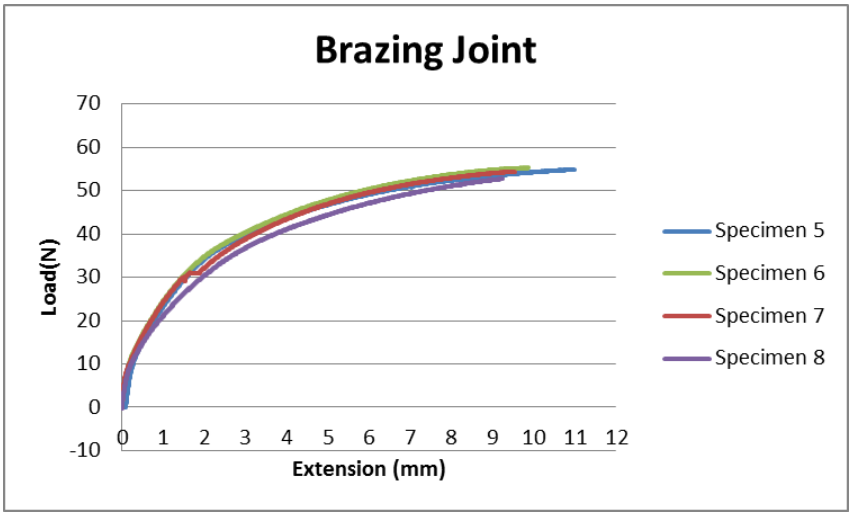

Figure 5.9: Tensile test result of brazing joints

5.3.3 Welded Joint

The maximum forces that the welded joints can tolerate varie, as shown in Figure 5.10. Additionally, the breaking force is also smaller than the breaking force of the brazed joint, as shown in Table 5.3. The primary reasons are the misalignment of the connected point (See Figure 5.11) and anisotropy of the welded joint. These two factors make the welded joint strength smaller than that of the brazed joint with silver solder paste.

Trial	Maximum Load (N)
9	21.87801
10	39.84961
11	28.83453
12	22.91417

Table 5.3: Maximum Load of welding joints

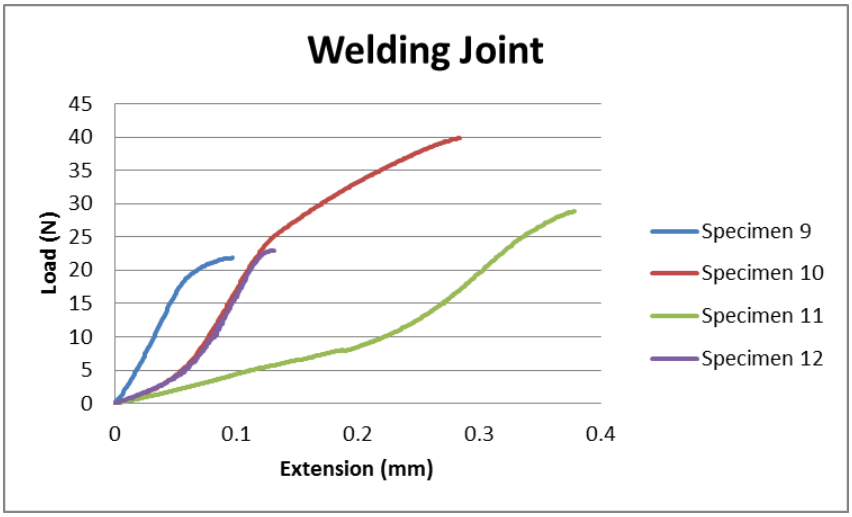

Figure 5.10: Tensile test result of welding joints

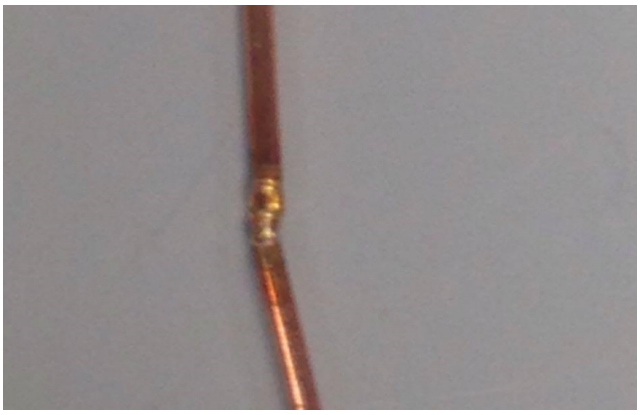

Figure 5.11: Misalignment of a welding joint

5.4 Time for Creating Single Joint

In order to maintain appropriate build speed, the time to create a single joint is determined.

5.4.1 Time for Brazing a Single Joint

The time for brazing a single joint was measured with a stopwatch. Time measurement does not include ignition and silver solder extrusion. In order to avoid the influence of the fixture, which works as a heat sink, the brazed end is hanged.

The time measurements are shown in Table 5.4. The first four trials were brazing directly. Trials 5 and 6 were preheated first before the brazing process began. Table 5.4 interprets that brazing a single joint can be completed within $6\,\mathrm{s}$.

Trial	Preheating Time (s)	Brazing Time (s)
1	-	4.53
2	-	4.45
3	-	5.28
4	-	5.51
5	2.88	3.83
6	3.55	3.45

Table 5.4: Time for brazing a single joint

5.4.2 Time for Welding Single Joint

The pulse TIG welding process is completed almost immediately, which makes it difficult to measure by a stopwatch. Therefore, the time estimation is based on the frequency that measured by the oscilloscope. According to Figure 5.3, the time to weld a single point is approximately $10\,\mathrm{m\,s}$, which is faster than the time for brazing a single joint.

5.5 Design Selection for the Discontinuous Joining System

A comparison table was developed based on the results of previous sections. Table 5.5 shows the comparison for pulse TIG welding and brazing.

	Pulse TIG Welding	Propane Brazing
Tensile Strength (Avg.)	$28.369\,\mathrm{N}$	$54.293\,\mathrm{N}$
Time (Avg.)	$10\,\mathrm{m\,s}$	$4.943\,\mathrm{s}$
Controllable	Easy	Medium
Cost	$\$4000$	$\$50$
Cleaning Area	$1.6\,\mathrm{mm}$	$<1.6\,\mathrm{mm}$

Table 5.5: Comparison table of discontinuous joining system

The breaking force and time for creating a single joint have been discussed in Section 5.3 and Section 5.4.

For control, two primary parameters in the pulse TIG welding process are current and voltage. Therefore, one can simply adjust current or voltage to create different penetration depths and welding bead sizes. However, the propane brazing process depends on several parameters, such as the tip of the torch, brazing temperature, and properties of filler material [108]. Therefore, the pulse TIG welding process is comparatively easy to control.

The cost of the equipment in the experiment is shown in Table 5.6 (Shipping fee is not included). However, the result of current measurement indicates that the current varies even when the setup is the same. A better quality machine is likely needed. However, the price for the average pulse TIG welding machine is higher than $\$3000$ [109], which makes the TIG welding process less preferable.

Brazing		
Item	Price	Citation
Worthington 310184 WT3401 propane torch	$24	[110]
Propane gas cylinder (14.1 Oz)	$3.22	[111]
EURO TOOL Inc. SS-75 silver solder paste (3 Oz)	$18.75	[112]
Welding		
Item	Price	Citation
DingXing DX-YQ0505 TIG Pulse Welder	$366	[113]
2% lanthanated electrode (per electrode)	$1.5	[114]

Table 5.6: Cost for the welding and brazing equipment

Another issue is the cleaning area. Oxidation is a common issue for thermal processing. For welding, the oxidation area is the area influenced by the plasma, which is smaller than the area of oxidation in the brazing process. In the experiment, the electrode was grounded before the welding process began. The average welding heat-affected zone is approximately $1.6\,\mathrm{mm}$ ($161\,\mathrm{V}$ and $1760\,\mathrm{A}$ within $5\,\mathrm{ms}$).

In summary, Table 5.5 shows that the TIG welding process is a better design choice because of quick welding time, ease of control, and smaller oxidation area. However, the strength of the welded joint and cost are disadvantages of the system. The strength of the welded joint can be improve with filler metal, but this makes the cost increase. Additionally, the high cost of the pulse TIG welding process is another issue for the development of the discontinuous joining process.

5.6 Chapter Summary

This chapter discusses experiments to choose a the design of the discontinuous joining process. There are two processes taken into account: pulse TIG welding and brazing. The selection criteria of the process include the strength of joints, time to create a single joint, control, cost, and cleaning area. According to Table 5.5, the pulse TIG welding process is recommended because

- It can create a single joint with just one pulse.
- The weld penetration can be simply controlled by current and voltage.
- The oxidation area is the same as the heat affected zone in the TIG welding process. Therefore, the oxidation that needs to be cleaned is smaller than that of brazing.

However, the primary disadvantage for the welding process is the joint strength and cost. Without filler metal, the breaking force of welded joint is $30\,\%$-$75\,\%$ less than the breaking force of copper wire. Additionally, the cost for the average pulse TIG welder is another potential issue for the design of the discontinuous joint process.

Chapter 6

Design of Wire Bender System

The discontinuous joining system and the wire bender system are two subsystems chosen for the desktop metal wire-feed prototyping machine. Chapter 5 focuses on investigating the feasibility of the discontinuous joining system. This chapter concentrates on evaluating the design of the wire bender for the desktop metal prototyping machine.

6.1 Literature Review for Benders

6.1.1 Tube Benders

The design of wire benders is analogous to tubing benders. There are four typical designs for tubing benders, which are roll bending, ram bending, compression bending and rotary draw bending. Figure 6.1 illustrates these four types of bending processes.

Rotary draw bending is the most common commercial bending process. The process includes a rotary bend die, clamp die, pressure die, and wiper die. When the bend die rotates, it also rotates the clamped tube. The pressure die is used to prevent excessive thinning of the exterior surface of the tube. Additionally, the primary function of the wiper die is to prevent wrinkling of the tube.

The concept of compression bending is similar to rotary draw bending. The primary difference is that the bend die is stationary in the compression bending process. Compression bending includes a stationary bend die, a clamp die, and a slide piece. The clamp die fixes and guides the position of a tube. The slide piece rotates and compresses the tube to the shape of the bend die.

The ram bending process is a relatively inexpensive bending process. The movement of the ram deforms the tube into an oval angle to create the desired shape.

Roller bending typically includes one top moving roller and two adjustable rollers. These rollers can have different alignments and create different bending angles. However, the process is limited to one single bending per cycle.

These four tube bending processes provide insight for the design of the wire bender system for the desktop metal wire-feed prototyping machine.

6.1.2 Freeform Bender

Besides these four bending processes, Murata and Kato [116] invented the MOS bending process, which is shown in Figure 6.2. The MOS bending process is based on two bending moments. The first bending moment comes from the vertical distance (μ) between the center of the guide cylinder and the center of the bending die and the guiding force (P_L). The second bending moment depends on the horizontal distance (V) between the exit of the guide cylinder and the center of the die and the contact force (P_u) by the bending die. The mechanism provides the benefit that there is no need to change the bending die when the bending radius

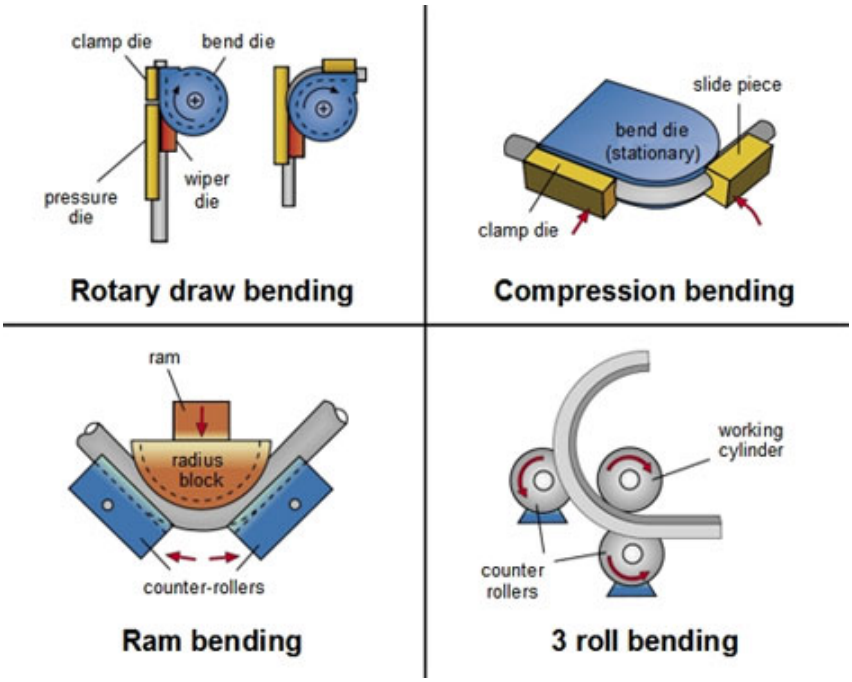

Figure 6.1: Four typical tube bending processes [115]

changes. The total bending moment is interpreted in Equation 6.1. The bending radii and bending angles can be completed by simply modifying the X and Y axial offsets (u_x and u_y) and penetration length (w_t), which represents the forward tube length toward the Z axis [117].

$$M = P_u \times V + P_L \times \mu \tag{6.1}$$

6.1.3 CNC Wire Bender System

One of the functional requirements for the desktop metal wire-feed prototyping machine is that the system needs to be automatic. Studying the existing

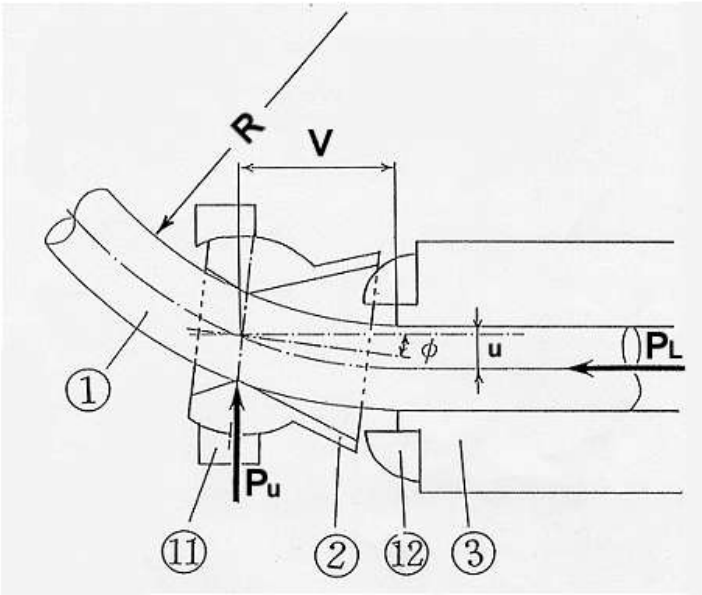

$$\mathbf{M = P_U \cdot V + P_L \cdot u}$$

1 - Tubular workpiece, 2 - Bending die, 3 - Guide cylinder
11 - Spherical bearing, 12 - Jig for control of die inclination

Figure 6.2: Components in the MOS bending head [116]

CNC wire benders can provide insight for this design.

PENSA Labs creates the first desktop CNC wire bending system, DIWire [97]. The specifications of DIWire are shown in Table 6.1. Note that there is a geometry constraint coming from the limitation of the bend angle, which is 135° in this case.

DIWire includes a wire straightening mechanism and a wire bending mechanism. The bending mechanism is similar to the compression bending type and is shown in Figure 6.3.

Specification	Value
Machine Dimensions	$24.1 \times 36.8 \times 17.1\ \mathrm{cm}$
Weight	$10.8\ \mathrm{kg}$
Operating Temperature	18-28 °C
Power Requirements	100-240 V 1.8 A 50-60 Hz
Materials	Steel Stainless Steel Aluminum Brass Copper Cold Bend Plastic
Diameter Range	1-4.7 mm
Maximum Bend Angle	135°

Table 6.1: The specification of the DIWire [97]

6.2 Function Structure of Wire Bender

The typical wire bender system includes straightening and bending mechanisms, as shown in Figure 6.3. However, a cutting process is required for automation process. Based on these requirements, a function structure of the wire bender system is illustrated in Figure 6.4.

The design of the wire geometry forming system for the desktop wire-feed prototyping machine can be modeled with this function structure.

6.3 Concept Generation for Wire Benders

Two concepts are proposed based on the function structure. Both concepts utilize a roller to transport the wire and a moving cutter to separate the wire.

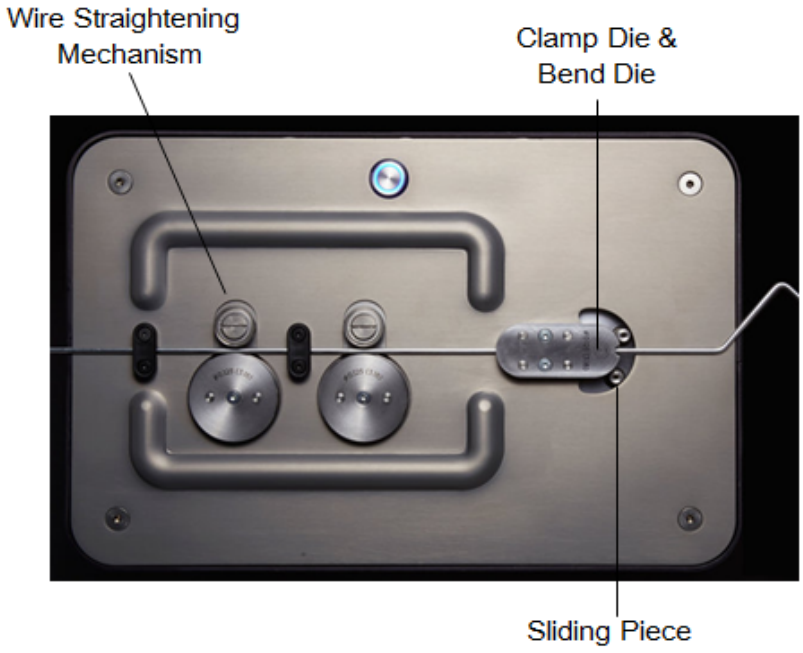

Figure 6.3: The DIWire straightening and bending mechanism (modified from [117])

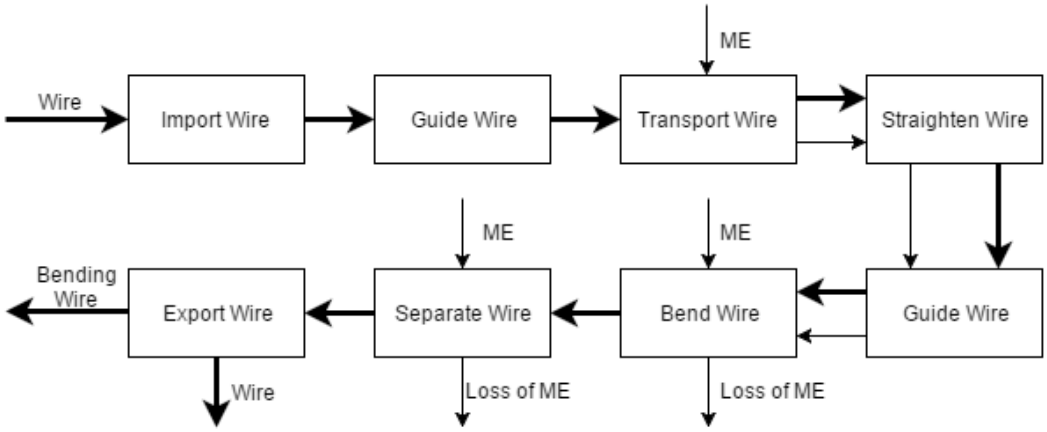

Figure 6.4: Function structure of the automatic wire bender system

The primary difference is that the first concept is based on the design of the compression bender (Figure 6.5), and the second one is similar to the concept of the freeform bending process (Figure 6.6).

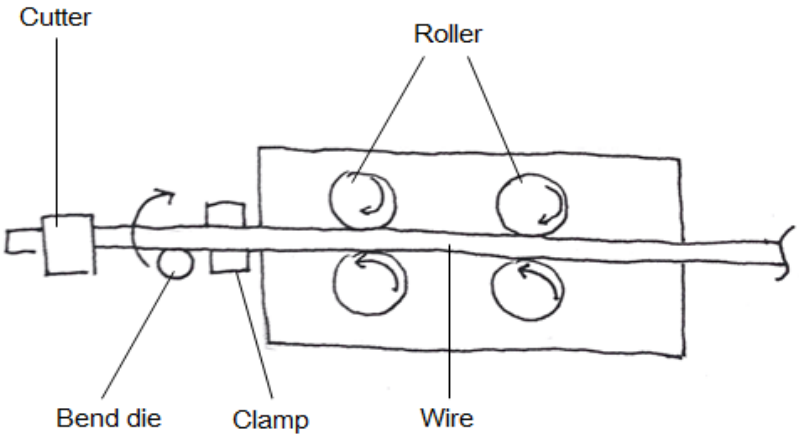

Figure 6.5: Compression bending concept (top view)

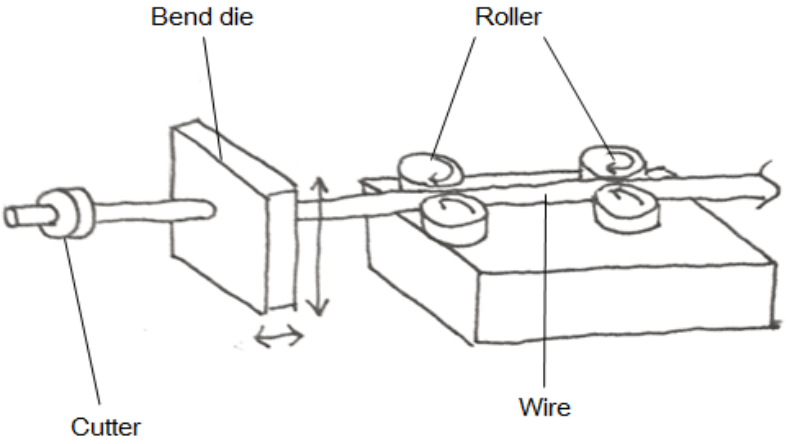

Figure 6.6: Freeform bending concept

In the compression bending concept, the clamp fixes the position of the wire and the bend die can rotate 180°. Movement in the z-direction is required to adjust the position of the bend die.

For the freeform fabrication concept, the bending die moves in the y and x directions to create different bending radii.

Geometry constraints and dimensional requirements are the primary concerns for the design selection criteria.

The process design of the bender can limit the resulting possible geometries design for the wire. For the compression bending concept, the design of the bend die determines the radius of the neutral axis of the wire. Therefore, the bending radius is fixed in the compression bending process unless the bend die is changed. On the other hand, freeform bending, such as MOS bending, can create multi-radii bends by adjusting the relative movement of the bending die and the guide cylinder. However, one of the significant geometry constraints for freeform bending is that the neutral radius of the bending wire is typically three times larger than the diameter of the wire. Therefore, it is impossible to create a tight radius by the freeform bending process.

Another consideration is dimensional requirements. The compression bending concepts utilize rotational motion to bend the wire. However, the freeform bedning process bends the wire by transitional motion, which makes the dimensional requirements of freeform bending relatively larger.

The compression bending concept is selected, the small-size bending ra-

dius is preferable for the artist application. Additionally, the desktop machine is considered. The CAD model and Bill of Materials (BOM) of this concept are developed in the next section.

6.4 Concept and CAD Model

This section presents the detailed design of the wire bender adapted for to the desktop wire-feed prototyping machine .

6.4.1 Further Consideration for the Wire Bender

6.4.1.1 Vertical Wire bender

Commonly wire benders are horizontal. However, for the automatic prototyping machine, it is necessary to consider how to position the wire to the target position.

One way to approach this issue is to create a vertical wire bender configuration with a moving platform. Therefore, the platform can move to the target position. When the wire is cut, it falls to the expected position.

In order to prevent the wire from moving during the transport process, the metal wire runs through a metal channel.

6.4.1.2 Cutting Mechanism

Another important consideration for the wire bender is separating the wire, which is illustrated in Figure 6.4.

Based on the experiment in Chapter 5, the metal wire can be cut by the

welding head when the output arc current increases. Therefore, we measure various output current setups to determine the energy needed to cut the wire. The experimental setup is similar to the experiment in Section 5.2.2.1. The arc voltage (V_{arc}) is kept at $161\,\mathrm{V}$. Table 6.2 shows the current measurement results using a $50\,\mathrm{mV}/200\,\mathrm{A}$ shunt. The output voltage (V_o) from the shunt is converted to the RMS voltage (V_{RMS}) first and then is converted to current (I_o). Therefore, the recommended energy should be higher than $8000\,\mathrm{J}$.

Trial	V_o (V)	V_{RMS} (V)	I_o (A)	E (J)	Cut or not?
1	1.92	1.357	5428	4369.545	No
2	2.8	1.98	7920	6375.6	No
3	3.36	2.375	9500	7647.5	No
4	3.52	2.489	9956	8014.58	Yes

Table 6.2: Wire cutting measurement result (V_{arc} =$161\,\mathrm{V}$ at $5\,\mathrm{ms}$)

6.4.2 Bending Wire Mechanism Design

Figure 6.7 shows a sketch of the wire bending mechanism design. The design includes a servo motor to control the position of the slide piece.

One of the issues for the compression bender is that the slide piece can only do bend in one direction (clockwise and counter-clockwise). Therefore, a solenoid is required to move down the slide pieces to complete inverse direction bending. Figure 6.8 the process of changing the direction of the sliding piece. In (a), the slide piece can only bend in the clockwise direction. In order to bend counter-clockwise, the solenoid retracts (b) to move the slide piece down, so it does not interface the wire (c). Once the slide piece moves to the left side, the solenoid extends to move

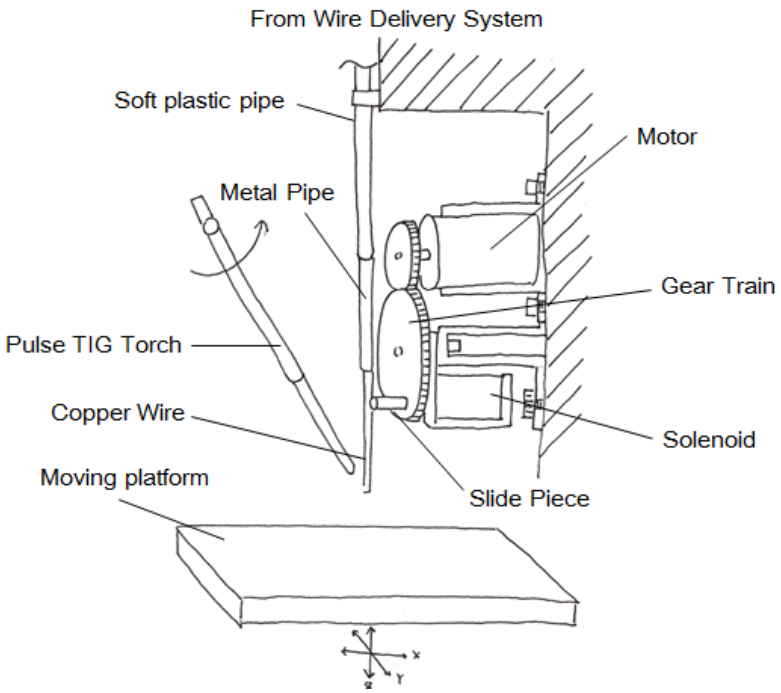

Figure 6.7: Schematic of the vertical wire bending system

slide piece back to the original height, and the counter-clockwise bending process can start.

6.4.2.1 Motor Torque Requirement

Based on the sketch presented in Figure 6.7, the servo motor should have the ability to support the solenoid. Therefore, it is preferable to pick a lightweight solenoid. The weight of an example solenoid (McMaster-Carr 70155K311) is 0.37 lb.

The simplified physical model of the bender system is illustrated in Figure 6.9. By assuming that the weight of the solenoid is uniform and the inertia of the

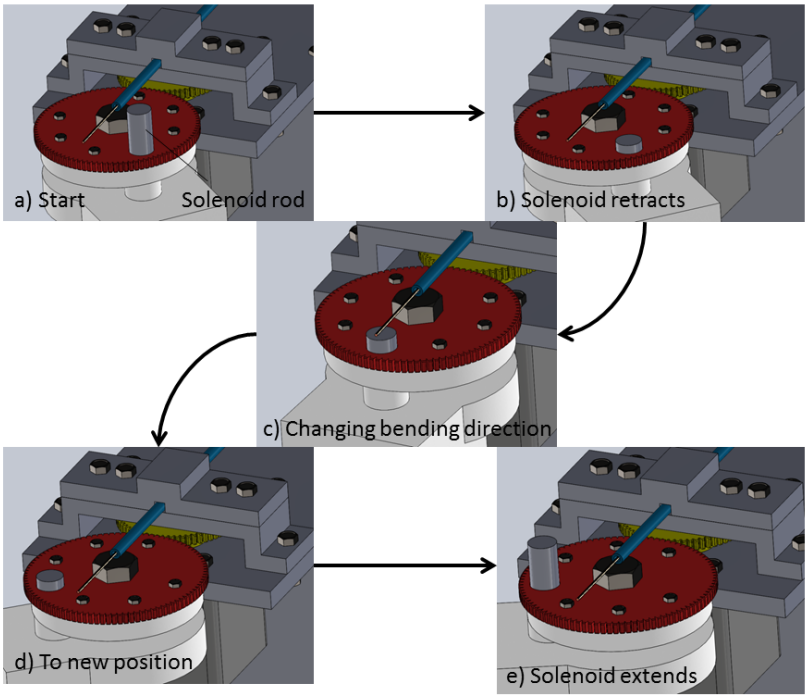

Figure 6.8: Process of changing the bending direction by a linear solenoid

gears is ignored due to the low-speed rotation, the sytem can be modeled as shown in Equation 6.2, where T is the torque from the motor, R is the gear ratio, w is the weight of the motor, and d_2 is the diameter of Gear 2.

$$\frac{T}{R} \geq \frac{wd_2}{2} \tag{6.2}$$

If the gear ratio between Gear 1 and Gear 2 is considered (Equation 6.3), Equation 6.2 can be rewritten as Equation 6.4. In Equation 6.3, N_1 and N_2 are the number of teeth, and d_1 is the diameter of the Gear 1.

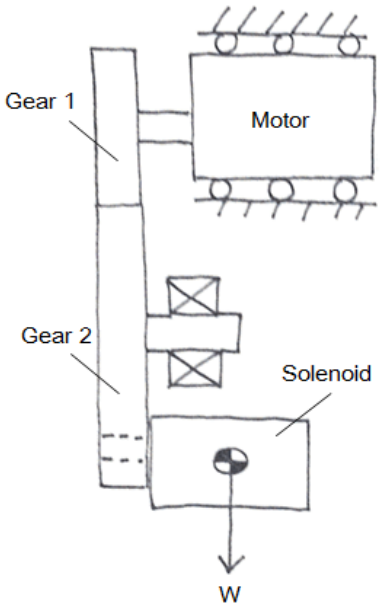

Figure 6.9: Physical model of the wire bender

$$R = \frac{N_1}{N_2} = \frac{d_1}{d_2} \tag{6.3}$$

$$T \geq \frac{w}{2} d_1 \tag{6.4}$$

As a result, the gear and stepper motor can be selected. The diameter of the first gear is similar to the length of the motor to avoid the interference when the solenoid is rotated. Their specification sheets are shown in Table 6.3 and Table 6.4.

	Gear 1	Gear 2
Pitch	48	48
Number of teeth	64	96
Pitch Diameter	1.333”	2”
OD	1.37”	2.04”
Vendor	McMaster-Carr	McMaster-Carr

Table 6.3: Specification sheet of Gear 1 and Gear 2

COMMON RATEING		SPECIVICATIONS	
STEP ANGLE	1.8°±5%	VOLTAGE	12V
PHASES	2	CURRENT	0.33A
INSULATION RESISTANCE	100Mohm(500V DC)	INDUCTANCE	46±20% Mh
CLASS OF INSULATION	B	RESISTANCE	34±10%
WEIGHT	0.20Kg	HOLDING TORQUE	0.23N.M

Table 6.4: Specification sheet of the SparkFun Electronics ROB-09238 stepper motor[118]

6.4.3 CAD Model and Bill of Materials

The CAD model of the vertical wire bender is shown in Figure 6.10. The BOM of the wire bender system is given in Table 6.6. The wire from the wire spool (22) is driven by the driver motor (7b) and guided by a steel pipe (14). The wire passes through the pipe (14) to the sliding piece (2). The sliding piece (2) can move from 90° to -90° to create bending.

Since the original plunger length of the solenoid is not long enough, an extender (2) is attached to it, as depicted in Figure 6.11.

The BOM of the wire bender system is given in Table 6.5. The prices for the

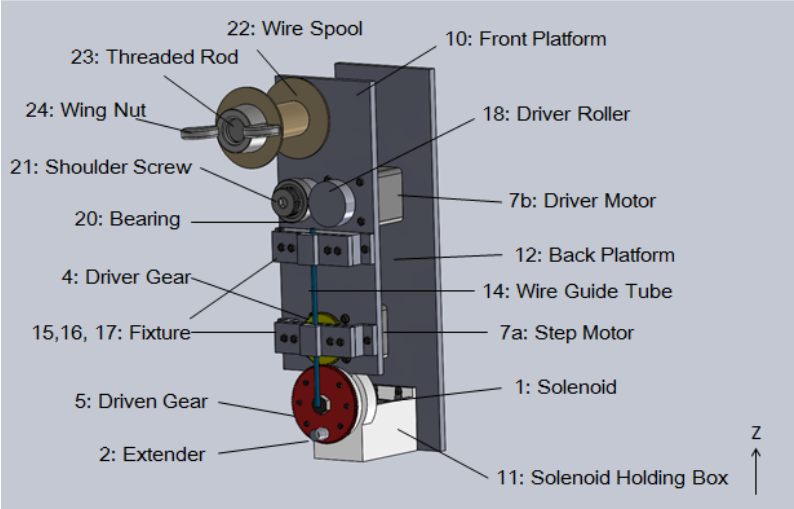

Figure 6.10: CAD Model of the vertical wire bender

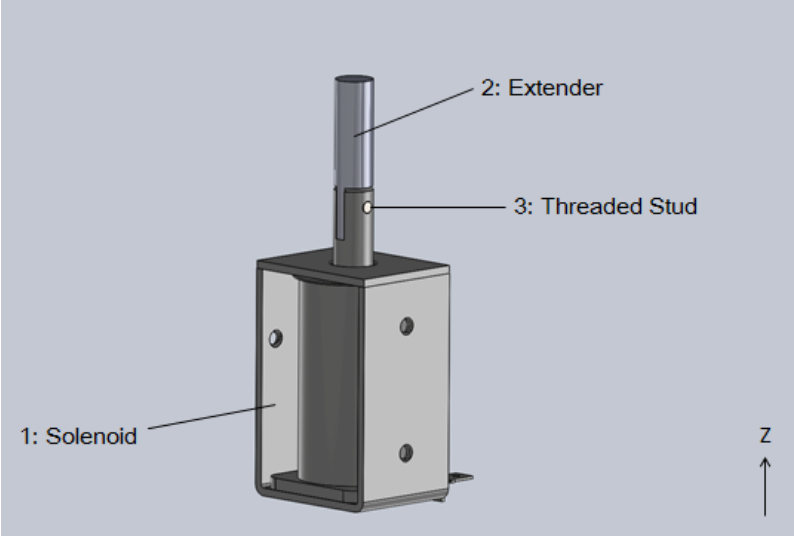

Figure 6.11: CAD model of solenoid assembly

machined components are estimated from the cost of raw material from McMaster-Carr pulse one-hour labor cost. The detailed dimensions of each component are presented in Appendix B.

Part	Part Name	QTY	Material	Processing	Price Per Unit
1	Solenoid	1	-	OEM McMaster 70155K111	$30.7 [119]
2	Extender	1	Low Carbon Steel	Machined	$6.29
3	Threaded Stud	1	316 Stainless Steel	OEM 4-40×5/16”	$3.5[120]
4	Gear Fixed Screw	6	304 Stainless Steel	OEM 4-40×3/8”	$0.05[121]
5	Driver Gear	1	Nylon	OEM/Drilled McMaster 57655K27	$10.44[122]
6	Driven Gear	1	Nylon	OEM/Drilled McMaster 57655K31	$9.68[123]
7a	Step Motor	1	-	OEM SparkFun Electronics ROB-09238	$14.95[124]
7b	Driver Motor	1	-	OEM SparkFun Electronics ROB-09238	$14.95[124]
8	Motor Screw	8	Class 4.8 Steel	OEM M3-0.5 × 10mm	$0.24[125]
9	Shoulder Screw	1	Alloy Steel	OEM Shoulder 1/4” ×5/8” Thread 10-24×3/8”	$1.236[126]
10	Front Platform	1	Low Carbon Steel	Machined	$23.765
11	Solenoid Holding Box	1	ABS	3D Printed	$13.13
12	Back Platform	1	Low Carbon Steel	Machined	$11.765
13	Hub Fixed Screw	2	304 Stainless Steel	OEM 4-40×1/8”	$0.06[127]
14	Wire Guide Tube	1	Steel	OEM OD: 1/8” ID: 0.069” L: 4.16”	$1.52[128]

Table 6.5: Bill of Material for the vertical wire bender

Part	Part Name	QTY	Material	Processing	Price Per Unit
15	Fixture A	1	Low Carbon Steel	Machined	$14.55
16	Fixture B	2	Low Carbon Steel	Machined	$14.55
17	Fixture C	1	Low Carbon Steel	Machined	$14.55
18	Driver Roller	1	Low Carbon Steel	Machined	$13.44
19	Spacer	1	Low Carbon Steel	Machined	$6.45
20	Bearing	1	Steel	OEM McMaster 60355K704	$8.74[129]
21	Shoulder Screw	1	316 Stainless Steel	OEM Shoulder $1/2$” $\times 5/16$” Thread $3/8$”-16$\times 5/8$”	$7.97[130]
22	Wire Spool + Wire	1	Spool: Plastic Wire:Copper	OEM Small Parts F22	$19.52[131]
23	Threaded Rod	1	Steel	OEM $3/4$”-10$\times 6.5$”	$2.61[132]
24	Wing Nut	1	Iron	OEM McMaster 90876A175	$4.25[133]
25a	Fixture Screw	4	Class 4.8 Steel	OEM M3-0.5 $\times$ 12mm	$0.08[134]
25b	Fixture Screw	4	Class 4.8 Steel	OEM M3-0.5 $\times$ 10mm	$0.06[134]
25c	Fixture Screw	4	Class 4.8 Steel	OEM M3-0.5 $\times$ 30mm	$0.1[134]
25d	Fixture nut	8	Class 4.8 Steel	OEM M3	$0.04[135]
26	Threaded Rod Nut	8	Stainless Steel	OEM $3/4$”-10	$1.1[136]

Table 6.5: Bill of Material for the vertical wire bender (*Continued*)

6.5 Summary

This chapter presents the design of the wire bending system. The total cost of the wire bending system is $272.14. Table 6.6 summarizes the function of the wire bender system from Figure 6.4.

Function	**Design**
Transport wire	Feed roller
Straighten wire	Roller
Guide wire	Steel pipe
Bend wire	Compression bender
Separate wire	Pulse TIG Welder

Table 6.6: Functions and designs for the wire bender system

A CAD model and BOM of the wire bender system are provided for future prototyping.

Chapter 7

Conclusion

Chapter 7 summarizes the work in this research and points out the future research direction.

7.1 Summary of Work

This research investigates the feasibility of a desktop metal wire-feed prototyping machine. The machine aims to provide an automatic layer-based process to create metal wire prototypes, such as metal wire sculptures. The primary challenge for the design is that the cost and domestic power supply limit the choice of the thermal joining process. Therefore, the objective of this research is to explore the different options of bonding processes. The primary contribution of the research includes:

- Review of current desktop metal additive manufacturing systems
- Develop conceptual design
- Investigate the feasibility of thermal joining methods
- Design a wire geometry forming system

Based on welding metallurgy models, simulations indicate that the design should have the following characteristics:

- *Include forming process to create the geometry*

  Due to the cost and domestic energy limitation, the desktop system cannot completely melt the wire with a scanning speed more than $20\,\mathrm{mm/s}$. Therefore, it is better to include the forming process to create the geometry instead of using thermal melting processes.

- *Utilize spot joining process to save build time*

  Based on the previous discussion, continuous extrusion also suffers from the low welding/brazing speed. Therefore, the spot welding/brazing process is recommended to save the build time.

7.2 Future Work

Several modules still require development before completing the design. Figure 7.1 depicts the CAD Model of the metal-wire prototyping system. The system includes a wire bending system, Pulse TIG Welder system, and two-axis platform. The welding torch can rotate to cut or weld the wire. The welding equipment is not included in the CAD Model. However, the welder can be placed near the machine and connected to the welding torch.

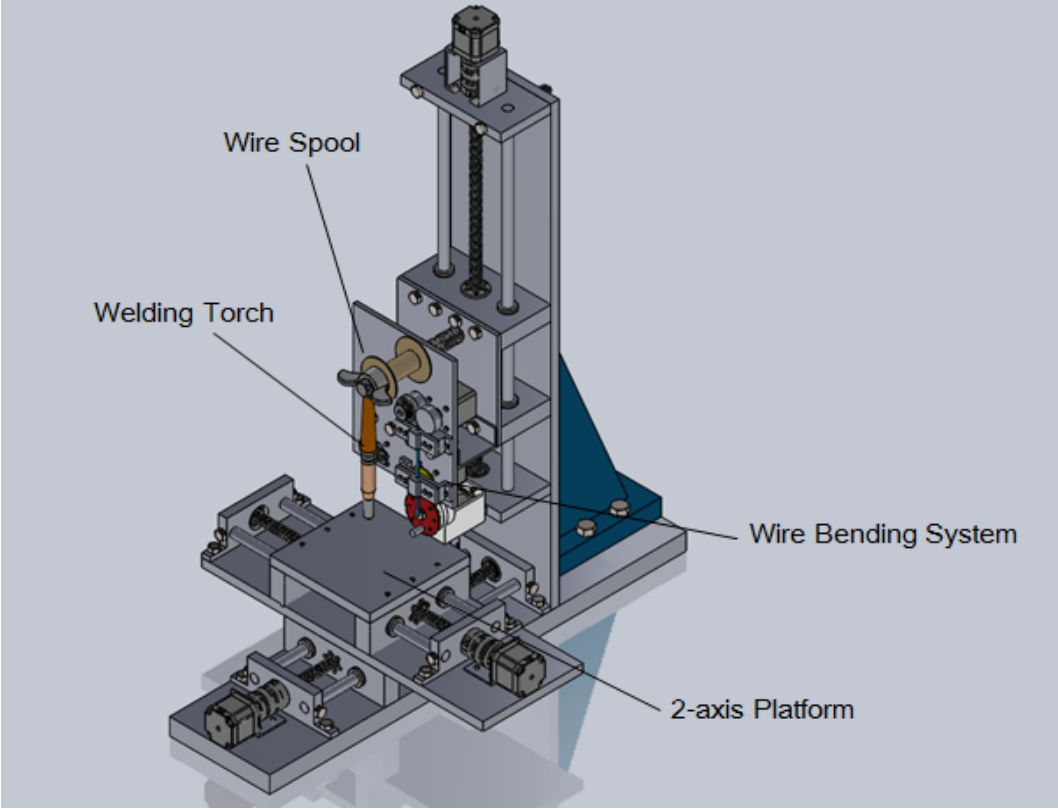

Figure 7.1: CAD Model for the desktop metal wire-feed prototyping machine (Welder is not included)

The CAD Model in Figure 7.1 illustrates the four primary areas for future works.

1. Develop three dimensional joining processes

   Because the continuous welding/brazing process increases the build time, other three-dimensional structures should be tested to make sure that the printed part can support itself. Figure 7.2 shows an example of a conventional layer-based build style and a possible build sytle for the metal wire-

feed system.

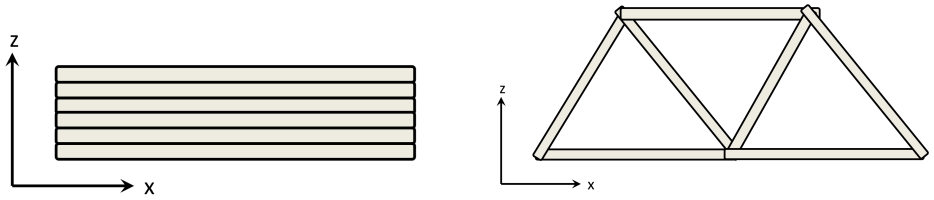

(a) Conventional layer-overlap (b) Possible layer-overlap

Figure 7.2: Different build structure

2. Design integrated joining and bender mechanism

   The design of the entire system is taken into consideration. The joining process should be applicable for three-dimensional bonding. The bender should be able to create complicated geometries and position the geometry on the build platform.

3. Detailed design of the system

   The original system utilizes the screw lead to guide the platform. Another possible choice is a belt drive. These options should be analyzed to determine whether either provides a technical or financial advantage. The torque of the screw lead motor should be at least 70 oz-in. However, detailed verification is still required before prototyping.

4. Program design for the system

   Since the system is not designed to create typical AM parts, design of the control program should be included in the research. The program should

accept a geometric model created by the user and control the desktop metal wire-feed prototyping system automatically. A starting point for program design of is DIWire, an open source wire bending system [137].

Appendices

Appendix A

List of Acronyms

3DP	Three Dimensional Printing
AM	Additive Manufacturing
CAD	Computer-Aided Design
EBM	Electron Beam Melting
FDM	Fused Deposition Modeling
FEF	Freeze-Form Extrusion Fabrication
IJP	Ink Jet Printing
LENS	Laser Engineered Net Shaping
LMD	Laser Metal Deposition
LOM	Laminated Object Manufacturing
MJM	Multi-Jet Modeling
PDM	Plasma Deposition Manufacturing
RFP	Rapid Freeze Prototyping
RP	Rapid Prototyping
SDM	Shape Deposition Manufacturing
SLA/SL	Stereolithography
SLM	Selective Laser Melting
SLS	Selective Laser Sintering
STL	Stereolithography (standard polygon file format)
UOC	Ultrasonic Object Consolidation

Appendix B

Engineering Drawings of Wire Bender Design Parts

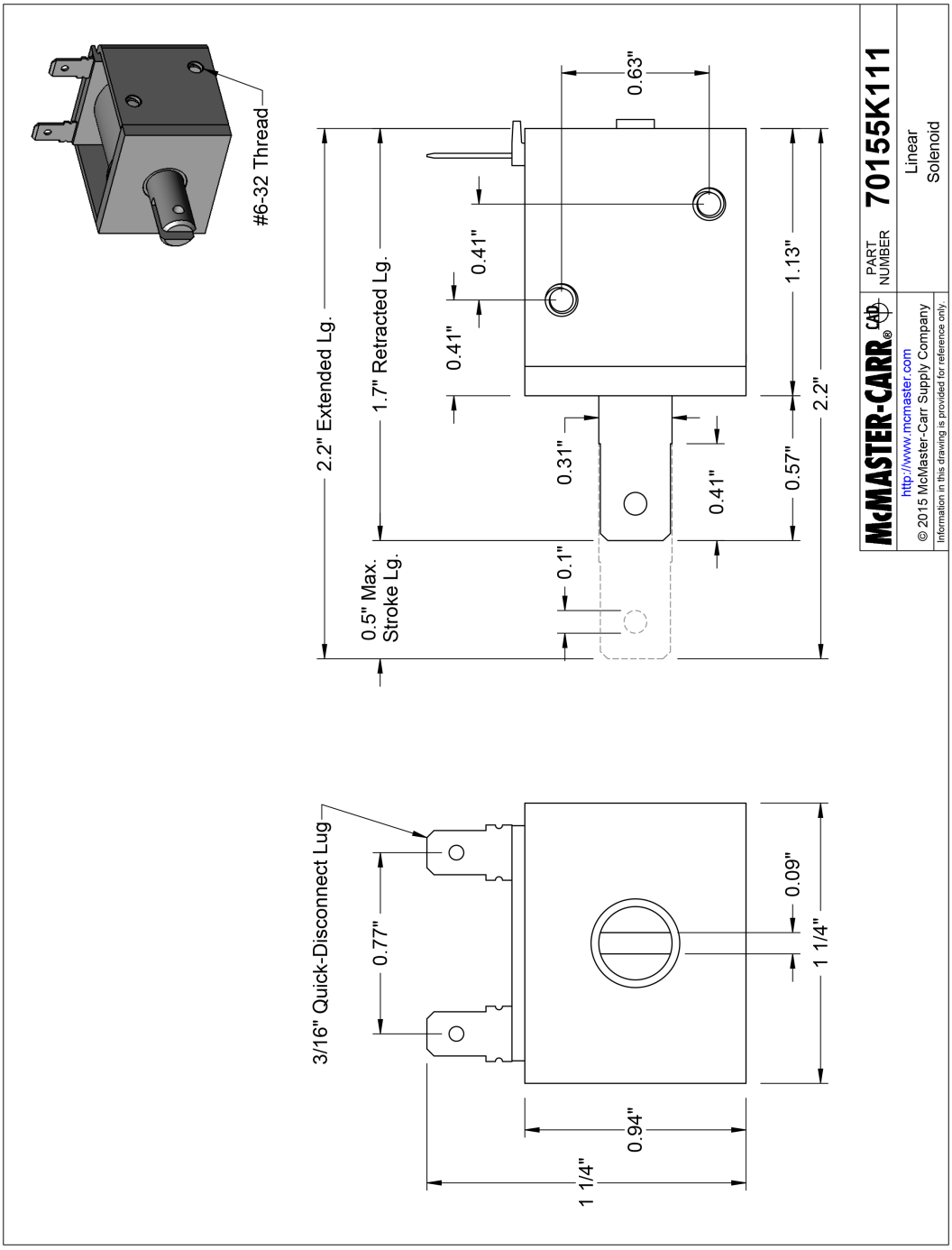
#6-32 Thread
2.2" Extended Lg.
1.7" Retracted Lg.
0.5" Max. Stroke Lg.
0.41"
0.41"
0.31"
0.1"
0.41"
0.63"
1.13"
0.57"
2.2"
3/16" Quick-Disconnect Lug
0.77"
0.94"
1 1/4"
0.09"
1 1/4"
McMASTER-CARR
http://www.mcmaster.com
© 2015 McMaster-Carr Supply Company
Information in this drawing is provided for reference only.
PART NUMBER
70155K111
Linear Solenoid

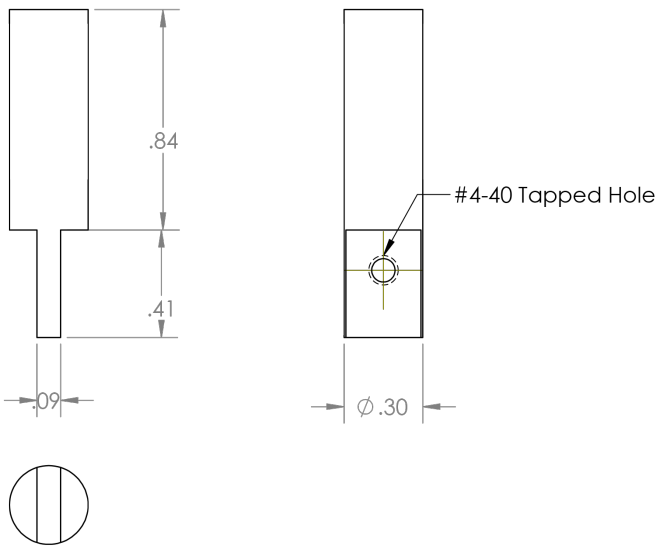

		UNLESS OTHERWISE SPECIFIED:		NAME	DATE
		DIMENSIONS ARE IN INCHES TOLERANCES: FRACTIONAL ± ANGULAR: MACH ± BEND ± TWO PLACE DECIMAL ± THREE PLACE DECIMAL ±	DRAWN		
			CHECKED		
			ENG APPR.		
			MFG APPR.		
		INTERPRET GEOMETRIC TOLERANCING PER:	Q.A.		
		MATERIAL Stee;	COMMENTS:		
NEXT ASSY	USED ON	FINISH			
APPLICATION		DO NOT SCALE DRAWING			

TITLE: Sliding Piece

SIZE	DWG. NO.	REV
A	2	

SCALE: 2:1	WEIGHT:	SHEET 1 OF 1

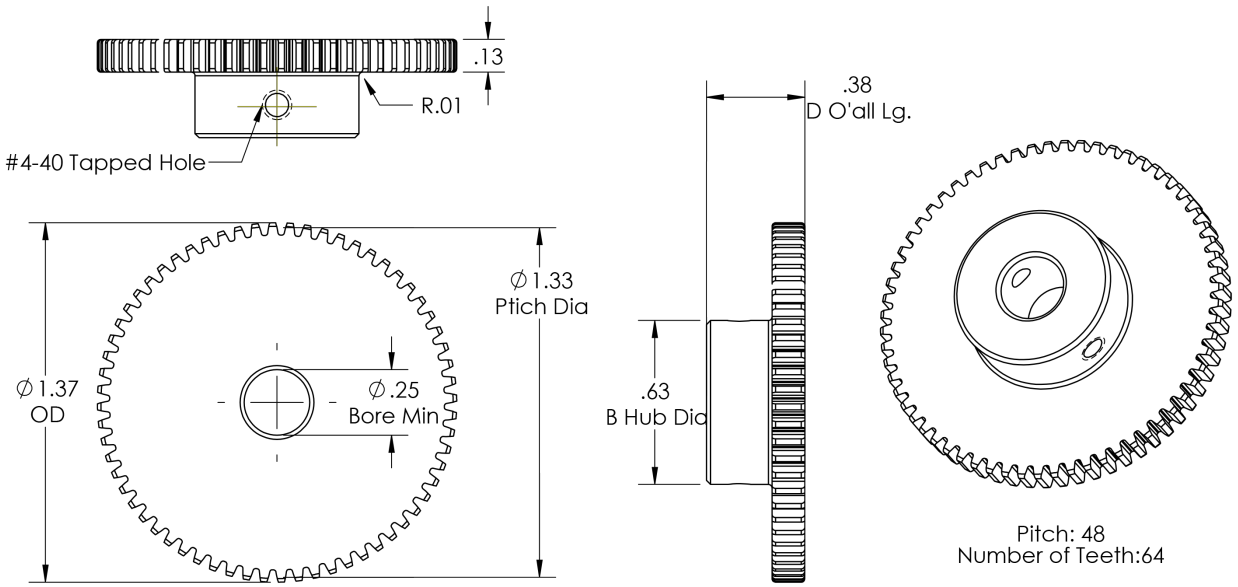

		UNLESS OTHERWISE SPECIFIED:		NAME	DATE
		DIMENSIONS ARE IN INCHES TOLERANCES: FRACTIONAL ± ANGULAR: MACH ± BEND ± TWO PLACE DECIMAL ± THREE PLACE DECIMAL ±	DRAWN		
			CHECKED		
			ENG APPR.		
			MFG APPR.		
		INTERPRET GEOMETRIC TOLERANCING PER:	Q.A.		
		MATERIAL Nylon	COMMENTS:		
NEXT ASSY	USED ON	FINISH			
APPLICATION		DO NOT SCALE DRAWING			

TITLE:

Driver Gear

SIZE	DWG. NO.	REV
A	5	
SCALE: 2:1	WEIGHT:	SHEET 1 OF 1

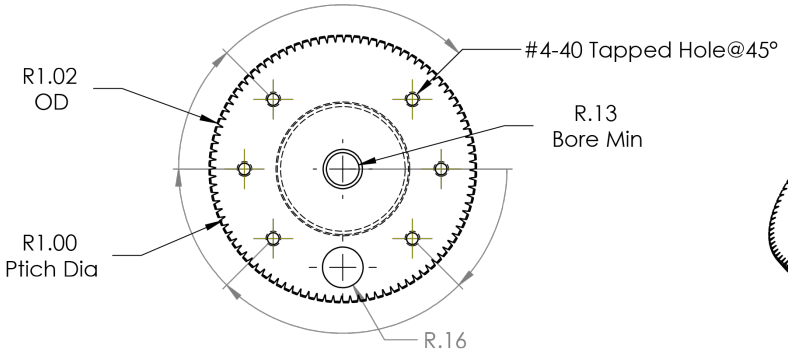

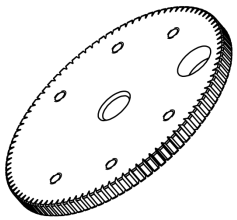

Pitch:48
Number of Teeth:96

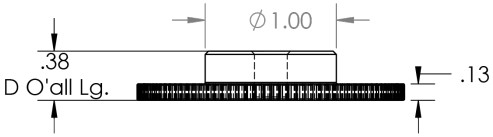

		UNLESS OTHERWISE SPECIFIED:		NAME	DATE
		DIMENSIONS ARE IN INCHES TOLERANCES: FRACTIONAL ± ANGULAR: MACH ± BEND ± TWO PLACE DECIMAL ± THREE PLACE DECIMAL ±	DRAWN		
			CHECKED		
			ENG APPR.		
			MFG APPR.		
		INTERPRET GEOMETRIC TOLERANCING PER:	Q.A.		
		MATERIAL Nylon	COMMENTS:		
NEXT ASSY	USED ON	FINISH			
APPLICATION		DO NOT SCALE DRAWING			

TITLE:

Driven Gear

SIZE	DWG. NO.	REV
A	6	

SCALE: 1:1	WEIGHT:	SHEET 1 OF 1

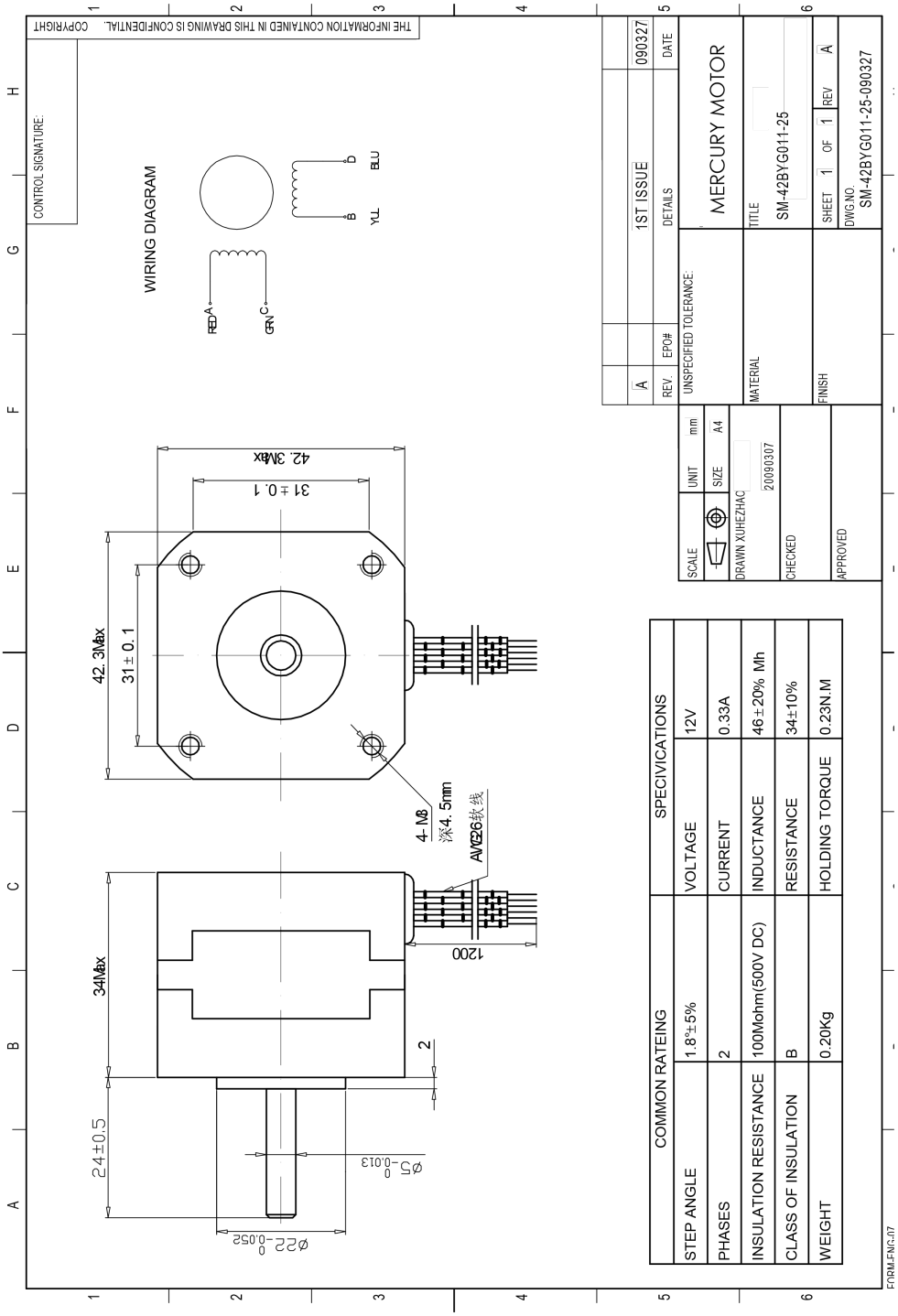
THE INFORMATION CONTAINED IN THIS DRAWING IS CONFIDENTIAL. COPYRIGHT
CONTROL SIGNATURE:
WIRING DIAGRAM
RED A
GRN C
B D
YEL BLU
REV. EPO# DETAILS DATE
A 1ST ISSUE 090327
UNSPECIFIED TOLERANCE:
MERCURY MOTOR
SCALE UNIT mm
SIZE A4
DRAWN XUHEZHAO
20090307
CHECKED
APPROVED
MATERIAL
FINISH
TITLE
SM-42BYG011-25
SHEET 1 OF 1 REV A
DWG.NO.
SM-42BYG011-25-090327
42.3Max
31±0.1
4-M3
深4.5mm
AWG26软线
1200
34Max
24±0.5
2
Ø5 0 -0.013
Ø22 0 -0.052
COMMON RATEING
STEP ANGLE 1.8°±5%
PHASES 2
INSULATION RESISTANCE 100Mohm(500V DC)
CLASS OF INSULATION B
WEIGHT 0.20Kg
SPECIVICATIONS
VOLTAGE 12V
CURRENT 0.33A
INDUCTANCE 46±20% Mh
RESISTANCE 34±10%
HOLDING TORQUE 0.23N.M
FORM-ENG-07

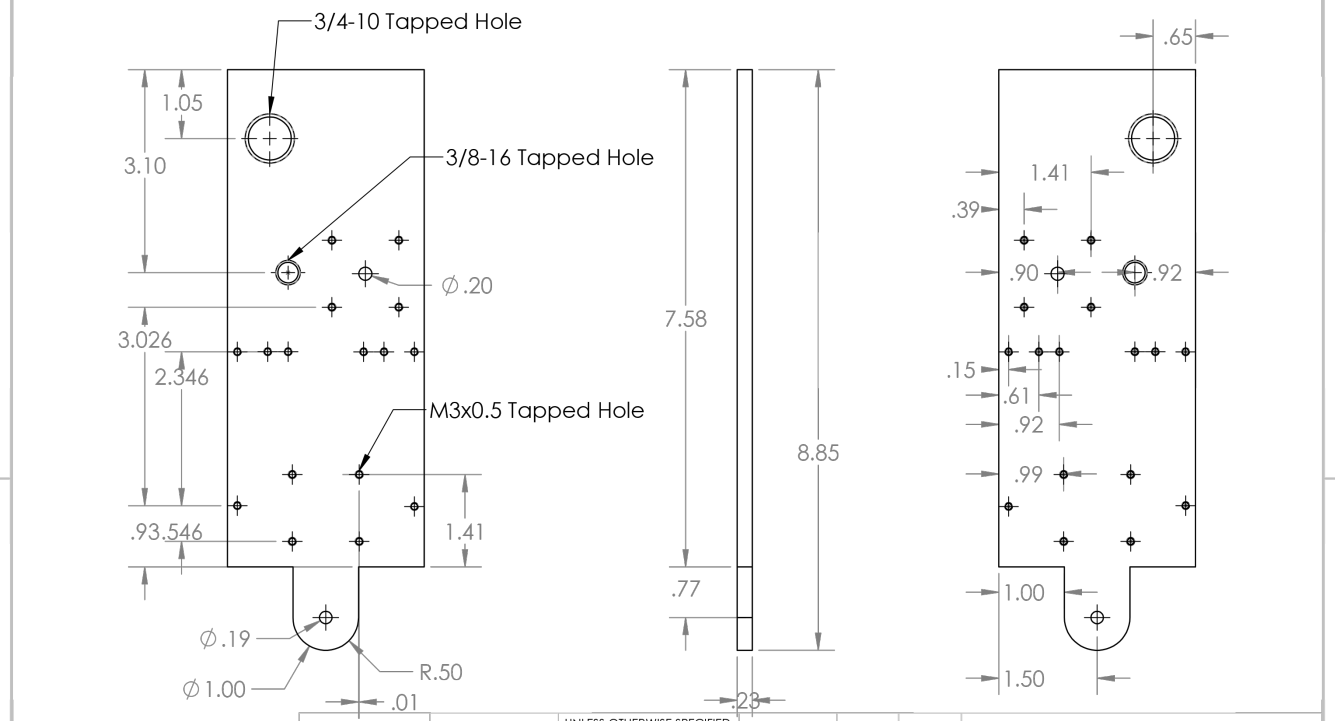

		UNLESS OTHERWISE SPECIFIED:		NAME	DATE
		DIMENSIONS ARE IN INCHES TOLERANCES: FRACTIONAL ± ANGULAR: MACH ± BEND ± TWO PLACE DECIMAL ± THREE PLACE DECIMAL ±	DRAWN		
			CHECKED		
			ENG APPR.		
			MFG APPR.		
		INTERPRET GEOMETRIC TOLERANCING PER:	Q.A.		
		MATERIAL Steel	COMMENTS:		
NEXT ASSY	USED ON	FINISH			
APPLICATION		DO NOT SCALE DRAWING			

TITLE:

Front Platform

SIZE	DWG. NO.	REV
A	10	

SCALE: 1:2 | WEIGHT: | SHEET 1 OF 1

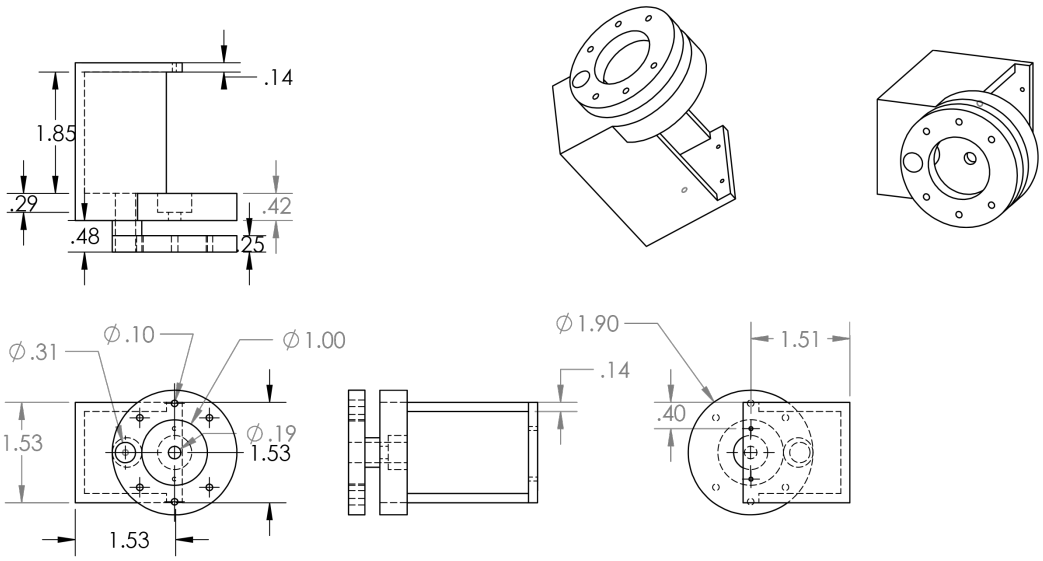

		UNLESS OTHERWISE SPECIFIED:		NAME	DATE
		DIMENSIONS ARE IN INCHES TOLERANCES: FRACTIONAL ± ANGULAR: MACH ± BEND ± TWO PLACE DECIMAL ± THREE PLACE DECIMAL ±	DRAWN		
			CHECKED		
			ENG APPR.		
			MFG APPR.		
		INTERPRET GEOMETRIC TOLERANCING PER:	Q.A.		
		MATERIAL ABS	COMMENTS:		
NEXT ASSY	USED ON	FINISH			
APPLICATION		DO NOT SCALE DRAWING			

TITLE:

Solenoid Holding Box

SIZE	DWG. NO.	REV
A	11	

SCALE: 1:2	WEIGHT:	SHEET 1 OF 1

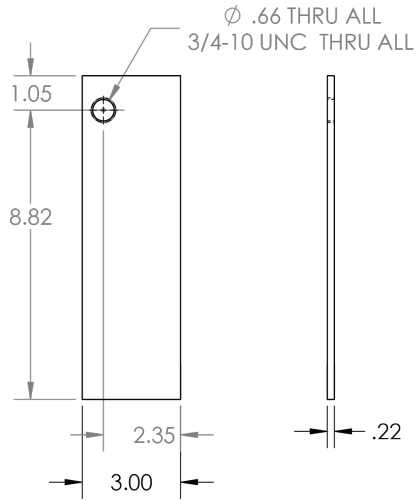

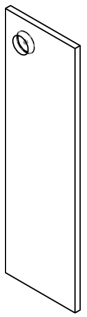

		UNLESS OTHERWISE SPECIFIED:		NAME	DATE
		DIMENSIONS ARE IN INCHES TOLERANCES: FRACTIONAL ± ANGULAR: MACH ± BEND ± TWO PLACE DECIMAL ± THREE PLACE DECIMAL ±	DRAWN		
			CHECKED		
			ENG APPR.		
			MFG APPR.		
		INTERPRET GEOMETRIC TOLERANCING PER:	Q.A.		
		MATERIAL Steel	COMMENTS:		
NEXT ASSY	USED ON	FINISH			
APPLICATION		DO NOT SCALE DRAWING			

TITLE:

Back Platform

SIZE	DWG. NO.	REV
A	12	

SCALE: 1:4	WEIGHT:	SHEET 1 OF 1

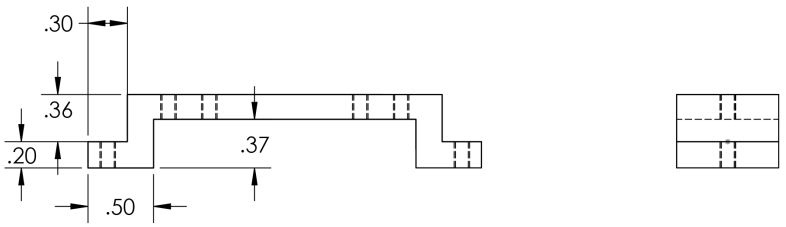

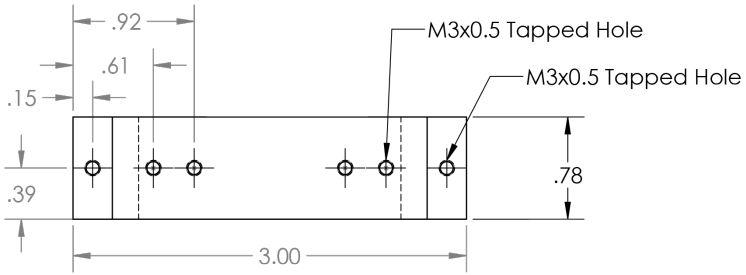

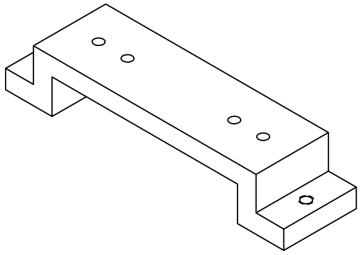

		UNLESS OTHERWISE SPECIFIED:		NAME	DATE
		DIMENSIONS ARE IN INCHES TOLERANCES: FRACTIONAL ± ANGULAR: MACH ± BEND ± TWO PLACE DECIMAL ± THREE PLACE DECIMAL ±	DRAWN		
			CHECKED		
			ENG APPR.		
			MFG APPR.		
		INTERPRET GEOMETRIC TOLERANCING PER:	Q.A.		
		MATERIAL Steel	COMMENTS:		
NEXT ASSY	USED ON	FINISH			
APPLICATION		DO NOT SCALE DRAWING			

TITLE: Fixture A

SIZE	DWG. NO.	REV
A	15	

SCALE: 1:1	WEIGHT:	SHEET 1 OF 1

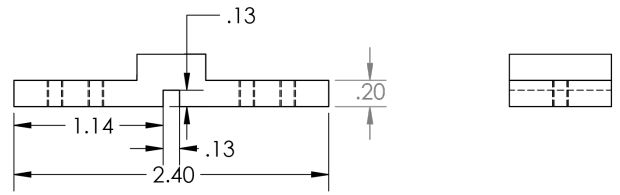

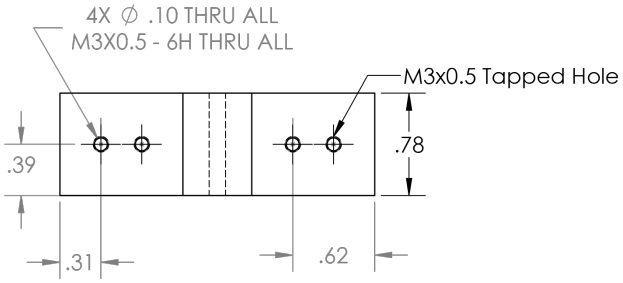

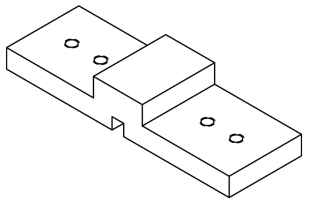

		UNLESS OTHERWISE SPECIFIED:		NAME	DATE
		DIMENSIONS ARE IN INCHES TOLERANCES: FRACTIONAL ± ANGULAR: MACH ± BEND ± TWO PLACE DECIMAL ± THREE PLACE DECIMAL ±	DRAWN		
			CHECKED		
			ENG APPR.		
			MFG APPR.		
		INTERPRET GEOMETRIC TOLERANCING PER:	Q.A.		
		MATERIAL Steel	COMMENTS:		
NEXT ASSY	USED ON	FINISH			
APPLICATION		DO NOT SCALE DRAWING			

TITLE: Fixture B

SIZE	DWG. NO.	REV
A	16	

SCALE: 1:1	WEIGHT:	SHEET 1 OF 1

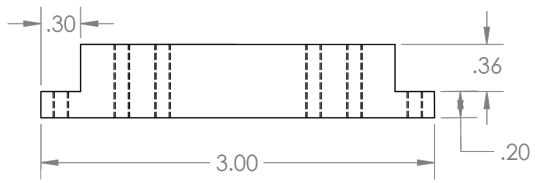

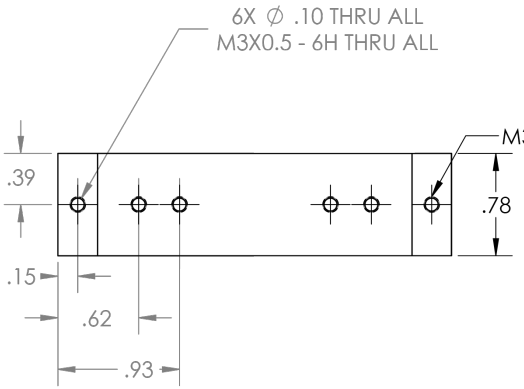

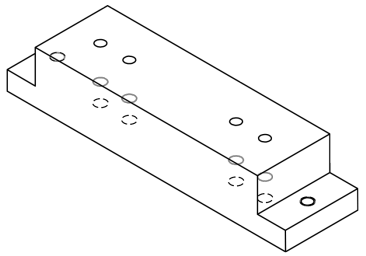

		UNLESS OTHERWISE SPECIFIED:		NAME	DATE
		DIMENSIONS ARE IN INCHES TOLERANCES: FRACTIONAL ± ANGULAR: MACH ± BEND ± TWO PLACE DECIMAL ± THREE PLACE DECIMAL ±	DRAWN		
			CHECKED		
			ENG APPR.		
			MFG APPR.		
		INTERPRET GEOMETRIC TOLERANCING PER:	Q.A.		
		MATERIAL Steel	COMMENTS:		
NEXT ASSY	USED ON	FINISH			
APPLICATION		DO NOT SCALE DRAWING			

TITLE: Fixture C

SIZE	DWG. NO.	REV
A	17	

SCALE: 1:1	WEIGHT:	SHEET 1 OF 1

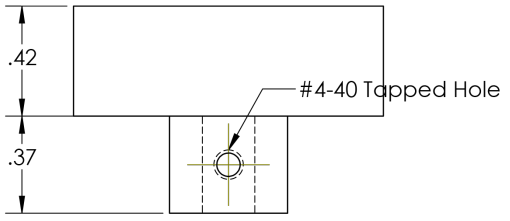

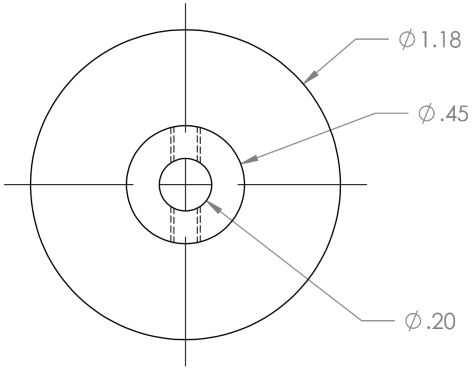

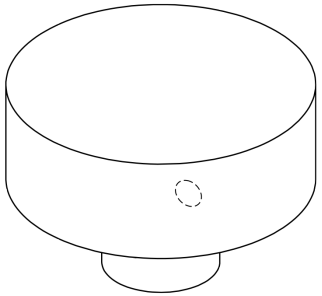

		UNLESS OTHERWISE SPECIFIED:		NAME	DATE
		DIMENSIONS ARE IN INCHES TOLERANCES: FRACTIONAL ± ANGULAR: MACH ± BEND ± TWO PLACE DECIMAL ± THREE PLACE DECIMAL ±	DRAWN		
			CHECKED		
			ENG APPR.		
			MFG APPR.		
		INTERPRET GEOMETRIC TOLERANCING PER:	Q.A.		
		MATERIAL Steel	COMMENTS:		
NEXT ASSY	USED ON	FINISH			
APPLICATION		DO NOT SCALE DRAWING			

TITLE:

Drive Roller

SIZE	DWG. NO.	REV
A	18	
SCALE: 2:1	WEIGHT:	SHEET 1 OF 1

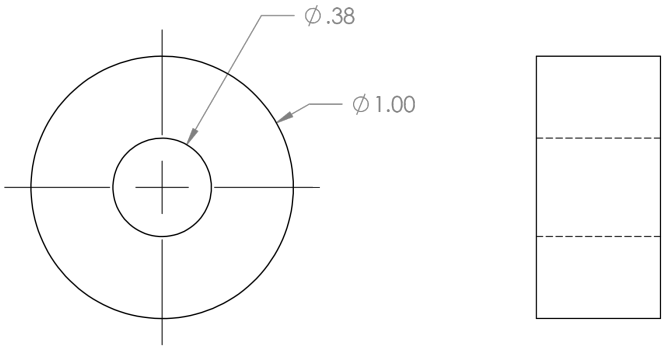

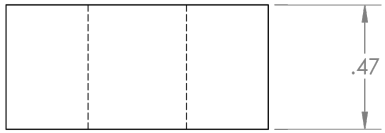

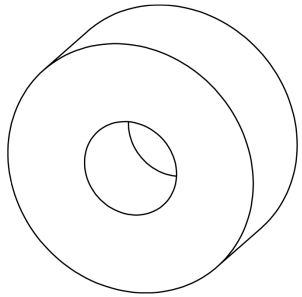

		UNLESS OTHERWISE SPECIFIED:		NAME	DATE
		DIMENSIONS ARE IN INCHES TOLERANCES: FRACTIONAL ± ANGULAR: MACH ± BEND ± TWO PLACE DECIMAL ± THREE PLACE DECIMAL ±	DRAWN		
			CHECKED		
			ENG APPR.		
			MFG APPR.		
		INTERPRET GEOMETRIC TOLERANCING PER:	Q.A.		
		MATERIAL Steel	COMMENTS:		
NEXT ASSY	USED ON	FINISH			
APPLICATION		DO NOT SCALE DRAWING			

TITLE: Spacer

SIZE	DWG. NO.	REV
A	19	

SCALE: 2:1	WEIGHT:	SHEET 1 OF 1

Trade Number: R8-2RS

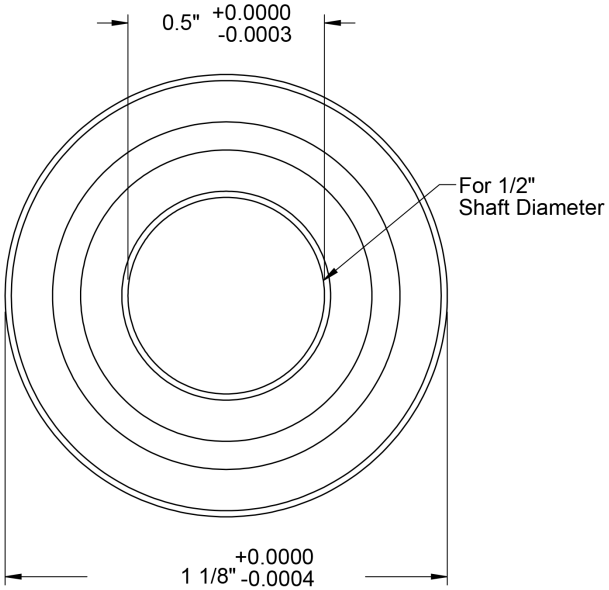

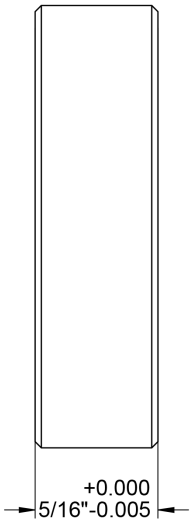

McMASTER-CARR® CAD

http://www.mcmaster.com

PART NUMBER **60355K704**

Ball Bearing

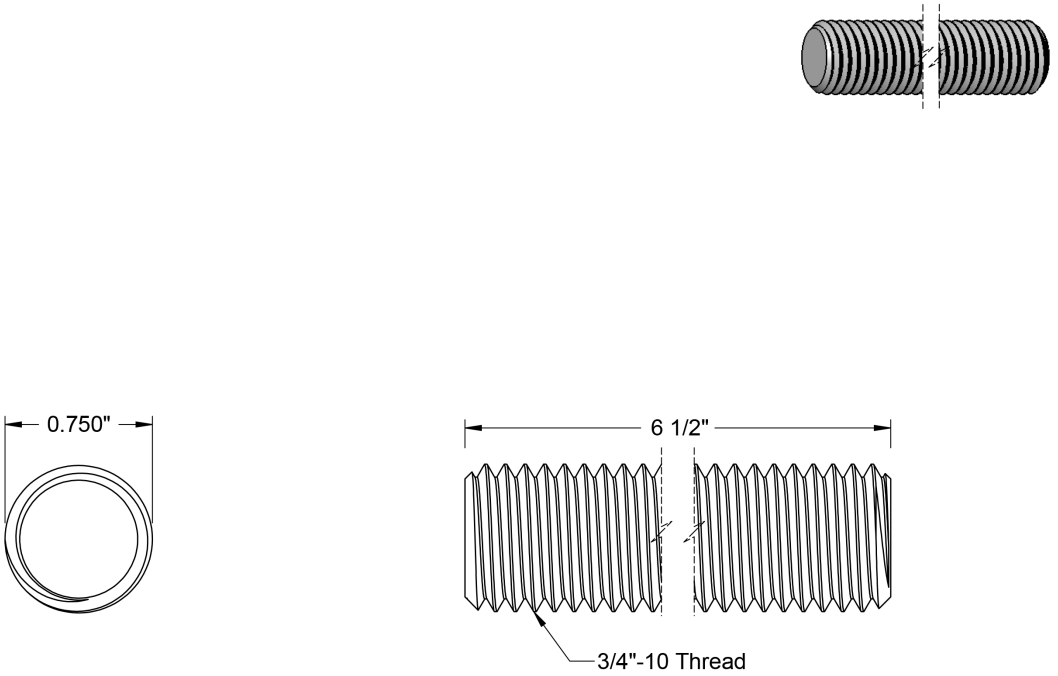

McMASTER-CARR® CAD

PART NUMBER **98750A318**

http://www.mcmaster.com

Information in this drawing is provided for reference only.

Medium-Strength Steel
Threaded Stud

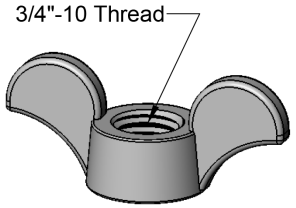

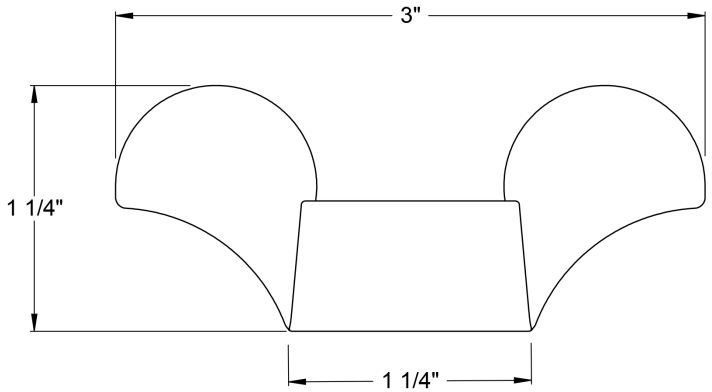

McMASTER-CARR® CAD	PART NUMBER 90876A175
http://www.mcmaster.com © 2015 McMaster-Carr Supply Company Information in this drawing is provided for reference only.	Wing Nut

Bibliography

[1] Neil Gershenfeld. *Fab: the coming revolution on your desktop–from personal computers to personal fabrication.* Basic Books, 2008.

[2] Thomas Campbell, Christopher Williams, Olga Ivanova, and Banning Garrett. Could 3d printing change the world. *Technologies, Potential, and Implications of Additive Manufacturing, Atlantic Council, Washington, DC*, 2011.

[3] Catarina Mota. The rise of personal fabrication. In *Proceedings of the 8th ACM conference on Creativity and cognition*, pages 279–288. ACM, 2011.

[4] Gerald C Anzalone, Chenlong Zhang, Bas Wijnen, Paul G Sanders, and Joshua M Pearce. A low-cost open-source metal 3-d printer. *Access, IEEE*, 1:803–810, 2013.

[5] William D Callister and David G Rethwisch. *Fundamentals of materials science and engineering: an integrated approach.* John Wiley & Sons, 2012.

[6] DA Roberson, D Espalin, and RB Wicker. 3d printer selection: A decision-making evaluation and ranking model. *Virtual and Physical Prototyping*, 8(3):201–212, 2013.

[7] K Jamshidi, S-H Hyon, and Y Ikada. Thermal characterization of polylactides. *Polymer*, 29(12):2229–2234, 1988.

[8] RepRap.org. ABS. http://reprap.org/wiki/ABS. (last accessed June 18, 2015).

[9] Mukesh Agarwala, David Bourell, Joseph Beaman, Harris Marcus, and Joel Barlow. Direct selective laser sintering of metals. *Rapid Prototyping Journal*, 1(1):26–36, 1995.

[10] Michael J Shkrum and David A Ramsay. *Forensic pathology of trauma*. Springer Science & Business Media, 2007.

[11] Samuel H Huang, Peng Liu, Abhiram Mokasdar, and Liang Hou. Additive manufacturing and its societal impact: a literature review. *The International Journal of Advanced Manufacturing Technology*, 67(5-8):1191–1203, 2013.

[12] Kevin Otto and Kristin Wood. *Product design: techniques in reverse engineering and new product development*. Pearson, 2003.

[13] George E Dieter. *Engineering design*. McGraw, 2009.

[14] Pero Raos, Ivica Klapan, and Tomislav Galeta. Additive manufacturing of medical models-applications in rhinology. *Collegium antropologicum*, 350:6134, 2013.

[15] Christopher S Huskamp and Victor Blakemore Slaughter. Design methodology to maximize the application of direct manufactured aerospace parts, March 31 2009. US Patent 7,509,725.

[16] Karen MB Taminger and Robert A Hafley. Electron beam freeform fabrication: a rapid metal deposition process. In *3rd Annual Automotive Composites Conference, Troy, MI, Sept*, pages 9–10, 2003.

[17] Terry Wohlers. *Wohlers report 2012*. Wohlers Associates, Inc, 2012.

[18] Kaufui V Wong and Aldo Hernandez. A review of additive manufacturing. *ISRN Mechanical Engineering*, 2012, 2012.

[19] Charles W Hull. Apparatus for production of three-dimensional objects by stereolithography, March 11 1986. US Patent 4,575,330.

[20] CK LEONG CHUA, KF LIM, and CS Rapid Prototyping. *Principles and Applications*. World Scientific, 2003.

[21] S Scott Crump. Apparatus and method for creating three-dimensional objects, June 9 1992. US Patent 5,121,329.

[22] Paul Calvert. Inkjet printing for materials and devices. *Chemistry of materials*, 13(10):3299–3305, 2001.

[23] Cheong Min Hong and Sigurd Wagner. Inkjet printed copper source/drain metallization for amorphous silicon thin-film transistors. *Electron Device Letters, IEEE*, 21(8):384–386, 2000.

[24] Thomas Boland, Tao Xu, Brook Damon, and Xiaofeng Cui. Application of inkjet printing to tissue engineering. *Biotechnology journal*, 1(9):910–917, 2006.

[25] Michael Feygin, Alexandr Shkolnik, Michael N Diamond, and Emmanuil Dvorskiy. Laminated object manufacturing system, March 24 1998. US Patent 5,730,817.

[26] T Himmer, T Nakagawa, and M Anzai. Lamination of metal sheets. *Computers in Industry*, 39(1):27–33, 1999.

[27] GD Janaki Ram, C Robinson, Y Yang, and BE Stucker. Use of ultrasonic consolidation for fabrication of multi-material structures. *Rapid Prototyping Journal*, 13(4):226–235, 2007.

[28] Christopher B Williams, Farrokh Mistree, and David W Rosen. Towards the design of a layer-based additive manufacturing process for the realization of metal parts of designed mesostructure. In *16th Solid Freeform Fabrication Symposium*, pages 217–230, 2005.

[29] Edson Costa Santos, Masanari Shiomi, Kozo Osakada, and Tahar Laoui. Rapid manufacturing of metal components by laser forming. *International Journal of Machine Tools and Manufacture*, 46(12):1459–1468, 2006.

[30] Carl R Deckard. Method and apparatus for producing parts by selective sintering, September 5 1989. US Patent 4,863,538.

[31] Emanuel M Sachs, John S Haggerty, Michael J Cima, and Paul A Williams. Three-dimensional printing techniques, April 20 1993. US Patent 5,204,055.

[32] Hermann Seitz, Wolfgang Rieder, Stephan Irsen, Barbara Leukers, and Carsten Tille. Three-dimensional printing of porous ceramic scaffolds for bone tis-

sue engineering. *Journal of Biomedical Materials Research Part B: Applied Biomaterials*, 74(2):782–788, 2005.

[33] John W Halloran, Vladislava Tomeckova, Susan Gentry, Suman Das, Paul Cilino, Dajun Yuan, Rui Guo, Andirudh Rudraraju, Peng Shao, Tao Wu, et al. Photopolymerization of powder suspensions for shaping ceramics. *Journal of the European Ceramic Society*, 31(14):2613–2619, 2011.

[34] Kathy Lu and William T Reynolds. 3dp process for fine mesh structure printing. *Powder technology*, 187(1):11–18, 2008.

[35] Jyoti Mazumder, Dwight Morgan, Timothy W Skszek, and Matthew Lowney. Direct metal deposition apparatus utilizing rapid-response diode laser source, July 27 2010. US Patent 7,765,022.

[36] SJ Randolph, JD Fowlkes, and PD Rack. Focused, nanoscale electron-beam-induced deposition and etching. *Critical reviews in solid state and materials sciences*, 31(3):55–89, 2006.

[37] Wei Zhang, Ming C Leu, Zhiming Ji, and Yongnian Yan. Rapid freezing prototyping with water. *Materials & design*, 20(2):139–145, 1999.

[38] Nannan Guo and Ming C Leu. Additive manufacturing: technology, applications and research needs. *Frontiers of Mechanical Engineering*, 8(3):215–243, 2013.

[39] Joseph Cesarano III and Paul D Calvert. Freeforming objects with low-binder slurry, February 22 2000. US Patent 6,027,326.

[40] J Xie, Aravinda Kar, James A Rothenflue, and William P Latham. Temperature-dependent absorptivity and cutting capability of co2, nd: Yag and chemical oxygen–iodine lasers. *Journal of Laser Applications*, 9(2):77–85, 1997.

[41] John G Bai, Kevin D Creehan, and Howard A Kuhn. Inkjet printable nanosilver suspensions for enhanced sintering quality in rapid manufacturing. *Nanotechnology*, 18(18):185701, 2007.

[42] Clint Atwood, M Ensz, D Greene, M Griffith, L Harwell, D Reckaway, T Romero, E Schlienger, and J Smugeresky. Laser engineered net shaping (lens (tm)): A tool for direct fabrication of metal parts. Technical report, Sandia National Laboratories, Albuquerque, NM, and Livermore, CA, 1998.

[43] Denis Cormier, Ola Harrysson, and Harvey West. Characterization of h13 steel produced via electron beam melting. *Rapid Prototyping Journal*, 10(1):35–41, 2004.

[44] GD Janaki Ram, Y Yang, and BE Stucker. Effect of process parameters on bond formation during ultrasonic consolidation of aluminum alloy 3003. *Journal of Manufacturing Systems*, 25(3):221–238, 2006.

[45] Douglas S Thomas and Stanley W Gilbert. Costs and cost effectiveness of additive manufacturing. *US Department of Commerce. Consulted at: http://nvlpubs. nist. gov/nistpubs/Special Publications/NIST. SP*, 11:76, 2014.

[46] Realizer GmbH. *SLM 300*, 2015.

[47] Realizer GmbH. *SLM 50*, 2015.

[48] EOS. *EOS M 290*, 2014. (last accessed November 1, 2016).

[49] 3D SYSTEM. *Sinterstation HiQ*, 2007.

[50] 3D SYSTEM. *Sinterstation Pro SLS System*, 2008.

[51] OPTOMEC. *LENS 450*, 2014.

[52] Arcam AB. *Arcam A2X*, 2015.

[53] Sciaky Inc. *Overview of EBAM Systems*, 2015.

[54] FABRISONIC. *Ultrasonic Additive Manufacturing Technology Overview*, 2012.

[55] Ph Buffat and Jean Pierre Borel. Size effect on the melting temperature of gold particles. *Physical Review A*, 13(6):2287, 1976.

[56] 3ders.org. Price Compare-3D Printers. http://www.3ders.org/pricecompare/3dprinters/. (last accessed March 10, 2016).

[57] Mini Metal Maker LLC. Mini Metal Maker. http://www.minimetalmaker.com/. (last accessed March 10, 2016).

[58] Miller Electric Mfg. Co. *Millermatic 140*, 2010.

[59] 3ders.org. Scientists build a $1,500 open-source 3d metal printer. http://www.3ders.org/articles/20131205-scientists-build-a-open-source-3d-metal-printer.html. (last accessed March 11, 2016).

[60] SIS-a new SFF method based on powder sintering, author=Khoshnevis, Behrokh and Asiabanpour, Bahram and Mojdeh, Mehdi and Palmer, Kurt, journal=Rapid Prototyping Journal, volume=9, number=1, pages=30–36, year=2003, publisher=MCB UP Ltd.

[61] Behrokh Khoshnevis, Mahdi Yoozbashizadeh, and Yong Chen. Metallic part fabrication using selective inhibition sintering (sis). *Rapid Prototyping Journal*, 18(2):144–153, 2012.

[62] John W Priest, Charles Smith, and Patrick DuBois. Liquid metal jetting for printing metal parts. In *Solid Freeform Fabrication Proceedings, University of Texas at Austin, TX*, pages 1–10, 1997.

[63] MetalClays.com. PM3 Silver Clay. http://www.metalclays.com/c/54/pmc3. (last accessed March 11, 2016).

[64] Jack M Ogden. Classical gold wire: some aspects of its manufacture and use. *Jewellery studies*, 5:95–105, 1991.

[65] Barbara A McGuire. *Wire in Design: Modern Wire Art & Mixed Media*. Krause Publications, 2002.

[66] AliExpress.com. Wire Sculpture. http://www.aliexpress.com/item/J8-LINESHOW-SCULPTURE-DECORATION-RACING-CAR-STAINLESS-HAND-MADE-ART-CRAFTS-HOME-OFFICE-GIFT/1403006234.html?spm=2114.40010308.4.97.OkKHt4. (last accessed March 11, 2016).

[67] Katholieke Universiteit Leuven. Production Processes - DTM 2000 Laser Sintering Machine. https://www.mech.kuleuven.be/pp/facilities/dtm2000. (last accessed March 11, 2016).

[68] National University of Singapore. Laminated Object Manufacturing. http://blog.nus.edu.sg/u0804594/common-rp-techniques/laminated-object-manufacturing-lom/. (last accessed March 11, 2016).

[69] CustomPartNet. Fused Deposition Modeling. http://www.custompartnet.com/wu/fused-deposition-modeling. (last accessed March 11, 2016).

[70] Great Britain. Health and Safety Executive (United Kingdom);. *Manual handling Manual Handling Operations Regulations 1992.* Sudbury (United Kingdom): HSE Books, 1992.

[71] MakerBot Industries. *MakerBot Replicator: User Manual.*

[72] Staples, Inc. Commercial Office Desk. http://www.staples.com/Commercial-Office-Desks/cat_CL164550. (last accessed March 11, 2016).

[73] Stratasys Data Sheets. The truth about speeds.

[74] Amazon.com. Artistic Wire Spiral Maker. http://www.amazon.com/Beadalon-228A-500-Artistic-Spiral-Maker/dp/B004DGITNM. (last accessed March 11, 2016).

[75] Christopher B Williams, Farrokh Mistree, and David W Rosen. A functional classification framework for the conceptual design of additive manufacturing technologies. *Journal of Mechanical Design*, 133(12):121002, 2011.

[76] Crescent Consultants Ltd. The filament winding process. http://www.cadfil.com/filamentwindingprocess.html, 2016. (last accessed March 11, 2016).

[77] VR Dave, JE Matz, and TW Eagar. Electron beam solid freeform fabrication of metal parts. In *Solid Freeform Fabrication Symposium*, pages 64–71, 1995.

[78] Karen M Taminger and Robert A Hafley. Electron beam freeform fabrication for cost effective near-net shape manufacturing. 2006.

[79] diy3dprinting. DIY 3D Printing. http://diy3dprinting.blogspot.com/2014/06/tig-welding-diy-metal-3d-printer-by.html. (last accessed March 11, 2016).

[80] Theodore L Bergman, Frank P Incropera, and Adrienne S Lavine. *Fundamentals of heat and mass transfer*. John Wiley & Sons, 2011.

[81] Seiji Katayama. *Handbook of laser welding technologies*. Elsevier, 2013.

[82] Full Spectrum Laser. Full spectrum laser. https://fslaser.com/Products/View/0. (last accessed March 11, 2016).

[83] Chad NelsoN and Jordan Crist. Predicting laser beam characteristics. *Laser Technik Journal*, 9(1):36, 2012.

[84] BJ Neubert and B Eppich. Influences on the beam propagation ratio m 2. *Optics communications*, 250(4):241–251, 2005.

[85] LaserStar Technologies Corporation. iWeld Laser Welding System. https://www.laserstar.net/welding-products/990-iweld.cfm. (last accessed March 11, 2016).

[86] Datalogic. *Green Laser*. (last accessed March 11, 2016).

[87] CrystaLaser. *Diode Pumped Green 523/527/542 n CrystaLaser*. (last accessed March 11, 2016).

[88] Chen Hui-Chi, Bi Guijun, and Sun Chen-Nan. High energy beam welding processes in manufacturing. In *Handbook of Manufacturing Engineering and Technology*, pages 617–639. Springer, 2015.

[89] Kikuo Ujihara. Reflectivity of metals at high temperatures. *Journal of Applied Physics*, 43(5):2376–2383, 1972.

[90] DL Cocke, R Schennach, MA Hossain, DE Mencer, H McWhinney, JR Parga, M Kesmez, JAG Gomes, and MYA Mollah. The low-temperature thermal oxidation of copper, cu 3 o 2, and its influence on past and future studies. *Vacuum*, 79(1):71–83, 2005.

[91] Guy Kendall White and SJ Collocott. Heat capacity of reference materials: Cu and w. *Journal of Physical and Chemical Reference Data*, 13(4):1251–1257, 1984.

[92] JP Moore, DL McElroy, and RS Graves. Thermal conductivity and electrical resistivity of high-purity copper from 78 to 400Âř k. *Canadian Journal of Physics*, 45(12):3849–3865, 1967.

[93] Li Wu, Huijun Kang, Zongning Chen, Ying Fu, and Tongmin Wang. Simulation study of al-1mn/al-10si circular clad ingots prepared by direct chill casting. *Metallurgical and Materials Transactions B*, 47(1):89–98, 2016.

[94] ASTRA ltd. *How much heat flux is that?*, 2009. (last accessed March 21, 2016).

[95] UltraFlex Power Technologies. *UltraHeat S Series*, 2014. (last accessed March 21, 2016).

[96] Amazon. Pulse Argon Spot Welder 400W for Welding Jewelry Gold Silver Platinum Palladium. https://www.amazon.com/Welder-Welding-Jewelry-Platinum-Palladium/dp/B00CO5EFMI/ref=sr_1_1?ie=UTF8&qid=1472683713&sr=8-1&keywords=argon+spot+welder, 2016. (last accessed August 31, 2016).

[97] PENSA LABS. *DIWire*, 2016. (last accessed March 21, 2016).

[98] Sinotech, Inc. 10-100 watt 40mm Brushless DC Motors. http://www.sinotech.com/Brushless_DC_Motors_10-100watt_40mm.html, 2014. (last accessed March 21, 2016).

[99] Skuit. *KM Kiln Specification Sheet*. (last accessed March 21, 2016).

[100] Kickstarter. DIWire: The First Desktop Wire Bender. https://www.kickstarter.com/projects/1638882643/diwire-the-first-desktop-wire-bender/description, 2014. (last accessed March 22, 2016).

[101] eBay Inc. ORIENTAL-MOTOR-100W-VEXTA-BRUSHLESS-DC-MOTOR-HBLM5100N-GFH-CUT-CABLE. http://www.ebay.com/itm/ORIENTAL-MOTOR-100W-VEXTA-BRUSHLESS-DC-MOTOR-HBLM5100N-GFH-CUT-CABLE-/290913551859?hash=item43bbcc85f3:g:5LEAAOSwZjJU~nDq, 2016. (last accessed March 22, 2016).

[102] eBay Inc. Mouse over image to zoom RapidFire-Pro-Programmable-Electric-Digital-Kiln-PMC-Jewelry-Making. http://www.ebay.com/itm/RapidFire-Pro-Programmable-Electric-Digital-Kiln-PMC-Jewelry-Making-/272172259244?hash=item3f5ebb17ac:g:VHgAAOSw1ZBUw~9Q, 2016. (last accessed March 22, 2016).

[103] Standard specification for soft or annealed copper wire. ASTM ASTM B3-13, ASTM International, West Conshohocken, PA, 2013.

[104] Peter W. Rowe. Silver solder. http://juxtamorph.com/silver-solder/, 2016. (last accessed October 11, 2016).

[105] Standard method for evaluating the strength of brazed joints. AWS AWS C3.2M/C3.2:2008, American Welding Society, 2008.

[106] Wikiwand. Diode bridge. http://www.wikiwand.com/en/Diode_bridge, 2016. (last accessed October 17, 2016).

[107] Standard test methods for tension testing of metallic materials. ASTM ASTM E8/E8M, ASTM International, West Conshohocken, PA, 2016.

[108] KJ Mathew. A review on brazing parameters and the experiments used to analyze the parameters.

[109] Rio Grande. Orion 100c pulse arc welding system. https://www.riogrande.com/Product/orion-100c-pulse-arc-welding-system/503107, 2016. (last accessed October 17, 2016).

[110] Amazon. Grade propane torch. https://www.amazon.com/Worthington-308639-WT4601i-Discontinued-Manufacturer/dp/B004FPZACY, 2016. (last accessed October 17, 2016).

[111] Home Depot. Propane gas cylinder. http://www.homedepot.com/p/Bernzomatic-14-1-oz-Propane-Gas-Cylinder-304182/202044700, 2016. (last accessed October 17, 2016).

[112] Amazon. Silver solder paste. https://www.amazon.com/Silver-Solder-Paste-Hard-Ss75-/dp/B00A97XWTU/ref=sr_1_1?ie=UTF8&qid=1473881504&sr=8-1&keywords=silver+solder+paste+hard, 2016. (last accessed October 17, 2016).

[113] Amazon. Pulse argon spot welder. https://www.amazon.com/gp/product/B00RYTMMH4/ref=oh_aui_detailpage_o02_s00?ie=UTF8&psc=1, 2016. (last accessed October 17, 2016).

[114] Amazon. Tig welding tungsten. https://www.amazon.com/gp/product/B013KZ042A/ref=oh_aui_detailpage_o06_s00?ie=UTF8&psc=1, 2016. (last accessed October 17, 2016).

[115] IEEE. Tube bending tooling information. http://www.globalspec.com/learnmore/manufacturing_process_equipment/machine_tool_components_accessories/tube_bending_tooling, 2016. (last accessed October 17, 2016).

[116] M Murata and T Kato. Highly improved function and productivity for tube bending by cnc bender. *TubeNet–The Site For Tube And Pipe Industries, http://www. tubenet. org [accessed March 2003]*, 2003.

[117] Peter Gantner, Herbert Bauer, David K Harrison, and Anjali KM De Silva. Free-bending: a new bending technique in the hydroforming process chain. *Journal of materials processing technology*, 167(2):302–308, 2005.

[118] SparkFun Electronics. *Stepper Motor*, 2016. (last accessed November 10, 2016).

[119] McMaster-Carr. Linear solenoid. https://www.mcmaster.com/#70155k311/=14zjcjq, 2016. (last accessed November 10, 2016).

[120] McMaster-Carr. Type 316 stainless steel fully threaded stud. https://www.mcmaster.com/#90575a141/=157pec9, 2016. (last accessed November 26, 2016).

[121] Grainger. 3/8" 18-8 (304) stainless steel machine screw with round head type and plain finish. https://www.grainger.com/product/GRAINGER-APPROVED-3-8-18-8-304-Stainless-Steel-2BB15?s_pp=false&picUrl=//static.grainger.com/rp/s/is/image/Grainger/1ME92_AW01?\protect\T1\

textdollarsmthumb\protect\T1\textdollar, 2016. (last accessed November 14, 2016).

[122] McMaster-Carr. Plastic gear - 14-1/2 degree pressure angle. https://www.mcmaster.com/#57655k27/=150xyd3, 2016. (last accessed November 14, 2016).

[123] McMaster-Carr. Plastic gear - 14-1/2 degree pressure angle. https://www.mcmaster.com/#57655k31/=150y2bs, 2016. (last accessed November 14, 2016).

[124] SparkFun Electronics. Stepper motor with cable. https://www.sparkfun.com/products/9238, 2016. (last accessed November 14, 2016).

[125] Grainger. 10mm property class 4.8 steel machine screw with pan head type and zinc plated finish. https://www.grainger.com/product/GRAINGER-APPROVED-10mm-Property-Class-4-8-Steel-6GU65?functionCode=P2IDP2PCP, 2016. (last accessed November 14, 2016).

[126] Grainger. Shoulder bolt, 1/4x5/8. https://www.grainger.com/product/GRAINGER-APPROVED-Shoulder-Bolt-1CA71?s_pp=false&picUrl=//static.grainger.com/rp/s/is/image/Grainger/38CZ28_AW01?\protect\T1\textdollarsmthumb\protect\T1\textdollar, 2016. (last accessed November 14, 2016).

[127] Grainger. 1/8" 18-8 (304) stainless steel machine screw with pan head type and plain finish. https://www.grainger.com/product/GRAINGER-

APPROVED-1-8-18-8-304-Stainless-Steel-1ZB33?s_pp=false&picUrl=//static.grainger.com/rp/s/is/image/Grainger/1ME92_AW01?\protect\T1\textdollarsmthumb\protect\T1\textdollar, 2016. (last accessed November 14, 2016).

[128] McMaster-Carr. Multipurpose 304/304l stainless steel tube. https://www.mcmaster.com/#8457k51/=151fzhb, 2016. (last accessed November 14, 2016).

[129] McMaster-Carr. Ball bearing. https://www.mcmaster.com/#60355k704/=1511s1r, 2016. (last accessed November 14, 2016).

[130] McMaster-Carr. Type 316 stainless steel shoulder screw. https://www.mcmaster.com/#97345a262/=150znry, 2016. (last accessed November 14, 2016).

[131] Amazon. Bare copper wire, bright, 22 awg, 0.025" diameter, $500'$ length. https://www.amazon.com/Copper-Bright-0-025-Diameter-Length/dp/B000IJYRK2/ref=sr_1_2?ie=UTF8&qid=1479087684&sr=8-2&keywords=22+gauge+copper+wire, 2016. (last accessed November 14, 2016).

[132] McMaster-Carr. Astm a193 grade b7 steel threaded stud. https://www.mcmaster.com/#98750a318/=150zmhn, 2016. (last accessed November 14, 2016).

[133] McMaster-Carr. Wing nut. https://www.mcmaster.com/#90876a175/=1511ugr, 2016. (last accessed November 14, 2016).

[134] Grainger. Property class 4.8 steel machine screw, phillips, pan head. https://www.grainger.com/product/GRAINGER-APPROVED-Property-Class-4-8-Steel-Machine-WP119869/_/N-8n0Z1z0ny1jZ1yzy9emZ1z09lw8?sst=subsetTest&s_pp=false&picUrl=//static.grainger.com/rp/s/is/image/Grainger/35EX91_AL01?\protect\T1\textdollarsmthumb\protect\T1\textdollar, 2016. (last accessed November 14, 2016).

[135] Grainger. Steel hex nut with m3-0.50 dia./thread size. https://www.grainger.com/product/GRAINGER-APPROVED-Steel-Hex-Nut-with-M3-0-50-38CR17?s_pp=false&picUrl=//static.grainger.com/rp/s/is/image/Grainger/38DM02_AW01?\protect\T1\textdollarsmthumb\protect\T1\textdollar, 2016. (last accessed November 14, 2016).

[136] Grainger. Stainless steel hex nut with $3/4$"-10 dia./thread size. https://www.grainger.com/product/GRAINGER-APPROVED-Stainless-Steel-Hex-Nut-with-1WB48?s_pp=false&picUrl=//static.grainger.com/rp/s/is/image/Grainger/22UK36_AS01?\protect\T1\textdollarsmthumb\protect\T1\textdollar, 2016. (last accessed November 14, 2016).

[137] DIwire. DIWire-Bender. https://github.com/diwire/DIWire-Bender, 2012. (last accessed April 4, 2016).

[138] Greg Miller. *Justifying, selecting and implementing tube bending methods*. Society of Manufacturing Engineers, 1998.

[139] The ExOne Company. *2013 Annual Report*, 2014.

[140] Girish Kelkar. Pulsed laser welding. *WJM Technologies, excellence in material joining, Cerritos, CA*, 90703, 2000.

[141] CS Wu and JS Sun. Modelling the arc heat flux distribution in gma welding. *Computational materials science*, 9(3):397–402, 1998.

[142] eBay Inc. DX-30A jewelry laser welder handheld mini laser spot welding machine. http://www.ebay.com/itm/DX-30A-jewelry-laser-welder-handheld-mini-laser-spot-welding-machine-/121859836611, 2016. (last accessed March 22, 2016).

[143] Low Power Lab LLC. Importing a laser cutter from China. http://lowpowerlab.com/blog/2014/05/26/importing-a-laser-cutter-from-china/, 2014. (last accessed April 6, 2016).